

# 1 **Contrasting the Penultimate and Last Glacial Maxima (140 and 21 ka** 2 **BP) using coupled climate-ice sheet modelling**

3 Violet L. Patterson<sup>1</sup>, Lauren J. Gregoire<sup>1</sup>, Ruza F. Ivanovic<sup>1</sup>, Niall Gandy<sup>2</sup>, Jonathan Owen<sup>1</sup>, Robin S.  
4 Smith<sup>3</sup>, Oliver G. Pollard<sup>1</sup>, Lachlan C. Astfalck<sup>4</sup>, [Paul J. Valdes<sup>5</sup>](#)

5 <sup>1</sup>School of Earth and Environment, University of Leeds, Leeds, UK

6 <sup>2</sup>Department of the Natural and Built Environment, Sheffield Hallam University, Sheffield, UK

7 <sup>3</sup>NCAS, Department of Meteorology, University of Reading, Reading, UK

8 <sup>4</sup>School of Physics, Mathematics and Computing, University of Western Australia, Perth, Australia

9 [<sup>5</sup>School of Geographical Sciences, University of Bristol, Bristol, UK](#)

10 *Correspondence to:* Violet L. Patterson (ee17vp@leeds.ac.uk)

11 **Abstract.** The configuration of the Northern Hemisphere ice sheets during the Penultimate Glacial Maximum differed to the  
12 Last Glacial Maximum. However, the reasons for this are not yet fully understood. These differences likely contributed to the  
13 varied deglaciation pathways experienced following the glacial maxima and may have had consequences for the interglacial  
14 sea level rise. ~~Therefore, a better understanding of how and why these two glacial maxima differed is crucial for developing~~  
15 ~~the full picture on why the Last Interglacial sea level was up to 9 meters higher than today, and thus may help constrain future~~  
16 ~~sea level rise.~~ To understand the differences between the North American Ice Sheet at the Last and Penultimate Glacial Maxima  
17 (21 and 140 ka BP), we perform two perturbed-physics ensembles of 62 simulations using a coupled ~~climateatmosphere~~-ice  
18 sheet model, FAMOUS-ice, ~~with prescribed surface ocean conditions~~, in which the North American and Greenland ice sheets  
19 are dynamically simulated with the Glimmer ice sheet model. ~~We select six~~ We apply an implausibility metric to find ensemble  
20 members that match reconstructed ice extent and volumes at the Last and Penultimate Glacial Maxima. ~~To understand~~ We use  
21 a resulting set of 'plausible' parameters to perform sensitivity experiments to decompose the role of climate forcings (orbit,  
22 greenhouse gases) and initial conditions on the final ice sheet configurations, ~~we use a factor decomposition technique.~~ This  
23 ~~reveals~~ confirms that the initial ice sheet conditions used in the model are extremely important in determining the difference in  
24 final ice volumes between both periods due to the large effect of the ice-albedo feedback. In contrast to evidence of a smaller  
25 Penultimate North American Ice Sheet, our ~~model shows~~ results show that the climate boundary conditions at these glacial  
26 maxima, if considered in isolation, imply a larger Penultimate Glacial Maximum North American Ice Sheet than at the Last  
27 Glacial Maximum, of around 6 meters sea level equivalent. This ~~suggests~~ supports the notion that the growth of the ice sheet  
28 prior to the glacial maxima is key in explaining the differences in North American ice volume.

## 29 **1 Introduction**

30 The Penultimate Glacial Maximum (PGM) occurred around 140,000 years ago, within Marine Isotope Stage 6 (MIS 6).  
31 Greenhouse gas (GHG) concentrations and global average insolation were similar to the Last Glacial Maximum (LGM; ~21  
32 ka BP) (Berger and Loutre, 1991; Loulergue et al., 2008; Bereiter et al., 2015) but the orbital configuration differed, affecting  
33 the seasonal and latitudinal distribution of incoming shortwave radiation (Berger, 1978; Colleoni et al., 2011). The global total  
34 ice sheet volume, and thus the global mean sea level, was likely similar between the two glacial maxima (~120-130 m below  
35 present), with larger uncertainty at the PGM (Rabineau et al., 2006; Masson-Delmotte et al., 2010; Rohling et al., 2017). Both  
36 geological evidence and numerical modelling suggest that despite the similarities in total ice volume between the PGM and  
37 the LGM, the configurations of the Northern Hemisphere ice sheets differed significantly (e.g. Svendsen et al., 2004; Colleoni  
38 et al., 2016; Batchelor et al., 2019).—

39 Some reconstructions suggest the Eurasian Ice Sheet (EIS) may have been up to ~50 % larger during the Penultimate Glacial  
40 Cycle (MIS 6: ~190-130 ka BP) than during the Last Glacial Cycle (~115-12 ka BP) ~~-(Svendsen et al., 2004), however).~~  
41 However, evidence of multiple advances and uncertainties in dating proxy records means that the maximum extent mapped at  
42 140 ka BP could correspond to previous advances during MIS 6 ~~(Svendsen et al., 2004)~~. Similarly, the timing of the maximum extent  
43 of the EIS at the LGM is also uncertain and areas of the ice margin likely reached their maximum extents at different times  
44 throughout the glacial cycle (Svendsen et al., 2004; Margari et al., 2014; Colleoni et al., 2016; Ehlers et al., 2018). The extent  
45 of the North American Ice Sheet (NAIS) during the PGM is even less well constrained due to a lack of glaciological evidence  
46 (e.g. moraines and till). The scarcity of empirical data in itself suggests that it was smaller in most areas than at the LGM  
47 because the subsequent larger ice sheet could have largely erased the evidence of prior glaciations (Dyke et al., 2002; Rohling  
48 et al., 2017). Additionally, evidence of reduced ice rafted debris (IRD) discharge from the Hudson Strait in the North Atlantic  
49 IRD belt (e.g. Hemming, 2004; Naafs et al., 2013; Obrochta et al., 2014), relative sea level assessment studies (e.g. Rohling et  
50 al., 2017) and climate, ice sheet and glacial isostatic adjustment modelling (e.g. Colleoni et al., 2016; Dyer et al., 2021) all  
51 point to a smaller volume PGM NAIS. For example, assuming a similar global mean sea level fall (and Antarctic ice sheet  
52 volume) at the PGM as at the LGM but with a larger volume EIS at the PGM (estimated at 33-53 m sea level equivalent (SLE)  
53 versus 14-29 m SLE at the LGM), this follows that the NAIS must have been smaller than at the LGM to compensate (39-59  
54 m SLE versus 51-88 m SLE) (Rohling et al., 2017).

55 The reason for these differences is likely complex and is not yet fully understood. The evolution and surface mass balance  
56 (SMB) of ice sheets depends on many factors such as; background climate, climate and ice sheet histories, dust deposition,  
57 vegetation, ice albedo and sea surface temperatures, as well as the interactions and feedbacks between them all (Kageyama et  
58 al., 2004; Krinner et al., 2006; 2011; Colleoni et al., 2009a; 2011; Liakka et al., 2012; Stone and Lunt, 2013). The ice sheets  
59 themselves also strongly influence the climate through their interactions with atmospheric and oceanic circulation and the  
60 energy balance. This alters global and local temperature and precipitation patterns which in turn affects ice sheet ablation and

61 accumulation (i.e. SMB) (e.g. Kageyama and Valdes, 2000; Abe-Ouchi et al., 2007; Beghin et al., 2014; 2015; Ullman et al.,  
62 2014; Liakka et al., 2016; Gregoire et al., 2015; 2018; Snoll et al., 2022; Izumi et al., 2023).—\_These interactions between the  
63 vast ice sheets and other components of the climate system exerted an important control on the initial climate state for the  
64 deglaciations, and hence on the subsequent chain of events, thus impacting the climate, ocean and sea level evolution during  
65 deglaciation. Thus, the contrasting configurations of the Northern Hemisphere ice sheets at the glacial maxima may have  
66 contributed to the different deglaciation pathways that followed. ~~The timings and magnitudes of the climate and ocean  
67 circulation changes that occurred during the Penultimate Deglaciation (~138-128 ka BP) differed to the Last Deglaciation  
68 (~19-11 ka BP) (Landais et al., 2013; Menviel et al., 2019). For example the Last Deglaciation experienced two abrupt climate  
69 changes associated with a weakened Atlantic Meridional Overturning Circulation, Heinrich Stadial 1 and the Younger Dryas  
70 (Denton et al., 2010; Ivanovic et al., 2016; 2018), compared to evidence of only one, much longer abrupt change towards the  
71 end of the Penultimate Deglaciation, Heinrich Stadial 11 (Cheng et al., 2009; Govin et al., 2015; Marino et al., 2015;  
72 JimenezAmat and Zahn, 2015). The deglaciations also led to interglacials with very different characteristics to one another,  
73 including average global surface temperatures 1-2 °C higher and sea level up to 9 m higher than the pre-industrial during the  
74 Last  
75 Interglacial (~129-116 ka BP) (Kopp et al., 2009; Turney and Jones, 2010; Grant et al., 2012; Dutton and Lambeck, 2012;  
76 Otto-Bliesner et al., 2013; Dutton et al., 2015; Dyer et al., 2021).~~

77 In this context, it is important to examine the complex physical interactions between the climate and the ice sheets to better  
78 understand why the last two glacial maxima had different ice sheet configurations and evaluate the ice sheets' sensitivities to  
79 changes in climate in relation to different orbits and greenhouse gas concentrations. To achieve this, numerical simulations of  
80 these periods are required using a coupled climate-ice sheet model that capture these complex, non-linear interactions. Previous  
81 studies on glacial-interglacial cycles, have relied on the coupling of relatively fast, low resolution and simplified Earth system  
82 Models of Intermediate Complexity (EMICs) to an ISM (e.g. Bonelli et al., 2009

83 ~~Despite the challenges in coupling Atmosphere Ocean General Circulation Models (AOGCMs) with ice sheet models due to  
84 the mismatch between the required spatial and temporal scales, recent technical advances have meant that this is now possible.;~~  
85 Ganopolski et al., 2010; Fyke et al., 2011; Heinemann et al., 2014; Beghin et al., 2014; Ganopolski and Brovkin, 2017; Quiquet  
86 et al., 2021; Poppelmeier et al., 2023; Willeit et al., 2024) or one-way forcing of an ice sheet model with climate forcing output  
87 by stand-alone climate simulations (e.g. Abe-Ouchi et al., 2013; Stone and Lunt, 2013; Gregoire et al., 2015; 2016). These  
88 computationally efficient techniques advanced our understanding of the roles of orbit and CO<sub>2</sub> in ice sheet evolution and  
89 proposed plausible reconstructions of past ice sheets (e.g. Robinson et al., 2011; Stone et al, 2013). They also highlighted  
90 important earth system interactions (e.g. Stone and Lunt, 2013; Willeit et al., 2024) such as with vegetation, dust, albedo,  
91 glacial isostatic adjustment, disparate ice sheets (Beghin et al., 2015) as well as internal ice sheet instabilities (Gregoire et al.,  
92 2012; Quiquet et al., 2021). However, the accuracy of these results has been limited by the simplified representation of climate

93 processes, atmospheric circulation and/or surface mass balance. A combination of increased computer power, the development  
94 of more computationally efficient, lower resolution ~~AOGCMs~~General Circulation Models (GCMs) and sub-grid scale schemes  
95 translating ice sheet relevant atmospheric processes onto the higher resolution ice sheet grid, has made bi-directional, coupled  
96 climate-ice sheet simulations over longer timescales, and in large ensembles, feasible (~~Fyke et al., 2011;~~ Vizcaino et al., 2013;  
97 Ziemen et al., 2014; Sellevold et al., 2019; Smith et al., 2021).— These coupled models have been used to simulate the climate-  
98 ice sheet interactions during past glacial periods including: glacial inception (Gregory et al., 2012); the LGM and the build up  
99 to it (Ziemen et al., 2014; Gandy et al., 2023; Sherriff-Tadano et al., 2023; Nui et al., 2024) and MIS 13 (Niu et al., 2021).

100 ~~This~~To better understand the differences between the Penultimate and Last Glacial Maxima ice sheet configurations, we seek  
101 to establish how the differences in climate forcings (such as orbit and greenhouse gases) between the two periods affected ice  
102 sheet surface mass balance and in turn their geometry. To this end, this study uses a coupled climate-ice sheet model, ~~called~~  
103 ~~(FAMOUS-ice-;~~ Smith et al., 2021), to perform ~~ensemble~~ensembles of simulations of the PGM and LGM to explore input  
104 climate and ice sheet parameter uncertainties, ~~and~~ and their effects on the North American ice sheet volume during each period,  
105 ~~and find parameter combinations.~~ We identify simulations that give a reasonable ice sheet configuration for both glacial  
106 maxima. The ensembles are also constrained based on match volume and extent ~~metrics and the ‘Not Ruled Out Yet’ (NROY)~~  
107 ~~simulations are analysed to try and understand the similarities and differences between both periods. We find that the~~  
108 ~~constraints and use these to perform a factorial decomposition of the effects of climate forcing and initial conditions used in~~  
109 ~~the LGM and PGM experiments played an important role in some of the differences seen and we quantify this impact through on~~  
110 ice volume difference between ~~the use of sensitivity tests and factor decomposition analysis.~~ two Glacial Maxima.

## 111 **2 Methods**

### 112 **2.1 Model description**

113 FAMOUS is a fast, low resolution AOGCM that is based on Hadley Centre coupled model HadCM3 and therefore retains all  
114 the complex processes represented in an AOGCM but uses only half the spatial resolution and a longer time step. Since it  
115 requires only 10 % of the computational costs of HadCM3, it has been successfully used for long transient palaeo simulations  
116 (Smith and Gregory, 2012; Gregory et al., 2012; Gregoire et al., 2012; Roberts et al., 2014; Dentith et al., 2019) and large  
117 ensembles for uncertainty quantification (Gregoire, 2010; Gandy et al., 2023). This study uses the atmospheric component,  
118 which is a ~~quasi~~-hydrostatic, primitive equation grid point model with a horizontal resolution of 7.5° longitude by 5° latitude  
119 with 11 vertical levels and a 1-hour time step (Williams et al., 2013). Land processes are modelled using the MOSES2.2 land  
120 surface scheme (Essery et al., 2003), which uses a set of sub-gridscale tiles in each grid box to represent fractions of nine  
121 different surface types, including land ice (Smith et al., 2021). Whilst this study prescribes sea surface temperatures and sea  
122 ice concentrations, FAMOUS can also be run fully coupled with a dynamical ocean (e.g. Dentith et al., 2019).—

123 FAMOUS now allows the direct two-way coupling to an ice sheet model in the configuration FAMOUS-ice (Smith et al.,  
124 2021). Here, we use FAMOUS in combination with Glimmer to interactively simulate the North American and Greenland ice  
125 sheets at 40km resolution. Glimmer is a fast running, 3D thermomechanical ice sheet model which uses the shallow ice  
126 approximation. This allows it to model ice sheet evolution over long timescales as it is more computationally efficient, and  
127 therefore has been used to simulate continental ice sheets over glacial-interglacial cycles (Rutt et al., 2009; Gregoire et al.,  
128 2016).

129 FAMOUS-ice accounts for the mismatch between atmosphere and ice sheet grid sizes by using a multilayer surface snow  
130 scheme to calculate SMB on ‘tiles’ at 10 set elevations within each grid box that contains land ice in FAMOUS. This SMB is  
131 then downscaled from the coarse FAMOUS grid to the much finer Glimmer grid at each model year (Smith et al., 2021).  
132 Glimmer uses this SMB field to calculate ice flow and surface elevation and passes this back to FAMOUS in which orography  
133 and ice cover is updated. In this study, to reduce computational costs further, FAMOUS-ice runs at 10 times ice sheet  
134 acceleration: for every year of climate integrated in FAMOUS, the simulated SMB field forces 10 years of ice sheet integration  
135 in Glimmer. Figure 1 shows a simplified diagram of this coupling process and full details can be found in Smith et al.,  
136 (2021). The current computational cost of this set up is around 50 decades (of climate years) per wallclock day using 8  
137 processors- (~ 192 core hours).

138 FAMOUS-ice has been shown to perform well in simulations of past and future ice sheets including Greenland and North  
139 America (Gregory et al., 2020; Smith et al., 2021; Gandy et al., 2023). In particular, the LGM North American Ice Sheet study  
140 of Gandy et al., (2023) was able to utilise the useful constraints of the LGM to infer the importance of parameters controlling  
141 ice sheet albedo on ice sheet configuration in this model.

Surface Mass Balance  
Surface temperature at bottom of snowpack

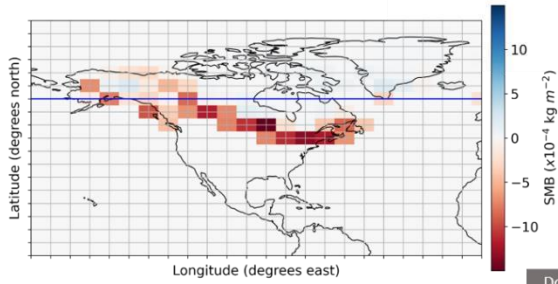
Every year

FAMOUS GCM  
(MOSES 2.2)

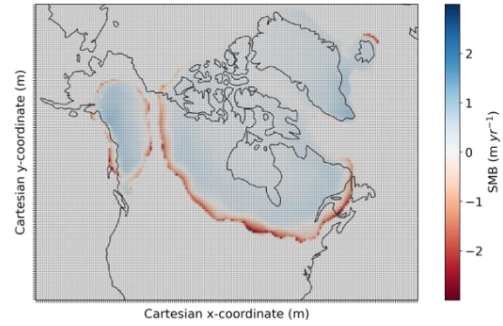
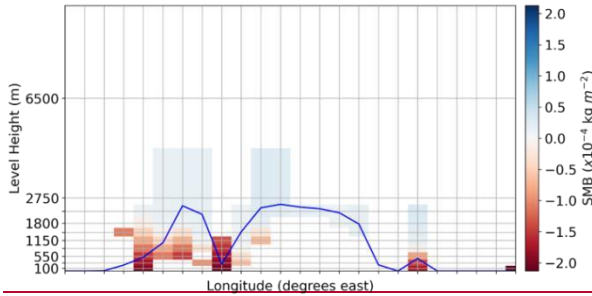
Glimmer CISM

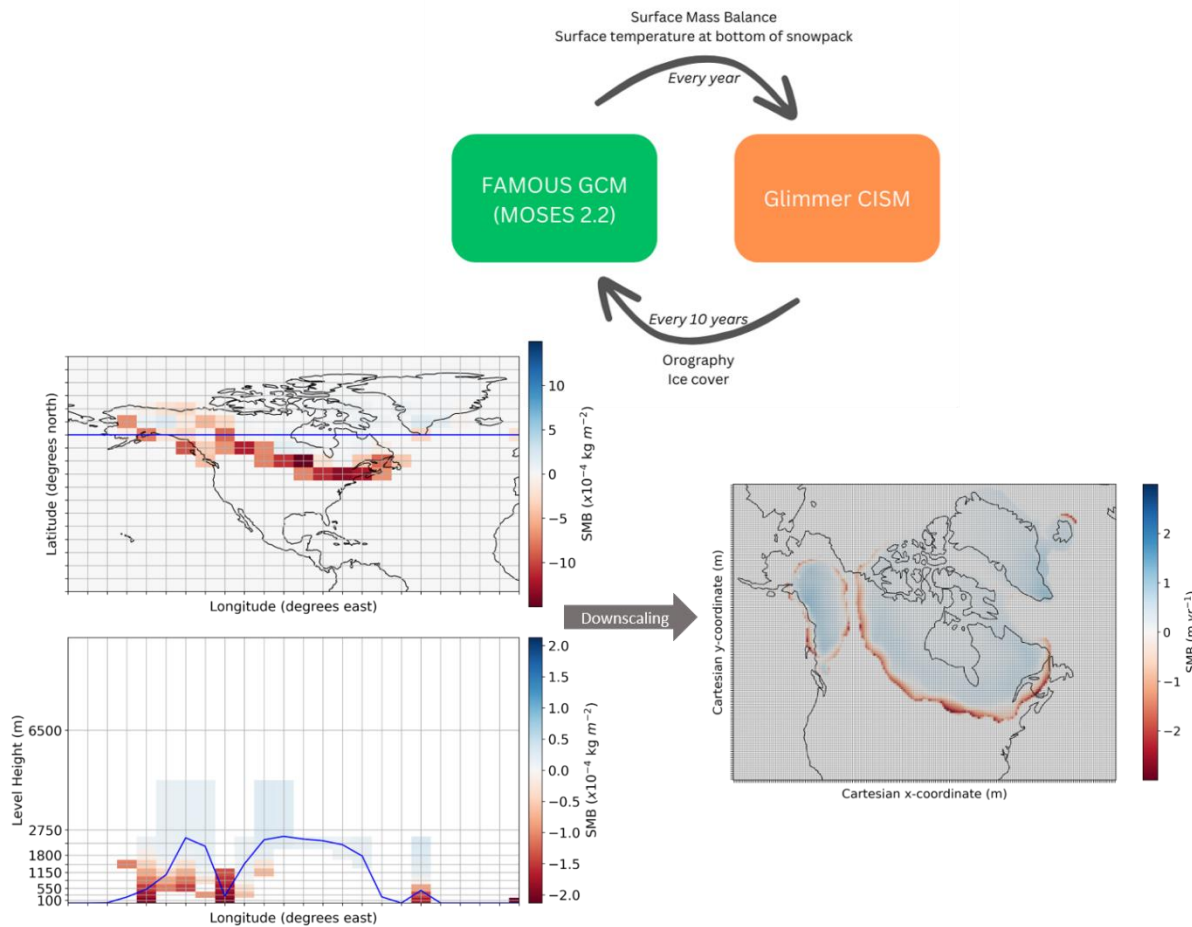
Every 10 years

Orography  
Ice cover



Downscaling





143  
 144 **Figure 1. Schematic illustrating the calculation of SMB along a specific transect across the ice sheet (blue line) at different elevations**  
 145 **on the FAMOUS grid followed by downscaling onto the Glimmer grid.**

146 **2.2 Experiment design**

147 **Our 2.2.1 Climate boundary conditions**

148 With the exception of including dynamic North American and Greenland ice sheets, our FAMOUS-ice simulations are set up  
 149 following the Paleoclimate Modelling Intercomparison Project Phase 4 (PMIP4) protocols for the LGM (Kageyama et al.,  
 150 2017) and PGM (Menviel et al., 2019). These protocols prescribe climatic boundary conditions, including orbital parameters  
 151 and GHG concentrations, the values of which can be found in Table 1. Concentrations of CO<sub>2</sub>, CH<sub>4</sub> and N<sub>2</sub>O are very similar  
 152 between the LGM and PGM but orbital parameters are significantly different. The larger eccentricity at the PGM enhances the  
 153 effect of precession compared to the LGM which affects the seasonal and latitudinal distribution of insolation. These changes

154 are important for ice sheet surface mass balance since melting is particularly sensitive to spring and summer temperatures  
155 (Huybers, 2006; Niu et al., 2019). The PGM received lower insolation in the Northern Hemisphere in late winter to early  
156 summer but higher levels in late summer to early winter, compared to the LGM (Fig. 2a).  
157 Subsequent to the completion of this work, it was discovered that the equation for the role of eccentricity on solar insolation



131— was incorrect in the model code. The magnitude of the error is larger for periods with higher eccentricity values and so a 132 sensitivity test was run to determine the effect this correction has on SMB and ice volume at the PGM. Details of this error 133—and the results of the sensitivity test can be found in Appendix A, but the impact was shown to be minimal (Fig. A1).

134—

135

Table 1. ~~Climatic~~Climatic boundary conditions used in the LGM and PGM experiments as prescribed by the PMIP4 protocols for each 136 period (Kageyama et al., 2017; Menviel et al., 2019).

	<del>Eccentricity</del>	<del>Obliquity</del>	<del>Perihelion</del>	<del>Solar Constant</del>	<del>CO<sub>2</sub></del>	<del>CH<sub>4</sub> (ppb)</del>	<del>N<sub>2</sub>O (ppb)</del>	
		(°)	180 (°)	(Wm <sup>-2</sup> )	(ppm)			
	<u>Eccentricity</u>	<u>Obliquity</u>	<u>Perihelion –</u>	<u>Solar</u>	<u>CO<sub>2</sub></u>	<u>CH<sub>4</sub></u>	<u>N<sub>2</sub>O</u>	<u>Orography and</u>
		(°)	180 (°)	<u>Constant</u>	<u>(ppm)</u>	<u>(ppb)</u>	<u>(ppb)</u>	<u>ice extent</u>
				<u>(Wm<sup>-2</sup>)</u>				
<b>LGM</b>	0.019	22.949	114	1360.7	190	375	200	<u>GLAC-1D</u>
<b>(21 ka)</b>								<u>(Tarasov et al.,</u>
<b>PGM</b>								<u>2012; Briggs et al.,</u>
<b>(140 ka)</b>								<u>2014; Ivanovic et</u>
<b>PGM</b>	0.033	23.414	73	1360.7	191	385	201	<u>al., 2016)</u>
<b>(140 ka)</b>								<u>Combined</u>
								<u>reconstruction</u>
								<u>(Abe-Ouchi et al</u>
								<u>2013; Briggs et al</u>
								<u>2014; Tarasov et al</u>
								<u>2012)</u>

137—

138

In the climate model, the global orography (including the Eurasian and Antarctic ice sheets) and land-sea mask for the LGM are calculated from the ~~139-GLAC1D~~GLAC-1D 21 ka BP reconstruction (Tarasov et al., 2012); Briggs et al., 2014; Ivanovic et al., 2016), which is one of ~~the two options~~three recommendations in the PMIP4 protocol (Kageyama et ~~140-~~al., 2017). For the PGM simulations we used the 140 ka BP combined ~~ice sheet~~ reconstruction (Tarasov et al., 2012; ~~Abe~~Abe-Ouchi et al., 2013; Briggs et al., 2014) detailed in the PGM PMIP4 protocol (Menviel et al., 2019). Vegetation is prescribed

142-based on a pre-industrial distribution and kept constant. As ice cover changes, the fractions of grid cells that are land ice versus  
143-other surface types changes proportionally, altering albedo. However, since there is no dynamical vegetation component, some  
144-important climate-ice-vegetation feedbacks are neglected, which could have a significant impact on ice sheet evolution (Stone 145  
and Lunt, 2013). ~~Sea Surface Temperature (SST) and sea ice concentration is also prescribed and constant and is taken from~~  
Because of the low resolution of the FAMOUS model, using a dynamical ocean and sea ice can introduce large biases in the simulated  
climate (Dentith et al. 2019). 146 HadCM3 simulations of 21 ka BP and 140 ka BP (Figs. B1 and B2). The modelled annual average  
SSTs are cooler at the LGM 147By prescribing Sea Surface Temperature (SST) and sea ice, we are able to limit the amplification of  
climate biases arising from atmosphere-ocean-sea ice interactions. Thus, SSTs and sea ice concentration are also prescribed and  
constant and are taken from higher resolution HadCM3 simulations of 21 ka BP (Fig. B1a; see details in Izumi et al., 2022) and 140  
ka BP (Fig. B1b). The 140 ka BP simulation is part of a suite of simulations covering the last 140,000 years (Allen et al., 2020). It was  
performed using a version of HadCM3 (specifically HadCM3B-M2.1aD, see Valdes et al., (2017), which was the same version as used  
by Izumi et al., (2022) for the LGM and Davies-Barnard et al., (2017)). The simulation was forced with 140 ka BP orbital configuration  
(Berger and Loutre, 1991) and greenhouse gases (Petit et al., 1999; Spahni et al., 2005; Loulergue et al., 2008). Ice sheet forcing and  
land sea mask were from DeBoer et al., (2013) who modelled the evolution of all the major ice sheets. It was run as a “snapshot”  
simulation for 3070 years which allowed the deeper ocean to attain near equilibrium.

FAMOUS atmosphere-ocean GCM has not been run for the PGM, and we lack sufficient data density for precisely dated PGM SSTs  
and sea-ice to produce statistically varied reconstructions, as in Gandy et al., (2023). Thus, for physical consistency between the LGM  
and PGM periods, HadCM3 output was used for the surface ocean boundary conditions. Of all possible options, HadCM3 output is the  
most appropriate choice for this because it is the parent model for FAMOUS; they share the same physics, differing mainly in their  
resolutions, and HadCM3 was used as the tuning target for FAMOUS during model development (Smith et al., 2008). We take the  
multi-year monthly mean “climatology” of SSTs and sea ice concentrations from the final 100 years of the simulations. These 12-  
month climatologies are repeated throughout the duration of the simulations to provide a seasonal forcing with no long-term trend and  
no interannual variability.

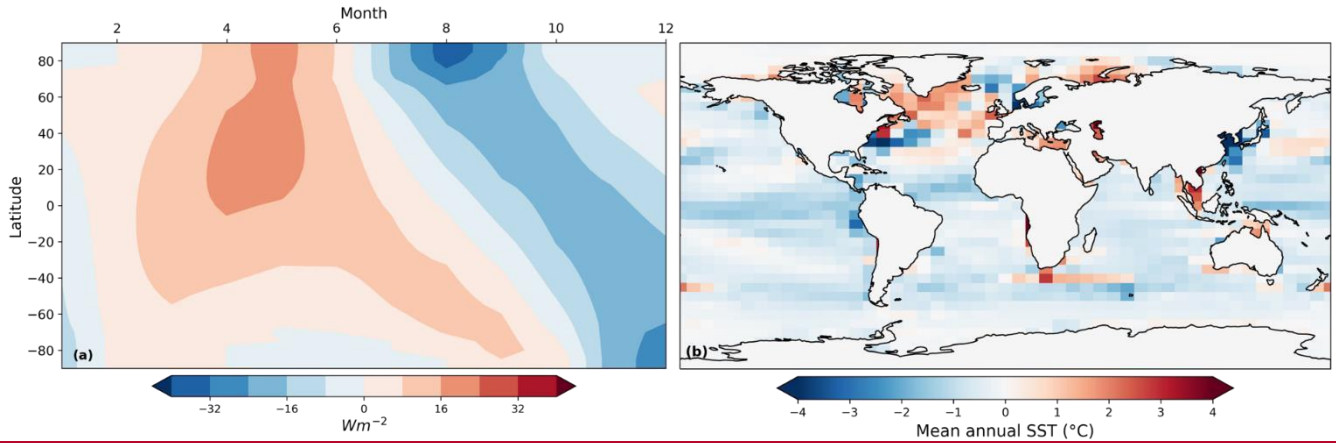
The modelled annual average SSTs are cooler at the LGM than at the PGM, everywhere, except in the North Atlantic due to less sea  
ice cover in this region (Fig. 2b). However, the 148-summer SSTs are warmer in the ~~NH~~Northern Hemisphere at the LGM compared  
to the PGM. ~~The decision to use these constant SST and sea ice 149 fields, rather than a statistical reconstruction as in Gandy et al.,~~  
(2023), was made due to the lack of both empirical and modelled 150 PGM SST data available to produce an equivalent reconstruction.  
(Fig. 2c). The HadCM3 LGM SSTs are colder on average than the reconstruction in Gandy et al., (2023), with the largest differences,  
of up to 6 °C, occurring in the tropics and mid-latitudes (Fig. B1c).

151 reconstruction in Gandy et al., (2023), with the largest differences, of up to 6 °C, seen in the tropics and mid-latitudes. This 152  
may introduce another source of uncertainty in the simulations. In the ice sheet model, we use the same ice sheet domain and 153 initial

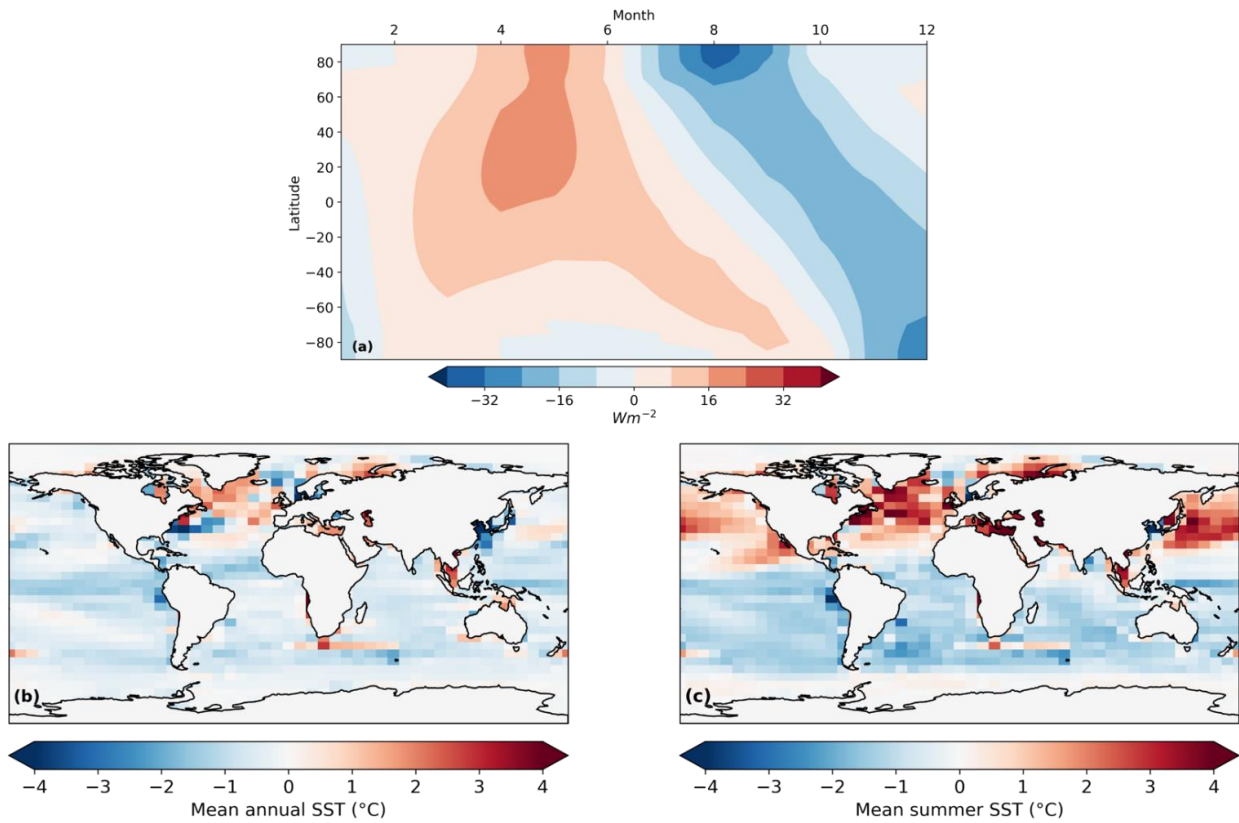
condition for the LGM and PGM, which is the same as used in Gandy et al., (2023). The interactive ice sheet model domain in Glimmer covers North America and Greenland, and the initial ice sheet extent, thickness and bedrock elevation is 155 from a previous Last Deglaciation ensemble of the NAIS, at 18.2 ka BP (Gregoire et al., 2016). This is a smaller intermediate

156  
157  
158

(MIS 3 like) ice sheet which is used as an approximate pre-glacial maximum extent from which to grow the ice sheet towards an equilibrium ice volume.



159



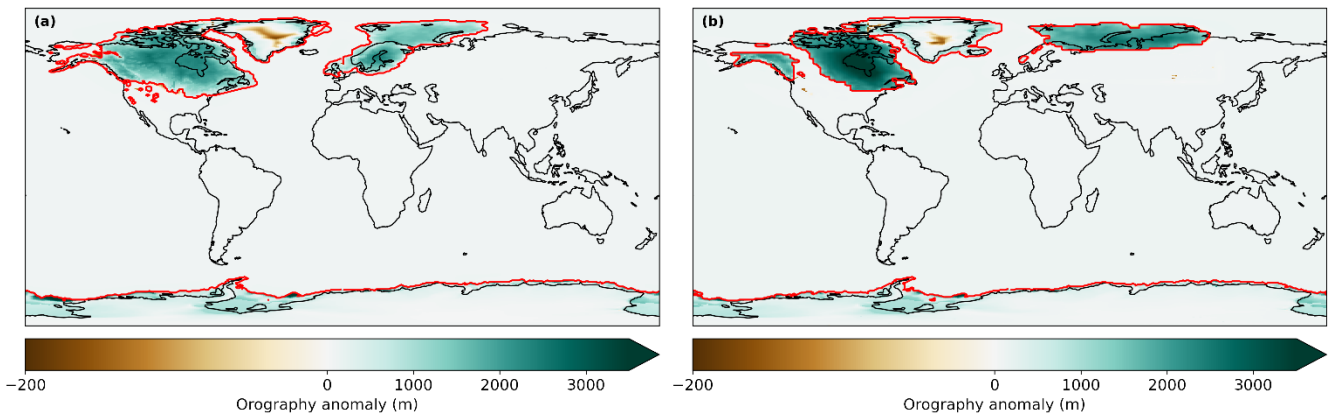
160

161 **Figure 2. Difference between the LGM and PGM (a) latitudinal distribution of incoming top of the atmosphere shortwave radiation**  
162 **each month, ~~and~~ (b) modelled annual sea surface temperatures, ~~and~~ (c) modelled summer (JJA) sea surface temperatures.**

### 163 2.2.2 Ice sheet boundary and initial conditions

164 In all our simulations, the ice sheet extent is set to the PMIP4 boundary conditions for the LGM and PGM as described in Table  
165 1, except in the interactive ice sheet model domain, which covers North America and Greenland. Here, we describe how the  
166 ice extent and elevation is initialised in FAMOUS and Glimmer over the interactive domain in our ensemble of PGM and LGM  
167 simulations and sensitivity experiments.

168 In our ensemble of LGM and PGM simulations, Glimmer is initiated from an 18.2 ka BP NAIS taken from a previous Last  
169 Deglaciation ensemble (Gregoire et al., 2016). This smaller intermediate (MIS 3-like) ice sheet was used in Gandy et al., (2023)  
170 as an approximate pre-glacial maximum extent from which to grow the ice sheet towards an equilibrium ice volume. For  
171 consistency, we used the same initial ice sheet conditions as in Gandy et al. (2023) when running our ensembles of LGM and  
172 PGM simulations. The coupling between the models passes this orography field from Glimmer to FAMOUS, updating the  
173 PMIP4 boundary condition that FAMOUS was initiated from. However, due to the technical formulation of the coupling, where  
174 entire gridboxes were initialised as covered in ice at all elevations in FAMOUS, the tiles in such gridboxes would not  
175 subsequently update to reflect the existence of any non-glaciated fractions that might exist in the Glimmer state. This means  
176 that when the initial conditions are radically different in FAMOUS and Glimmer (as in our ensemble of simulations), the  
177 FAMOUS ice extent over the North American continent is not updated to match the Glimmer initial conditions. Thus, in our  
178 ensemble of LGM simulations, the albedo remains high throughout the saddle region (the area between the Laurentide and  
179 Cordilleran ice sheets) because the FAMOUS ice extent remains as large as the atmospheric model's initial conditions (i.e. the  
180 GLAC-1D 21 ka BP reconstruction) for the duration of the simulations (Fig. 3). The different ice sheet configurations used in  
181 FAMOUS and Glimmer in the ensembles, are outlined in our table of experiments, Table 2 (experiments 1 and 2). The impact  
182 of this set-up compared to an ice sheet configuration matched in FAMOUS and Glimmer is explored in Sect. 3.2 and Appendix  
183 C.



185  
186 **Figure 3. Topography anomaly from present day used as the initial condition in FAMOUS and the ice masks (red lines) for (a) the**  
187 **LGM and (b) the PGM.**

188 We perform two sets of sensitivity experiments to understand the relative impact of the initial ice sheet conditions and the  
189 climate forcing on the resulting LGM and PGM NAIS volumes. The first set of experiments uses matching ice sheet  
190 configurations in FAMOUS and Glimmer, set either to the LGM GLAC-1D reconstruction or to the end of one of our PGM  
191 coupled simulations (Table 2; experiments 3 – 6). The second set uses the same initial ice sheet configurations as in the  
192 ensemble, i.e. GLAC-1D and PMIP4 reconstructions in FAMOUS and the 18.2 ka ice sheet in Glimmer (Table 2; experiments  
193 7 - 10). A full description of the initial conditions and methods used in these sensitivity experiments can be found in Sect. 2.5.  
194

195 Table 2. Table of experiments performed in this study detailing the ‘climate forcing’ (orbital configuration, trace gases and global  
 196 orography as outlined in Table 1 and SSTs/sea ice from HadCM3), initial ice extent set in FAMOUS over Greenland and North  
 197 America, initial Glimmer ice sheet conditions and input parameter values. NROY are the simulations that are ‘Not Ruled Out Yet’  
 198 after applying the implausibility metric described in Sect. 2.4.

<u>Experiments</u>	<u>Climate forcing</u>	<u>FAMOUS initial ice extent</u>	<u>Glimmer initial condition</u>	<u>Input parameter values</u>
<u>1) LGM ensemble</u>	<u>LGM</u>	<u>PMIP4 LGM (GLAC-1D)</u>	<u>18.2 ka ice sheet</u>	<u>Randomly sampled from Table 3 ranges (See Sect. 2.3)</u>
<u>2) PGM ensemble</u>	<u>PGM</u>	<u>PMIP4 PGM</u>	<u>18.2 ka ice sheet</u>	<u>Randomly sampled from Table 3 ranges (See Sect. 2.3)</u>
<u>3) <math>V_{i1}</math> (full LGM)</u>	<u>LGM</u>	<u>PMIP4 LGM (GLAC-1D)</u>	<u>PMIP4 LGM GLAC-1D</u>	<u>Matching NROYa simulation</u>
<u>4) <math>V_{e1}</math></u>	<u>PGM</u>	<u>PMIP4 LGM (GLAC-1D)</u>	<u>PMIP4 LGM GLAC-1D</u>	<u>xpken/xpkyn (See Sect. 2.4 and 3.1)</u>
<u>5) <math>V_{i1}</math></u>	<u>LGM</u>	<u>PGM NROYa (xpkyn)</u>	<u>PGM NROYa (xpkyn)</u>	
<u>6) <math>V_{e1}</math> (full PGM)</u>	<u>PGM</u>	<u>PGM NROYa (xpkyn)</u>	<u>PGM NROYa (xpkyn)</u>	
<u>7) <math>V_{i2}</math> (NROYa LGM)</u>	<u>LGM</u>	<u>PMIP4 LGM (GLAC-1D)</u>	<u>18.2 ka ice sheet</u>	
<u>8) <math>V_{e2}</math></u>	<u>PGM</u>	<u>PMIP4 LGM (GLAC-1D)</u>	<u>18.2 ka ice sheet</u>	
<u>9) <math>V_{i2}</math></u>	<u>LGM</u>	<u>PMIP4 PGM</u>	<u>18.2 ka ice sheet</u>	
<u>10) <math>V_{e2}</math> (NROYa PGM)</u>	<u>PGM</u>	<u>PMIP4 PGM</u>	<u>18.2 ka ice sheet</u>	

### 2.3 Ensemble design

201 The ensemble by Gandy et al., (2023) showed that uncertainty in parameters controlling SMB, ice sheet dynamics and climatic  
 202 conditions over the ice sheets had a significant influence on the extent and volume of the LGM NAIS, with albedo parameters  
 203 explaining the majority of the variation in model output. Since these parameters needed re-tuning from simulations of the  
 204 present day Greenland ice sheet to produce an acceptable LGM NAIS configuration in FAMOUS-ice under LGM climate  
 205 conditions, the PGM may also show different sensitivities to the uncertain parameters. Therefore, we ~~run~~ ran new ensembles of  
 206 the LGM and PGM in order to ~~quantify~~ explore uncertainties and identify combinations of climate and ice sheet parameters that  
 207 perform well for both periods.

208 Following on from Gandy et al., (2023), a second wave of simulations was performed and compared to reconstructions of ice  
 209 sheet extent and volume to identify ‘Not Ruled Out Yet’ (NROY) parameter combinations (see methodology in Appendix ED),  
 210 the results of which formed the basis of the ensemble design in this study. We reran the LGM ensemble to allow for slight

211 changes in the experiment design compared to Gandy et al., (2023): we use orbital parameters for 21 ka BP rather than 23 ka  
212 BP and HadCM3 SSTs instead of a statistical reconstruction (see Sect. 2.2.1). Table 23 details the 13 parameters that were  
213 varied in these simulations. Out of the 176 NROY parameter combinations from the Wave 2, a representative subset of 62 were  
214 selected which provided adequate coverage of the NROY space (see Appendix CD for details). Each was run for 1000 climate  
215 years (10,000 ice sheet years) for both the LGM and PGM set-upexperiments until the majority of the ice sheet ~~has~~ reached  
216 close to equilibrium. Despite differences in the model set up between this study and Gandy et al., (2023), we expect the 62  
217 samples chosen from their design to be a good estimate to an optimal parameter design for our set-upexperiment design  
218 (Appendix C-D).



Table 23. Description of parameters varied in the ensembles. Adapted from Gandy et al., (2023).

**Parameter** — **Description**

<u>Parameter</u>	<u>Range</u>	<u>Description</u>
<i>Lapse Rate</i>	<u>-0.01 – -0.002</u> <u>K km<sup>-1</sup></u>	Prescribed lapse rate for air temperature used to downscale FAMOUS near-surface ice sheet climate onto surface elevation tiles. <u>Downwelling</u> Downwelling longwave radiation is also adjusted for consistency. <u>More negative values lead to stronger lapse rate effects (Smith et al., 2021).</u>
<del><i>Daice</i></del>		
<del><i>Rho</i></del>		
<del><i>AV_GR</i></del>		
<del><i>RHerit</i></del>		
<del><i>VFI</i></del>		
<del><i>CT</i></del>		
<del><i>CW</i></del>		
<del><i>Entrainment</i></del>		
<del><i>Coefficient</i></del>		
<del><i>Alpham</i></del>		
<del><i>Basal Sliding</i></del>		
<del><i>Mantle</i></del>		
<del><i>Relaxation Time</i></del>		
<del><i>Flow</i></del>		
<del><i>Enhancement</i></del>		
<del><i>Factor</i></del>		
<u><i>Daice</i></u>	<u>-0.4 - 0 K<sup>-1</sup></u>	Sensitivity of bare-ice albedo to surface air temperatures once the surface is in a melt regime. <u>Albedo reduced to as low as 0.15 with minimum value (Smith et al., 2021)</u>

<u><i>F<sub>snow</sub></i></u>	<u>350 – 800 kg m<sup>-3</sup></u>	The threshold in surface snow density at which the FAMOUS albedo scheme switches from a scattering paradigm appropriate for a conglomeration of snow grains to one more appropriate for a solid surface. <u>Higher values correspond to using brighter albedos for denser snow, increasing ice sheet albedo (Smith et al., 2021)</u>
<u><i>AV<sub>GR</sub></i></u>	<u>0 – 0.01 μ m<sup>-1</sup></u>	Sensitivity of the snow albedo to variation in surface grain size. <u>Higher values enhance the darkening of snow over time, decreasing the albedo (Smith et al., 2021).</u>
<u><i>RH<sub>crit</sub></i></u>	<u>0.6 - 0.9 Pa<sup>-1</sup></u>	The threshold of relative humidity for cloud formation (R. Smith, 1990). A higher value means clouds can form less easily.
<u><i>VF<sub>I</sub></i></u>	<u>1 – 2 m s<sup>-1</sup></u>	The precipitating ice fall-out speed (Heymsfield, 1977).
<u><i>CT</i></u>	<u>5x10<sup>-5</sup> - 4x10<sup>-4</sup> s<sup>-1</sup></u>	The conversion rate of cloud liquid water droplets to precipitation (R. Smith, 1990).
<u><i>CW</i></u>	<u>1x10<sup>-4</sup> – 2x10<sup>-3</sup> kg m<sup>-3</sup></u>	The threshold values of cloud liquid water for formation of precipitation (R. Smith, 1990). Only the value for the land is varied.
<u><i>Entrainment Coefficient</i></u>	<u>1.5 - 6</u>	<del>Convection Scales rate</del> <u>Rate</u> of mixing between environmental air and convective plume. <u>Higher values enhance mixing of convective plumes with ambient dry air.</u>
<u><i>Alpham</i></u>	<u>0.2 - 0.65</u>	The sea ice <del>low</del> <u>lowest</u> albedo (Crossley & Roberts, 1995).
<u><i>Basal Sliding</i></u>	<u>0.5 - 20 mm yr<sup>-1</sup></u>	The basal sliding rate. A higher value allows increased ice velocity.
<u><i>Mantle Relaxation Time</i></u>	<u>300 – 9000 yrs</u>	The relaxation time of the mantle, a lower value <del>essentially</del> making the mantle less viscous, thus allowing a quicker topographic rebound.
<u><i>Flow Enhancement Factor</i></u>	<u>1 - 10</u>	<del>The softness of ice.</del> <u>Glen's Flow Law enhancement factor.</u> Increasing the factor makes the ice softer and more deformable (Rutt et al., 2009).

## 2.4 Implausibility criteria

To filter out implausible ice sheet configurations in the results, a set of constraints, based on southern ice sheet extent and volume, were applied to the LGM ensemble. Both ensembles were filtered based on the LGM results since the extent of the NAIS is very well constrained by geological data and there are more estimates of ice volume for the LGM than the PGM. This is because there is a lack of empirical data (over both space and time) on ice

sheet configuration at the PGM due to destruction of evidence by subsequent glaciations and difficulties with dating what is available (Parker et al., 2022). Thus, most of the reconstructions of NAIS PGM extent are actually the maximum extent reached over the whole of MIS 6 (190-132 ka BP) and are mostly based on numerical modelling combined with this scarce proxy data (e.g. Colleoni et al., 2016; Batchelor et al., 2019). This leaves a set of plausible or 'Not Ruled Out Yet' (NROY) LGM simulations that can then be compared to the corresponding PGM simulations to determine whether parameters that performed well for the LGM also give plausible PGM results. LGM ice extent was assessed against the reconstruction by Dalton et al. (2020). We focus our evaluation of ice extent on the southern NAIS area and chose to disregard regions of known model bias. This includes marine margins that are subject to processes not included in Glimmer and the Alaskan regions where small climate model biases lead to ice sheet overgrowth (e.g. Ganopolski et al., 2010; Ziemen et al., 2014; Gregoire et al. 2016, Sherriff-Tadano et al., 2023). Additionally, ice lobes are not well captured in many models as they are likely to be transient, short-lived features that may be caused by complex ice dynamics (e.g. Zweck and Huybrechts, 2005). Therefore, we do not expect our simulations to perfectly match the reconstructed Southern NAIS extent. To account for the expected mismatch between model and data, we applied a tolerance on the Southern ice sheet area of  $1.79 \times 10^6 \text{ km}^2$ , equivalent to three-times the area of the lobes (Fig. 4). We thus calculate the Southern NAIS ice area as the integrated area within the large box shown in Fig. 4 at the end of each LGM simulation and selected simulations that matched the reconstructed area from Dalton et al. (2020) within plus or minus  $1.79 \times 10^6 \text{ km}^2$ . The volume of the NAIS is not as well constrained by proxy data and so estimates rely on ice sheet, glacial isostatic adjustment and sea level modelling studies. Based on a number of these studies (Marshall et al., 2002; Tarasov and Peltier, 2002; 2004; Tarasov et al., 2012; Lambeck et al., 2014; Peltier et al., 2015; Rohling et al., 2017; Batchelor et al., 2019; Gowan et al., 2021), a minimum NAIS (including Greenland) volume of 70 m SLE ( $2.8 \times 10^7 \text{ km}^3$ ) was applied to the ensemble. The translation of ice volumes into meters of sea level equivalent are calculated based on present day ocean area.

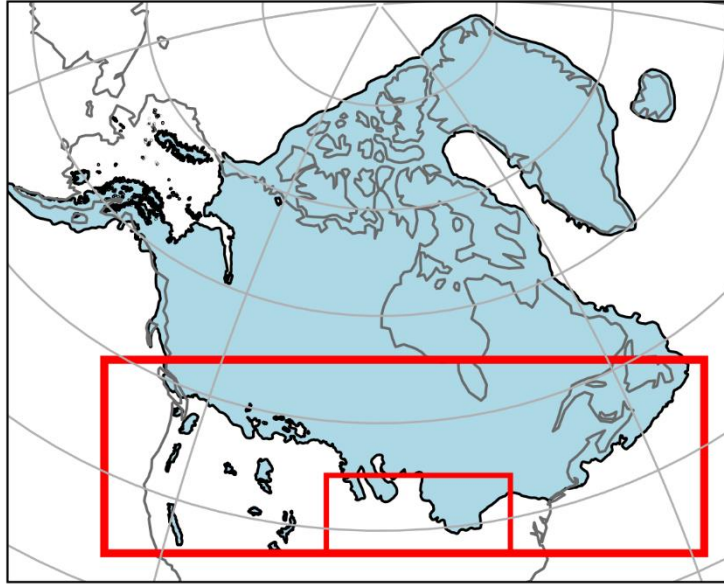


Figure 4. Outline of the LGM North American Ice Sheet by Dalton et al. (2020). The large red box shows the region used to calculate reconstructed and modelled Southern NAIS area. The small red box shows the region used to calculate the area of the lobes from which we set the upper and lower target bounds for southern ice extent (See Sect. 2.4).

## 2.5 Sensitivity analysis

We choose one of the resulting NROY parameter combinations, NROYa (specifically experiments xpken/xpkyn), which has LGM and PGM ice volumes lying in the middle of estimated ranges and the least excess ice growth over Alaska, to investigate the relative impact of the initial conditions versus the climate on the resulting ice sheet configurations. This is achieved through a sensitivity analysis along with factorisation based on the method used in Lunt et al., (2012) and Gregoire et al. (2015). We divided the differences in inputs between LGM and PGM into two factors; the initial ice sheet configurations used in FAMOUS and Glimmer and the climate boundary conditions (orbital parameters, greenhouse gases and SSTs/sea ice). Thus, the total difference in final ice volume ( $\Delta V$ ) between the LGM and the PGM can be written as Eq. (1):

$$\Delta V = dV_{ice} + dV_{climate} \tag{1}$$

where  $dV_{ice}$  is the difference in final ice volume due to the different initial ice sheet configurations and  $dV_{climate}$  is the difference due to the difference climate boundary conditions used.

The factorisation method requires  $2^N$  simulations (where N is the number of different components) to determine the contribution of each component to ice volume difference, therefore  $2^2 = 4$  experiments are needed that systematically change one variable. These experiments are listed in Table 2. The relative contributions of the initial conditions and climate can be calculated by Eqs. (2) and (3):

$$dV_{ice} = \frac{1}{2}((V_i - V) + (V_{ci} - V_c)),$$

(2)

$$dV_{climate} = \frac{1}{2}((V_c - V) + (V_{ci} - V_i)),$$

(3)

To properly understand the effect of the initial conditions, we performed two sets of sensitivity experiments. In the first set, labelled  $V_i$ ,  $V_c$ ,  $V_{i-1}$  and  $V_{c-1}$  (Table 2; experiments 3 – 6), both the topography and ice cover are set to be consistent between the climate and ice sheet model components. Specifically, for the LGM, the Glimmer initial bedrock topography and ice surface elevation was prescribed from the GLAC-1D reconstruction used in the FAMOUS LGM boundary condition.

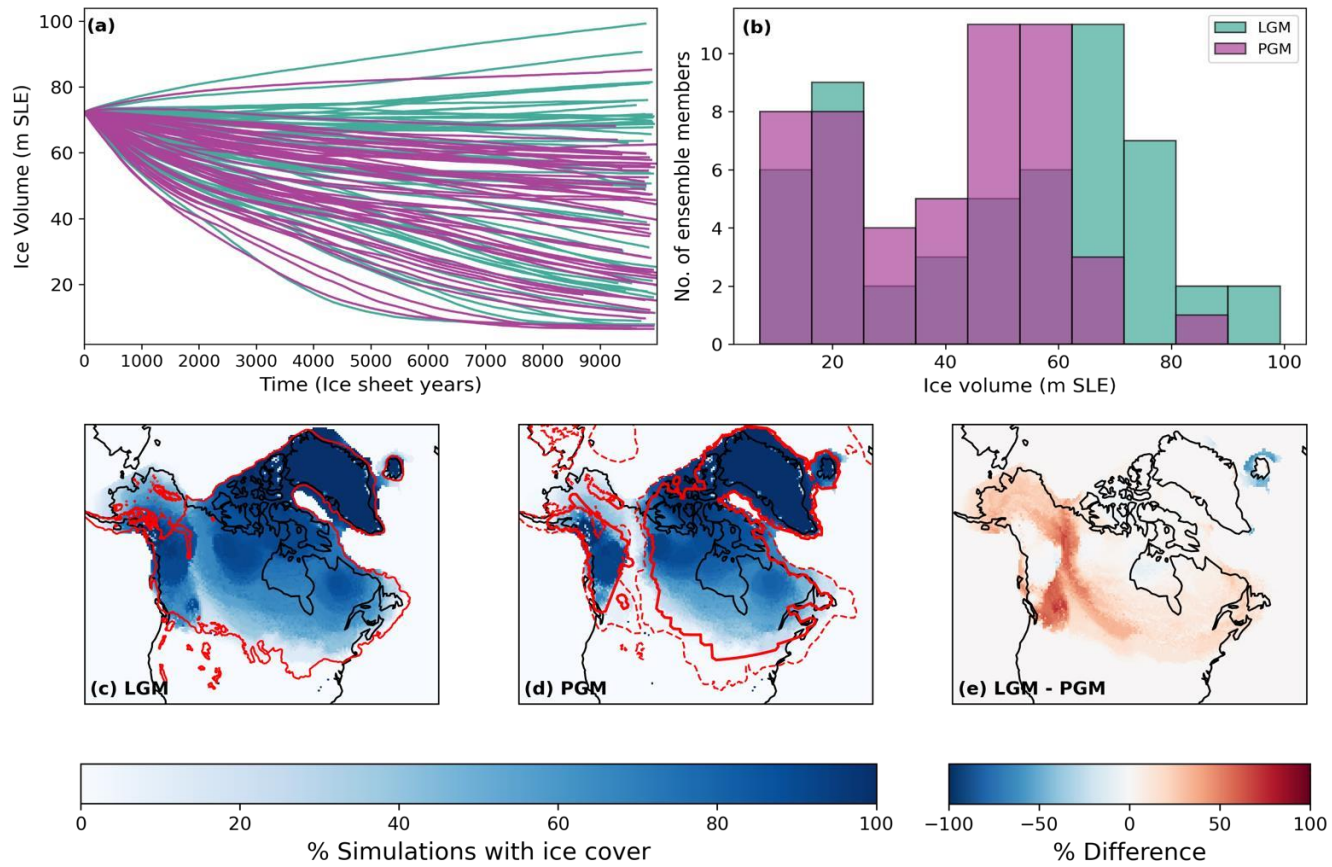
181 For the PGM, the ice thickness data needed for the PMIP4 reconstruction to be converted to the Glimmer initial condition were  
182 not available. Instead, both Glimmer and FAMOUS were initialised with the final timestep of the NROYa PGM (xpkyn)  
183 experiment since it closely resembles the PMIP4 reconstruction. Experiment  $V_{i_1}$  corresponds to a full LGM simulation and  
184  $V_{ci_1}$  corresponds to a full PGM simulation. In the second set of sensitivity experiments, we use the initial Glimmer ice sheet  
185 used in the ensembles, i.e. the 18.2 ka mid-size ice sheet, only varying the FAMOUS initial ice sheets to see how this difference  
186 in orography between the climate and ice sheet models may have impacted the result. These experiments are labelled  $V_{i_2}$ ,  $V_{c_2}$ ,  
187  $V_{i_2}$  and  $V_{ci_2}$  (Table 2: experiments 7 – 10), with  $V_{i_2}$  corresponding to the LGM NROYa (xpken) and  $V_{ci_2}$  corresponding to  
188 the PGM NROYa (xpkyn).

### 189 **3 Results ~~and discussion~~**

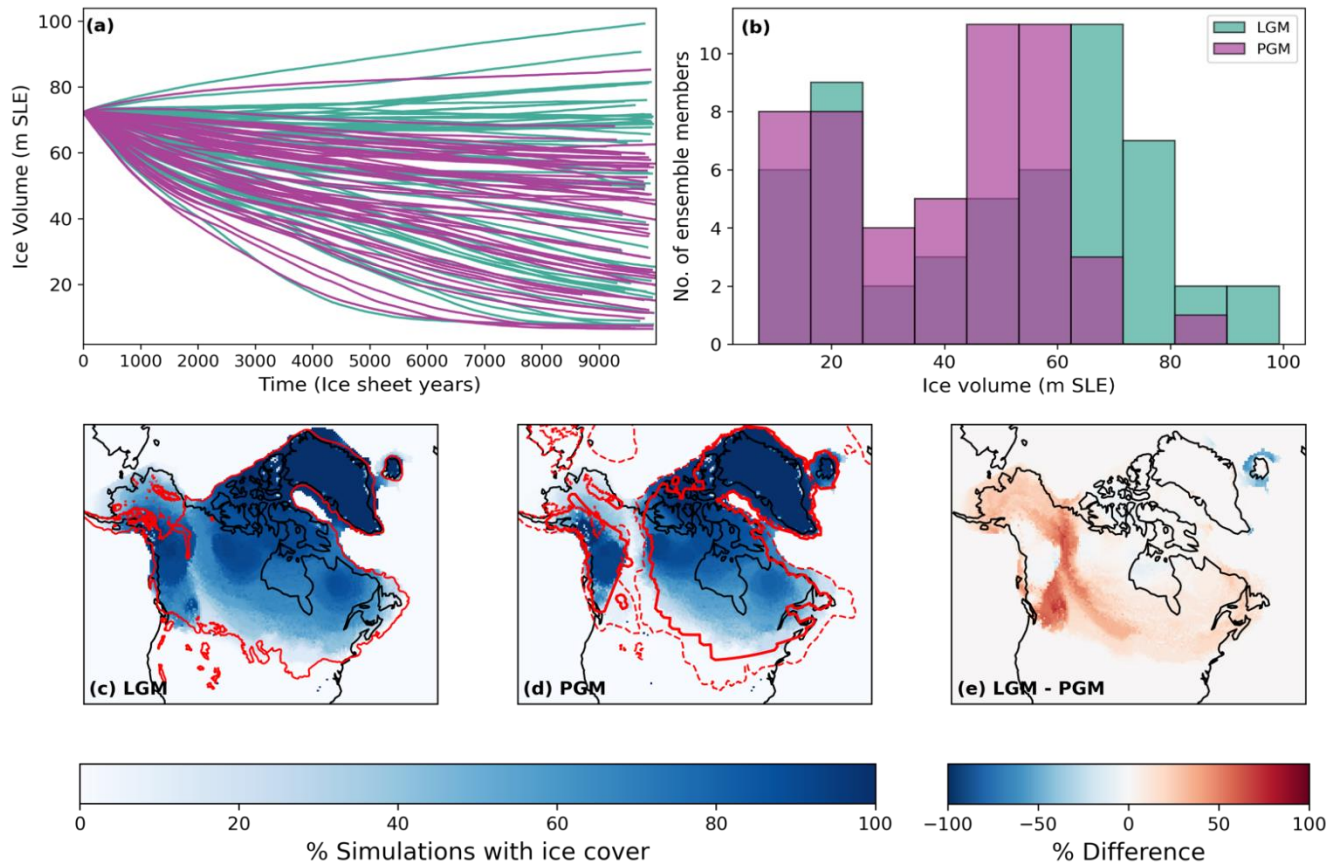
#### 190 **3.1 Ensembles**

##### 191 **3.1.1. Unconstrained ensembles**

192 Our ensembles of 62 North American Ice Sheet configurations spans uncertainty in model parameters and reveals the wide  
193 range of possible modelled ice sheet evolutions. Over the full ensembles, we find that the set-up of the original Wave 2 meant  
194 that the albedo values were too high and so the use of more realistic albedos in these ensembles led to many of the runs  
195 deglaciating to very low volumes as shown in Fig. 35 (see Appendix [ED](#) for more detail).



197  
198



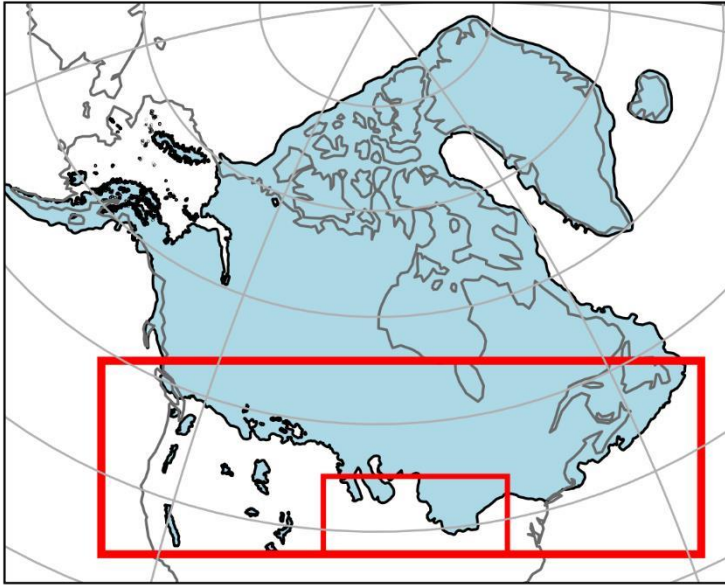
199  
 200 **Figure 35.** (a) Ice volume evolution over modelled time, and (b) density distribution of final ice volumes for the full LGM and PGM  
 201 ensembles. Percentage of simulations with ice cover for (c) LGM (with the Dalton et al., (2020) reconstructed margin shown in red);  
 202 (d) PGM (with the PMIP4 PGM modelled margin shown in solid red and the Batchelor et al., (2019) reconstructed maximum MIS 6  
 203 margin shown in dashed red), and (e) the difference between the LGM and PGM, at the end of the simulations.

### 204 **3.1.2. Constrained ensembles**

205 ~~To filter out implausible ice sheet configurations in the results, a set of constraints, based on southern ice sheet extent and~~  
 206 ~~volume, were applied to the LGM ensemble. Both ensembles were filtered based on the LGM results since the extent of the~~  
 207 ~~NAIS is very well constrained by geological data and there are more estimates of ice volume for the LGM than the PGM. This~~  
 208 ~~is because there is a lack of empirical data (over both space and time) on ice sheet configuration at the PGM due to destruction~~  
 209 ~~by subsequent glaciations and difficulties with dating what is available (Parker et al., 2022). Thus, most of the reconstructions~~  
 210 ~~of NAIS extent for this period are actually the maximum extent over the whole of MIS 6 (190-132 ka BP) and are mostly based~~



211 ~~on numerical modelling combined with this scarce proxy data (e.g. Colleoni et al., 2016; Batchelor et al., 2019). The NROY~~  
212 ~~LGM results can then be compared to the corresponding PGM results to advance understanding of the differences that occurred~~  
213 ~~and reveal whether parameters that performed well for the LGM also give plausible PGM results. Ice extent was assessed~~  
214 ~~against the reconstruction by Dalton et al. (2020). We focus our evaluation of ice extent on the southern NAIS area and chose~~  
215 ~~to disregard regions of known model bias. This includes marine margins that are subject to processes not included in Glimmer~~  
216 ~~and the Alaskan regions where small climate model biases lead to ice sheet overgrowth (e.g. Ganopolski et al., 2010; Gregoire~~  
217 ~~et al. 2016, Sherriff-Tadano et al., 2023). Additionally, ice lobes are not well captured in many models so we do not expect~~  
218 ~~our simulations to perfectly match the reconstructed Southern NAIS extent. To account for this, we applied a tolerance on the~~  
219 ~~Southern ice sheet area of  $1.79 \times 10^6 \text{ km}^2$ , equivalent to 3 times the area of the lobes (Fig. 4). We thus calculate the Southern~~  
220 ~~NAIS ice area as the integrated area within the large box shown in Fig. 4 at the end of each LGM simulation and selected~~  
221 ~~simulations that matched the reconstructed area from Dalton et al. (2020) within plus or minus  $1.79 \times 10^6 \text{ km}^2$ . The volume of~~  
222 ~~the NAIS is not as well constrained by proxy data and so estimates rely on ice sheet, glacial isostatic adjustment and sea level~~  
223 ~~modelling studies. Based on a number of these studies, a minimum NAIS (including Greenland) volume of 70 m SLE ( $2.8 \times$~~   
224  ~~$10^7 \text{ km}^3$ ) was applied to the ensemble (Marshall et al., 2002; Tarasov and Peltier, 2002; 2004; Tarasov et al., 2012; Lambeck~~  
225 ~~et al., 2014; Peltier et al., 2015; Rohling et al., 2017; Batchelor et al., 2019; Cowan et al., 2021). The volumes in meters sea~~  
226 ~~level equivalent are calculated based on present day ocean area.~~



217  
 218 **Figure 4.** Outline of the LGM North American Ice Sheet by Dalton et al. (2020). **The large red box shows the region we use to**  
 219 **calculate reconstructed and modelled Southern NAIS area. The small red box shows the region used to calculate the area of the**  
 220 **lobes for setting as the upper and lower target bounds.**

221 **Table 34.** Average volumes (NAIS + Greenland) and southern NAIS areas and their standard deviations (SD) of the NROY LGM and  
 222 PGM simulations. Also shown are estimated values from literature for comparison.

223

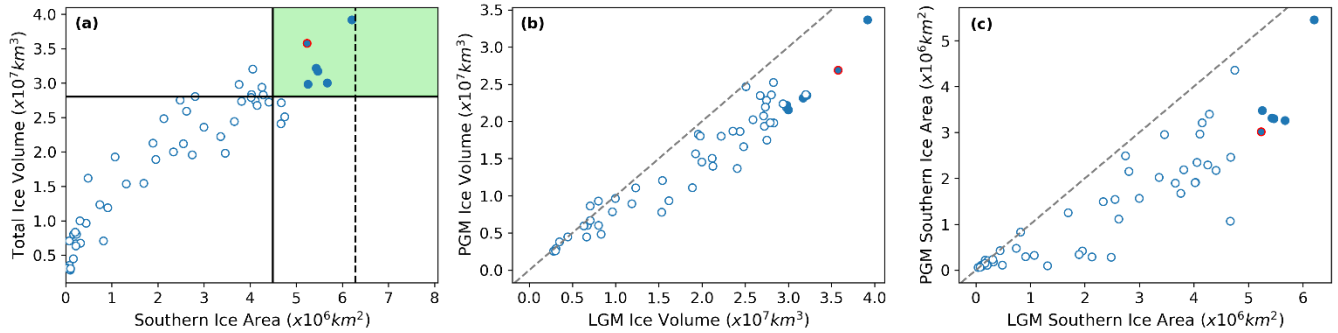
	<u>Mean Total Volume</u> <u>(SD), m SLE</u>	<u>Estimated Total Volume,</u> <u>m SLE</u>	<u>Mean Southern Area</u> <u>(SD), x 10<sup>6</sup> km<sup>2</sup></u>	<u>Estimated Southern</u> <u>Area, x 10<sup>6</sup> km<sup>2</sup></u>
	<u>Mean Total Volume</u> <u>(SD), m SLE</u>	<u>Estimated Total Volume,</u> <u>m SLE</u>	<u>Mean Southern Area</u> <u>(SD), x 10<sup>6</sup> km<sup>2</sup></u>	<u>Estimated Southern</u> <u>Area, x 10<sup>6</sup> km<sup>2</sup></u>
<b><i>LGM</i></b>	82.1 (8.29)	61-98 (Rohling et al., 2017)	5.55 (0.33)	6.28 (Dalton et al., 2020)
<b><i>PGM</i></b>				
<b><i>PGM</i></b>	62.3 (10.3)	49-69 (Rohling et al., 2017)	3.64 (0.82)	3.32 (Menviel et al., 2019)

224

225

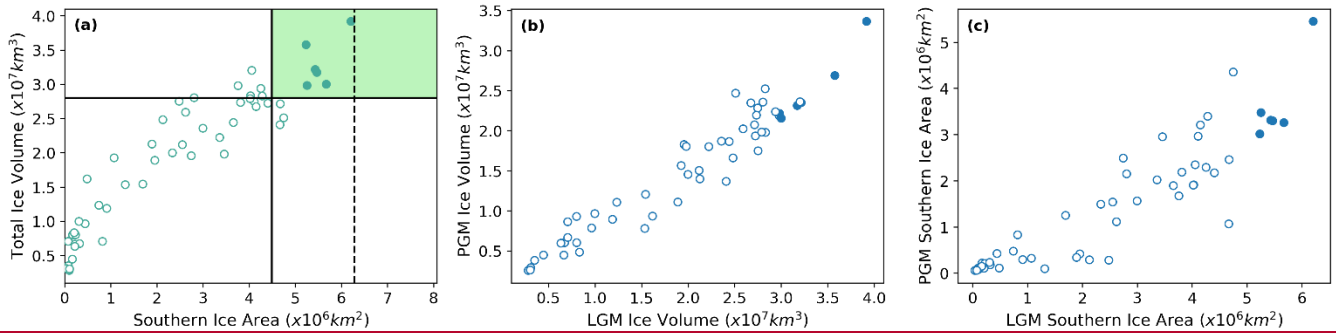
After applying our ~~metric constraints,~~implausibility criteria (Sect. 2.4), six non-implausible or NROY LGM simulations remained. Table 34 gives the average ~~226~~ volumes and areas of these six simulations and the corresponding six PGM ice sheets compared to estimated values from ~~227~~ empirical and model data. All six LGM simulations show an overgrowth of ice in Alaska of varying magnitudes, as a result of ~~228~~ the previously mentioned climate model bias. However, in other regions the simulations display a very similar ice extent, with ~~229~~ the southern area only varying by  $9.7 \times 10^5 \text{ km}^2$ . None of the simulations form ice lobes, as expected, but they do show a close match ~~230~~ to reconstructed ice extent in our target area, although towards the lower end of the plausible range, and in the marine regions (Fig. 6a and 7a). There is a minimum ice volume of 73.9 m

231 SLE and a maximum of 97.1 m SLE. The maximum ice thickness varies by around 300 m but the overall shapes of the ice sheets  
 232 remain the same, with the thickest ice towards the east of the ice sheet over Hudson Bay.



234 **Figure 6. (a) The relationship between final ice volume and southern area for the LGM ensemble, and the relationship between the LGM**  
 235 **and PGM (b) final ice volume, and (c) final southern areas. The filled in blue dots represent the six NROY LGM simulations and the solid**  
 236 **lines on panel (a) show the minimum volume and area constraints applied to the ensemble. The ensemble member chosen as NROYa is**  
 237 **outlined in red (Sect 2.5).**

238 All the PGM ice sheets were smaller in volume than their LGM counterpart (Figs. 56 and 67) and displayed a smaller extent in the  
 239 southern margin and the saddle region between the western Cordilleran Ice Sheet and eastern Laurentide Ice Sheet. However, the  
 240 PGM simulations also displayed more variability in their ice extent and volumes. The ice volumes range from 53.4 m SLE to 83.37  
 241 m SLE and the southern extent varies by  $2.44 \times 10^6 \text{ km}^2$ . The range in maximum ice thickness is also over double the LGM, varying  
 242 by around 613 m. These PGM configurations also look plausible compared to the less well constrained extent data available,  
 243 including previous empirical and modelled reconstructions of the PGM/MIS 6 extent (Menviel et al., 2019; Batchelor et al., 2019;  
 244 Fig. 6b7b). For example, all the simulations maintain an ice-free corridor between the Laurentide and Cordilleran ice sheets which  
 245 is a common feature in these PGM reconstructions. In addition, the excess Alaskan ice seen in LGM simulations is also present at  
 246 the PGM, however the growth is not as excessive. ~~We therefore conclude that in our model, based on the available empirical~~  
 247 ~~constraints, parameters that produce a good LGM NAIS also produce a plausible PGM NAIS using PGM boundary and initial~~  
 248 ~~conditions (orbital parameters, SSTs and orography). Our simulations can thus be compared and analysed to understand the causes~~  
 249 ~~of the different configurations between the two periods.~~

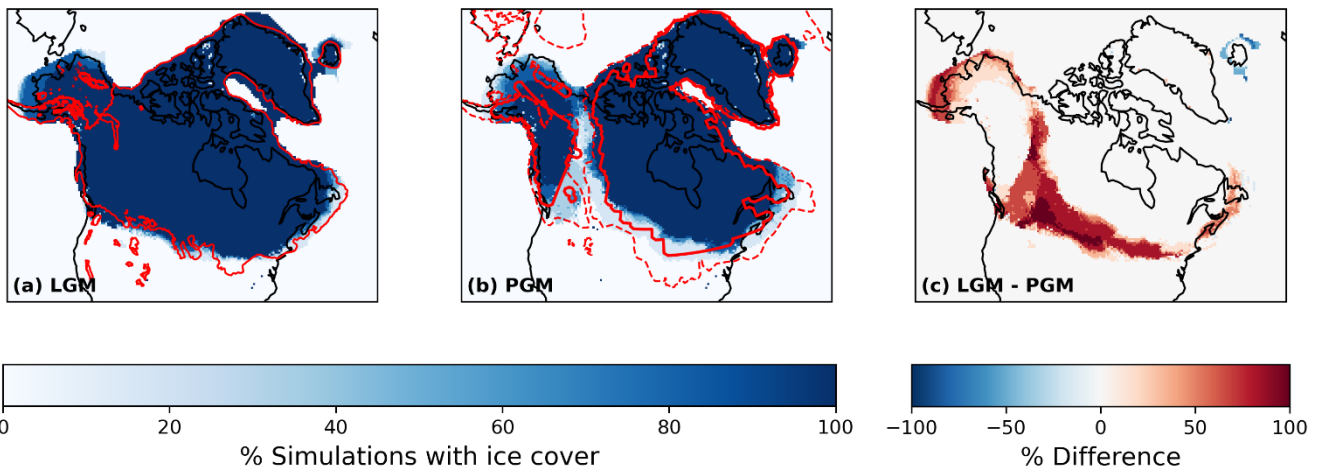


251

252

**Figure 5. (a) The relationship between final ice volume and southern area for the LGM ensemble, and the relationship between the LGM and PGM; (b) final ice volume, and (c) final southern areas.**

253

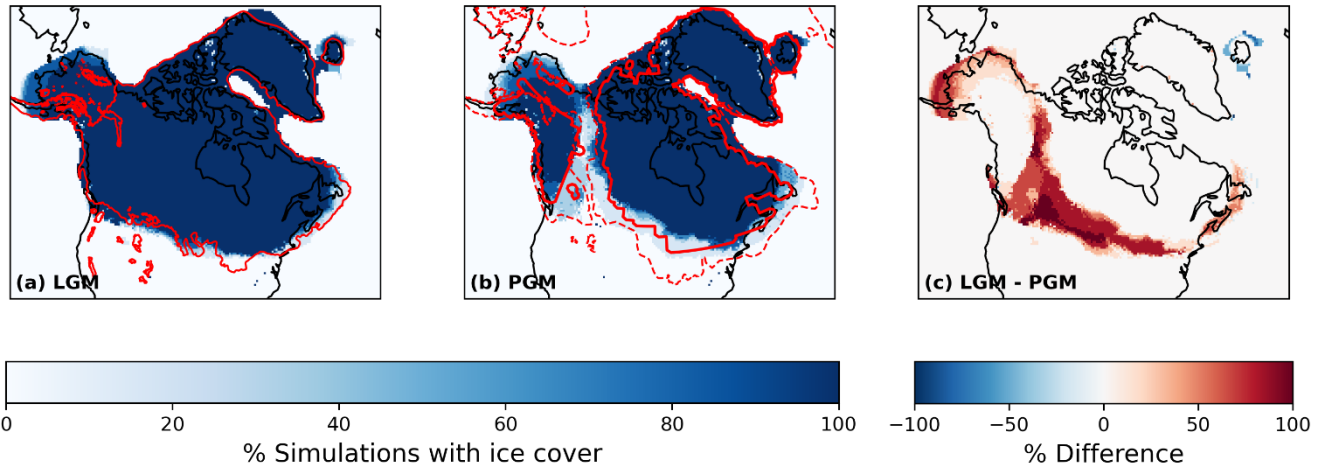


254

255

**Figure 7. The filled in blue dots represent the six NROY LGM simulations and the solid lines on panel (a) show the minimum volume and area constraints applied to the ensemble.**

256



257  
258  
259  
260  
261  
262  
263  
264  
265  
266  
267  
268  
269  
270  
271

**Figure 6.** Percentage of simulations with ice cover for (a) LGM with the Dalton et al., (2020) reconstructed margin shown in red; (b) PGM with the PMIP PGM modelled margin shown in solid red and the Batchelor et al., (2019) reconstructed maximum MIS 6 margin shown in dashed red, and (c) the difference between the LGM and PGM, at the end of the simulations for the six NROY ensemble members.

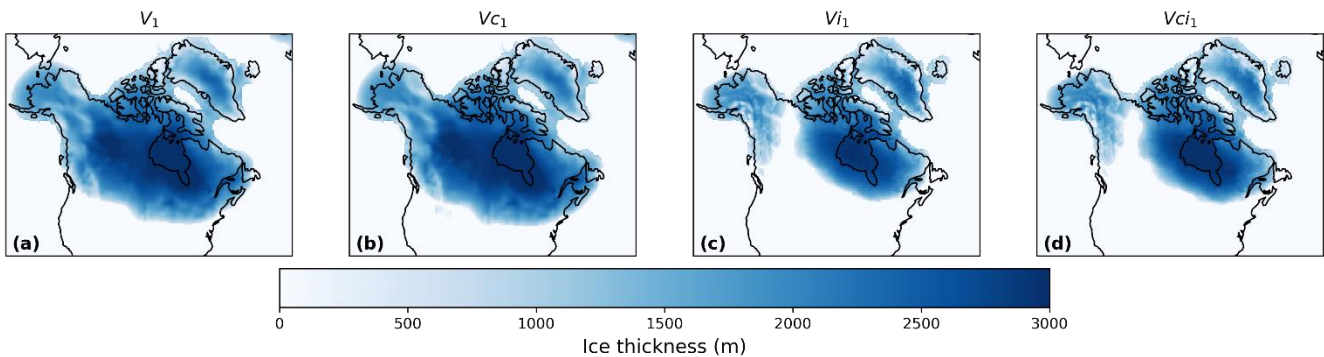
### 3.2 Impact of initial ice sheet vs climate

Out of our six NROY model configurations, we selected the parameters of a pair of LGM and PGM experiments  $x_{pken}/x_{pkyn}$  (NROYa; Fig. 6) to perform two sets of four sensitivity experiments to decompose the effects of climate forcing and initial conditions on the final ice sheet volume. This included repeating  $x_{pken}$  and  $x_{pkyn}$  using matching FAMOUS and Glimmer LGM and PGM initial conditions respectively (Table 2, experiments 3 and 6). For both glacial maxima, using the matching initial conditions resulted in more excess ice over Alaska (Fig. C1), though the southern ice extents are relatively similar between the two sets of experiments. Overall, for the LGM, using the GLAC-1D reconstruction in Glimmer ( $V_{i1}$ ) resulted in an ice sheet 9.7 m SLE larger than if the 18.2 ka ice sheet was used ( $V_{i2}$ ) (Table 5; Fig. C1a). For the PGM, the matching initial conditions ( $V_{ci1}$ ) resulted in only 0.45 m SLE increase from the NROYa simulation ( $V_{ci2}$ ) due to a decrease in ice volume over the Laurentide ice sheet (Table 5; Fig. C1b).

272 **Table 5. Final ice volumes of the four sensitivity experiments performed with matching climate model and ice sheet model ice sheets and**  
 273 **the equivalent four performed with different initial ice sheets in each model**

<u>Experiment</u>	<u>Final ice volume</u> <u>(m SLE)</u>	<u>Experiment</u>	<u>Final ice volume</u> <u>(m SLE)</u>
<u><math>V_{i1}</math> (full LGM)</u>	<u>100.3</u>	<u><math>V_{i2}</math></u>	<u>90.6</u>
<u><math>V_{c1}</math> (LGM ice, PGM climate)</u>	<u>104.2</u>	<u><math>V_{c2}</math></u>	<u>97.1</u>
<u><math>V_{i1}</math> (PGM ice, LGM climate)</u>	<u>64.7</u>	<u><math>V_{i2}</math></u>	<u>63.0</u>
<u><math>V_{ci1}</math> (full PGM)</u>	<u>68.6</u>	<u><math>V_{ci2}</math></u>	<u>68.1</u>

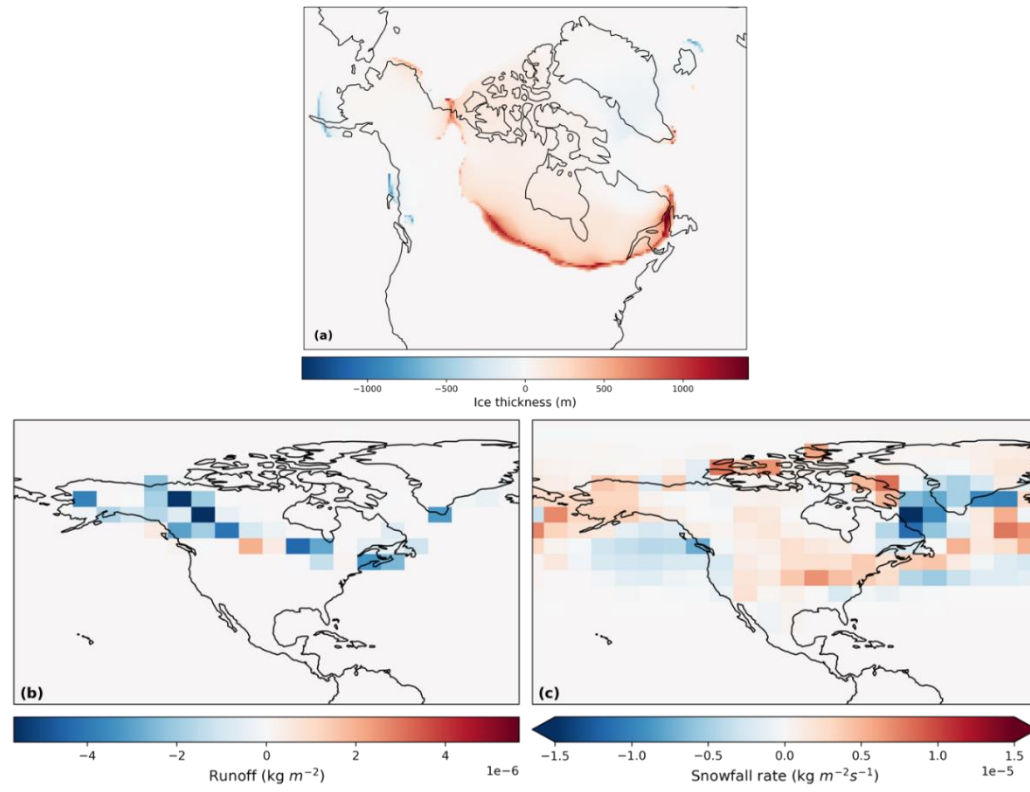
274  
 275 The final ice sheet volumes from the first set of four sensitivity experiments (Table 2; experiments 3 – 6) are displayed in Table 5  
 276 and shown in Fig. 8. The results of the second set of four experiments (Table 2; experiments 7 – 10) are also included in Table 5.  
 277 The results of the factor decomposition analysis show that the simulated ice volume at the PGM was 31.7 m SLE ( $1.25 \times 10^7 \text{ km}^3$ )  
 278 lower than at the LGM ( $dV_{i1}$ ). The initial ice sheet configuration ( $dV_{i1}$ ) alone caused a 35% decrease in volume, but this was  
 279 partially offset by the climatic conditions ( $dV_{c1}$ ), which resulted in an increase in volume of 4%. The result was similar for the  
 280 second set of experiments, with the initial ice sheet configuration ( $dV_{i2}$ ) causing a decrease of 31% in ice volume at the PGM  
 281 compared to the LGM, but the climate ( $dV_{c2}$ ) caused a 6% increase in volume.



282  
 283 **Figure 8. Final ice thickness in the sensitivity tests using (a) LGM ice sheets and LGM climate; (b) LGM ice sheets and PGM climate; (c)**  
 284 **PGM ice sheets and LGM climate, and (d) PGM ice sheets and PGM climate.**

285 The PGM climate is conducive to growing a larger ice sheet (Fig. 9a) because the orbital configuration results in the Northern  
 286 Hemisphere receiving less incoming solar radiation in spring and early summer (Table 1; Fig 2a). This reduces the melting of snow  
 287 that has accumulated in winter (Fig. 9b). The winter snow accumulation is also higher at the PGM than at the LGM (Fig. 9c) due to  
 288 the PGM having warmer air temperatures in autumn and winter, because of the orbital forcing, leading to a wetter climate. Summer

289 SSTs are also cooler at the PGM (Fig. 2c) due to lower spring insolation, further contributing to reduced runoff. In contrast, the  
290 Greenland ice sheet decreases in size due to PGM climate conditions (Fig. 9a), likely due to higher sea ice concentration south of  
291 Greenland reducing the moisture source available for precipitation.



292  
293 **Figure 9. Difference between experiment  $V_{ci-1}$  (full PGM) and  $V_{i-1}$  (PGM ice sheet with LGM climate) isolating the effect of LGM climate**  
294 **vs PGM climate on (a) final ice thickness simulated by Glimmer and (b) spring (MAM) runoff and (c) winter (DJF) snowfall over the first**  
295 **10 years.**

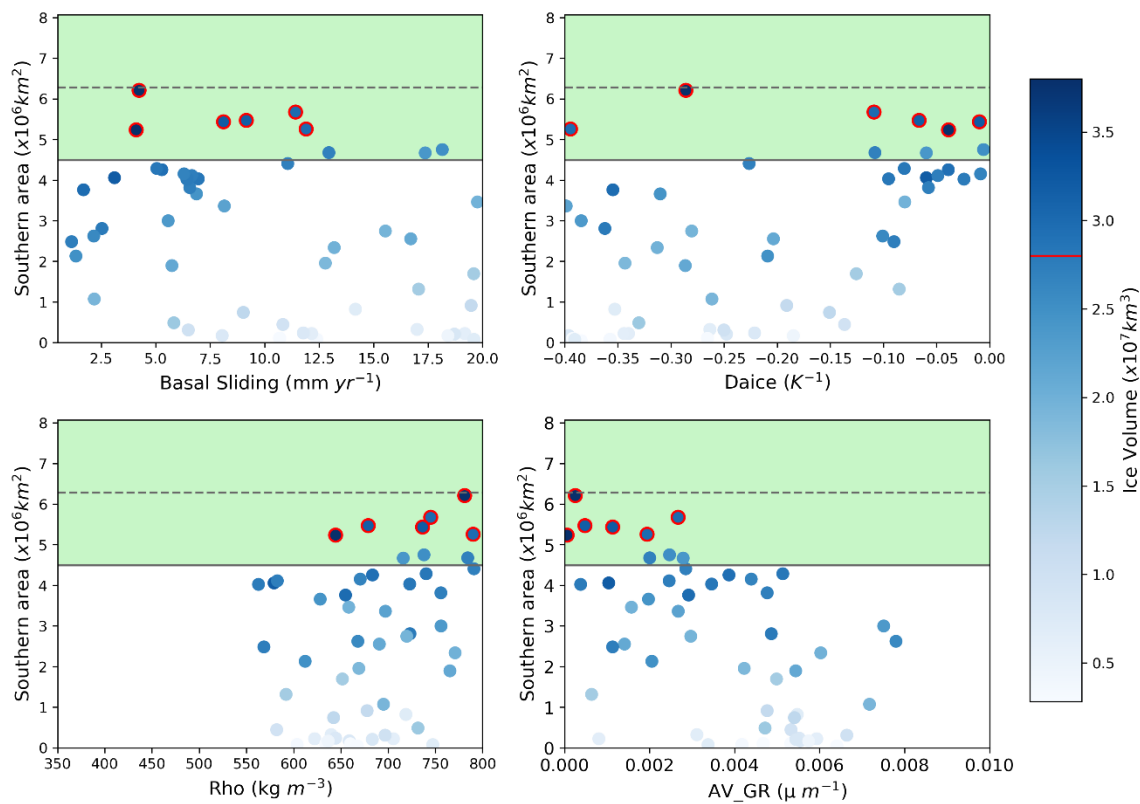
### 296 **3.3 Uncertainty due to model parameters**

297 Most Due to the sampling strategy, this ensemble does not have an optimal design for analysing the sensitivity of the ice sheets  
298 during the two time periods to the different model parameter values because our ensemble of simulations does not uniformly span  
299 the uncertain parameter space. For this, we refer the reader to the studies of Gandy et al., (2023) and Sherriff-Tadano et al., (2023),  
300 which present larger ensembles of experiments. Here, we first evaluate if our results are consistent with these two studies before  
301 examining if the difference between the PGM and LGM ice sheets is sensitive to specific model parameters.

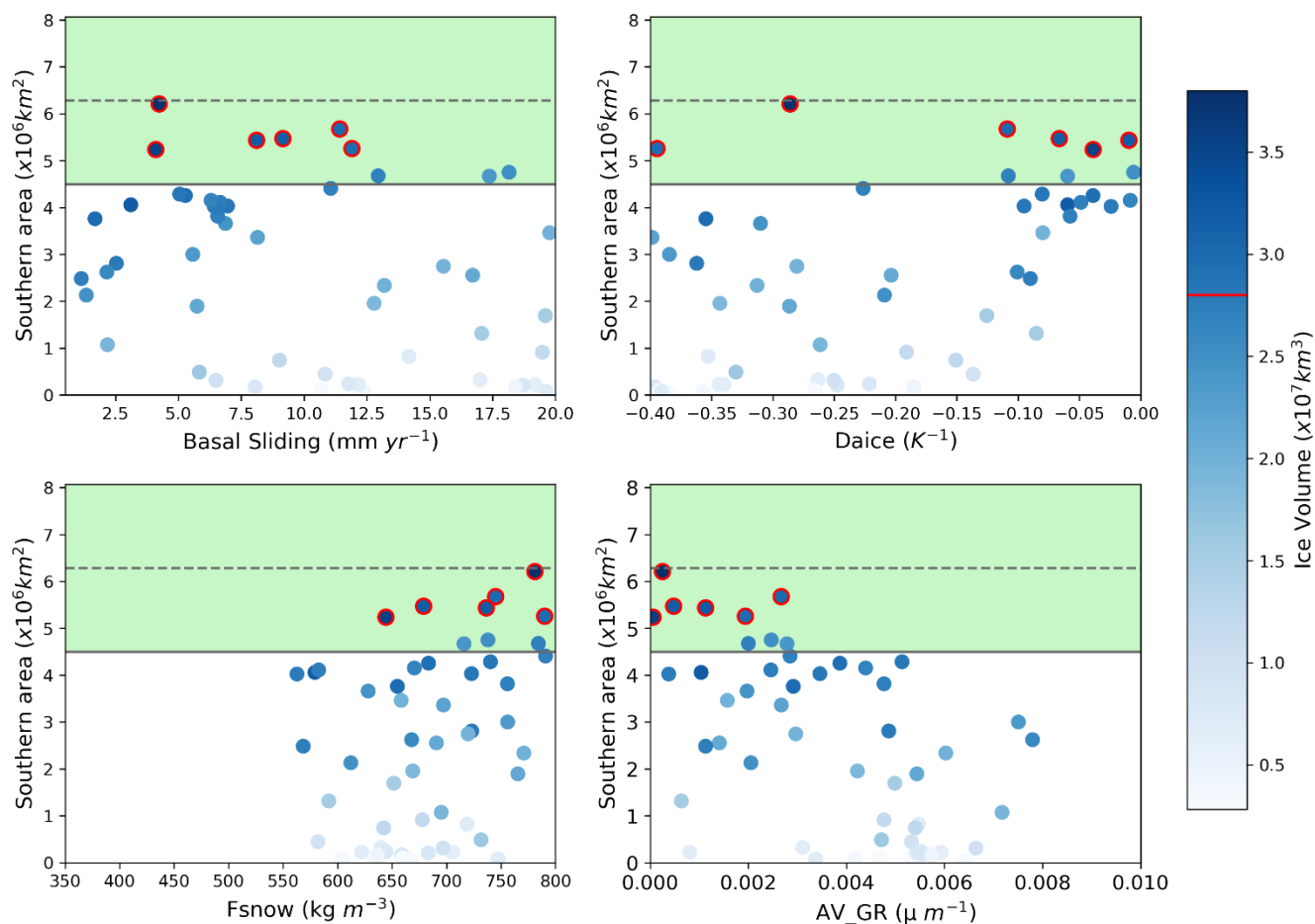
302 Based on correlations between the parameters and ice sheet area and volume, we find that the LGM and PGM behave similarly  
303 across the parameter ranges (Figs. E1 and E2) and most of the uncertainty in the results for both ~~the LGM and PGM periods~~ can be



304 explained by parameters that affect the surface albedo of the ice sheet (~~*Daice*, *Rho* and *AV\_GR*~~) and *basal* and to a lesser extent,  
305 *Fsnow*. Higher values of *Daice* and *Fsnow* and lower values of *AV GR* cause higher albedos and lead to larger ice sheets (Table 3).  
306 *Basal sliding* (Fig. 7). Similar conclusions were drawn by Gandy et al., (2023), on which this study is based, as well as other  
307 ensemble based studies exploring the sensitivity of the LGM NAIS to model parameters (e.g. Sherriff Tadano et al., 2023). The  
308 similar behaviour between the LGM and PGM across the parameter ranges (Figs. D1 and D2) further implies that similar model  
309 parameter values are appropriate for use when modelling both periods and within the bounds of available model and data constraints,  
310 our results show that retuning the model would not lead to significant changes in predicted ice sheet configurations between the  
311 LGM and PGM. However, since the ice volume is most sensitive to surface albedo and most simulations deglaciate under low  
312 values of *Daice*, this suggests that the value of bare ice albedo in the model may need to be increased for future work. also influences  
313 the volume of the ice sheet, with less impact on the area, with lower values and thus lower ice velocities causing larger volume ice  
314 sheets. The cloud parameter *CW* also shows a relatively high positive correlation for the PGM (Fig. 10). This is consistent with the  
315 findings of previous studies and current understanding on the importance of albedo for ice sheet evolution (Willeit and Ganopolski,  
316 2018; Sherriff-Tadano et al., 2023; Gandy et al., 2023).  
317 Additionally, ~~the~~ there is a negative correlation between the difference in ice volume and area between the LGM and PGM ~~is most~~  
318 ~~influenced by~~ and the parameters *AV GR*, *Daice* and *basal sliding*, ~~however the effect of these parameters on the differences seen~~  
319 ~~is minor (Fig. D3),~~ and *RHCrit*. Conversely, there is a positive correlation between the LGM-to-PGM difference in ice volume/area  
320 and *Daice* (Fig. E3). This suggests that the lower values of *AV GR* and higher the values of *Daice* and thus a higher albedo and, as  
321 well as lower the ice sheet velocity, the and more cloud, make the ice sheet more sensitive ~~the ice sheet is~~ to changes in radiative  
322 forcings from the orbital boundary conditions. ~~Due to the sampling strategy, this ensemble is not the best design to analyse the~~  
323 ~~sensitivity of the ice sheets during the two time periods to the different parameters and would require a larger ensemble and a~~  
324 ~~sensitivity analysis with Gaussian Process emulation (e.g. Pollard et al., 2023), as is presented in Gandy et al. (2023) and Sherriff-~~  
325 ~~Tadano et al. (2023).~~



327  
328



329  
 330 **Figure 710.** Relationship between LGM southern area and the four most influential parameters. The green shaded region shows the  
 331 southern area constraint applied with the dotted line showing the exact area of the reconstruction and the solid line the minimum bound  
 332 applied. The colour scale represents ice volume and the dots outlined in red are the six NROY LGM simulations with the red line on the  
 333 colour bar showing the volume constraint.

#### 334 4 Discussion

335 After constraining our ensembles based on the available empirical and model data for the LGM, we find that the model was able to  
 336 successfully simulate the ice sheet at both periods under different LGM and PGM climate boundary conditions (orbital parameters,  
 337 SSTs and global orography) and initial ice sheets. However, the southern extents of the constrained LGM simulations all fall towards  
 338 the lower end of the plausible range, which is a common feature seen in other simulations using a low resolution atmosphere model  
 339 due to biases that cause a reduced stationary wave effect over this region (Ziemen et al., 2014; Sherriff-Tadano et al., 2023; Gandy

et al., 2023). Additionally, the ice lobes that are present over the Great Lakes are not captured in these simulations. Again, this is common in ice sheet models and is likely a result of missing subglacial processes or the low resolution of the climate and ice sheets models.

**Analysis of the behaviour of the modelled ice sheets across the parameter spaces reveals that both the LGM and PGM ice volume and extent have similar sensitivities to parameter uncertainties. We therefore conclude that parameters that produce a good LGM NAIS also produce a plausible PGM NAIS under PGM boundary conditions and thus similar model parameters are appropriate for use when modelling both periods. Our simulations can thus be compared and analysed to understand the causes of the different configurations between the two periods.**

### 3.3 Climate-ice sheet interactions

The main cause of the difference in configurations between the LGM and PGM in this study is the less negative SMB at the LGM in the saddle region (Fig. 8). This is mostly a result of much lower ablation rates (runoff) in the summer months (JJA) at the LGM compared to the PGM, and to a lesser extent in spring and autumn (MAM and SON), and an increase in sublimation. The accumulation (snowfall) is similar between the two periods and does not contribute much to the SMB difference.

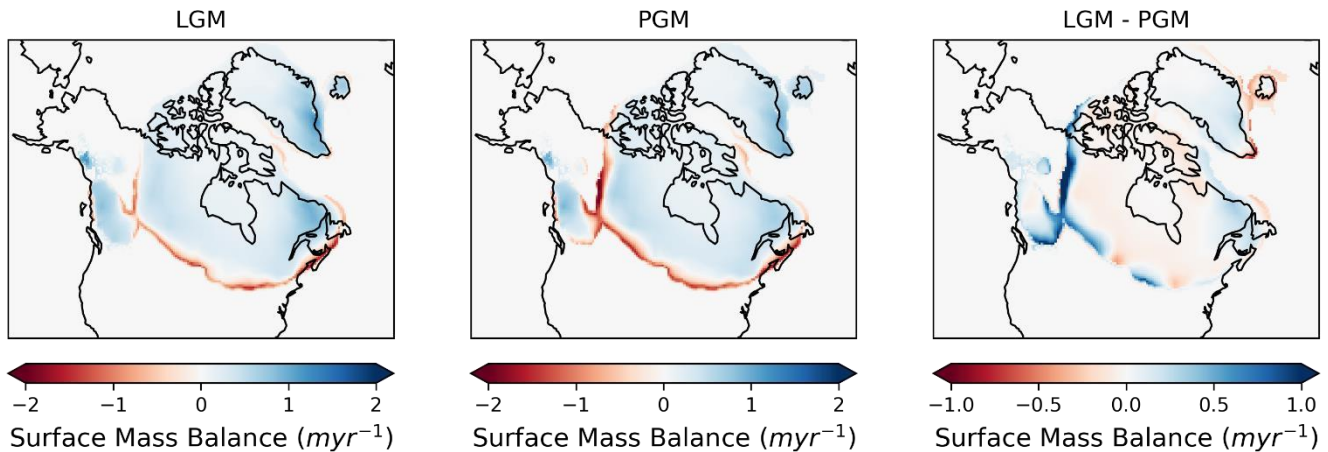
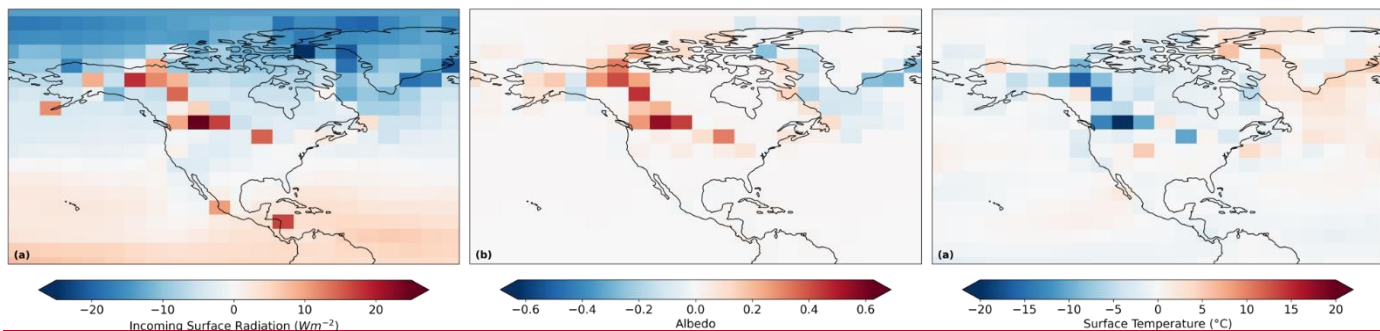


**Figure 8. Mean surface mass balance of the constrained LGM and PGM ensembles averaged over model years 10–20 of the simulations and the difference between them.**

This reduction in runoff occurs despite the LGM receiving more incoming top of the atmosphere shortwave radiation in early summer and more incoming surface radiation over North America at this time (Fig. 9a). Therefore, the positive SMB anomaly is a result of much more of this shortwave radiation being reflected back off the surface causing lower surface temperatures than at the PGM, allowing ice to build up and be maintained. In other words, the LGM has a higher albedo in this saddle region resulting in a more positive ice-albedo feedback (Figs. 9b and 9c). In contrast, the PGM has much lower albedo over the southern margin and saddle region, preventing ice growth in these regions.

362 During the analysis of these runs, we found that the coupling in the model was not passing all reductions in ice sheet area from  
363 Glimmer to FAMOUS in certain regions, particularly where entire FAMOUS gridboxes were initially covered in ice at all  
364 elevations (i.e. the saddle region at the LGM). This would have tended to reinforce the initial high albedo, positive mass  
365 balance surface conditions in the saddle region for the LGM configuration but would not have prevented the PGM simulations  
366 from growing ice in that area. To assess the role played by the initial conditions in our model simulations, we present an  
367 additional sensitivity analysis in the following section.

368



369

303 ~~Figure 9. Mean difference between the NROY LGM and PGM simulations of mean summer (a) incoming surface shortwave 304 radiation; (b) albedo, and (c) surface temperature. All plots show the June July August average over model years 10-20 of the 305 simulations.~~

### 306 ~~3.4 Sensitivity analysis~~

307 To investigate the sensitivity of the final ice volumes to these differences in the initial conditions versus the differences in the 308 climate, a sensitivity analysis was carried out along with factorisation based on the method used in Lunt et al., (2012), also 309 used in Gregoire et al. (2015). We divided the differences in inputs between LGM and PGM into two factors; the initial ice 310 sheet configuration used in FAMOUS and the climate boundary conditions (orbital parameters, greenhouse gases and SSTs/sea 311 ice). However, since the ice volume is most sensitive to surface albedo and most simulations deglaciates under low values of  $D_{ice}$ , this suggests that the value of bare ice albedo in the model may need to be increased for future work. Thus, the total difference in final ice volume ( $\Delta V$ ) between the LGM and the PGM can be written as Eq. (1):

$$312 \quad \Delta V = dV_{ice} + dV_{climate}, \quad (1)$$

313 where  $dV_{ice}$  is the difference in final ice volume due to the different initial ice sheet configurations and  $dV_{climate}$  is the 314 difference due to the difference climate boundary conditions used.

315 The factorisation method requires  $2^N$  simulations (where N is the number of different components) to determine the 316 contribution of each component to ice volume difference, therefore  $2^2 = 4$  experiments are needed that systematically change 317 one variable. These experiments are listed in Table 4. We chose one of the NROY pairs of simulations (xpkcn and xpkyn 318 respectively) to carry out this analysis, these thus correspond to the full LGM and PGM simulations ( $E$  and  $E_{ei}$  respectively) 319 in the factorial decomposition. We further performed the two additional simulations needed for the decomposition (Table 4).

320 ~~The relative contributions of the initial conditions and climate can be calculated by Eqs. (2) and (3):~~

$$321 \quad dV_{ice} = \frac{1}{2} ((V_i - V) + (V_{ei} - V_e)), \quad (2)$$

$$322 \quad dV_{climate} = \frac{1}{2} ((V_e - V) + (V_{ei} - V_i)), \quad (3)$$

323  
324 **Table 4. Ice sheet and climate conditions in each of the four experiments used in**

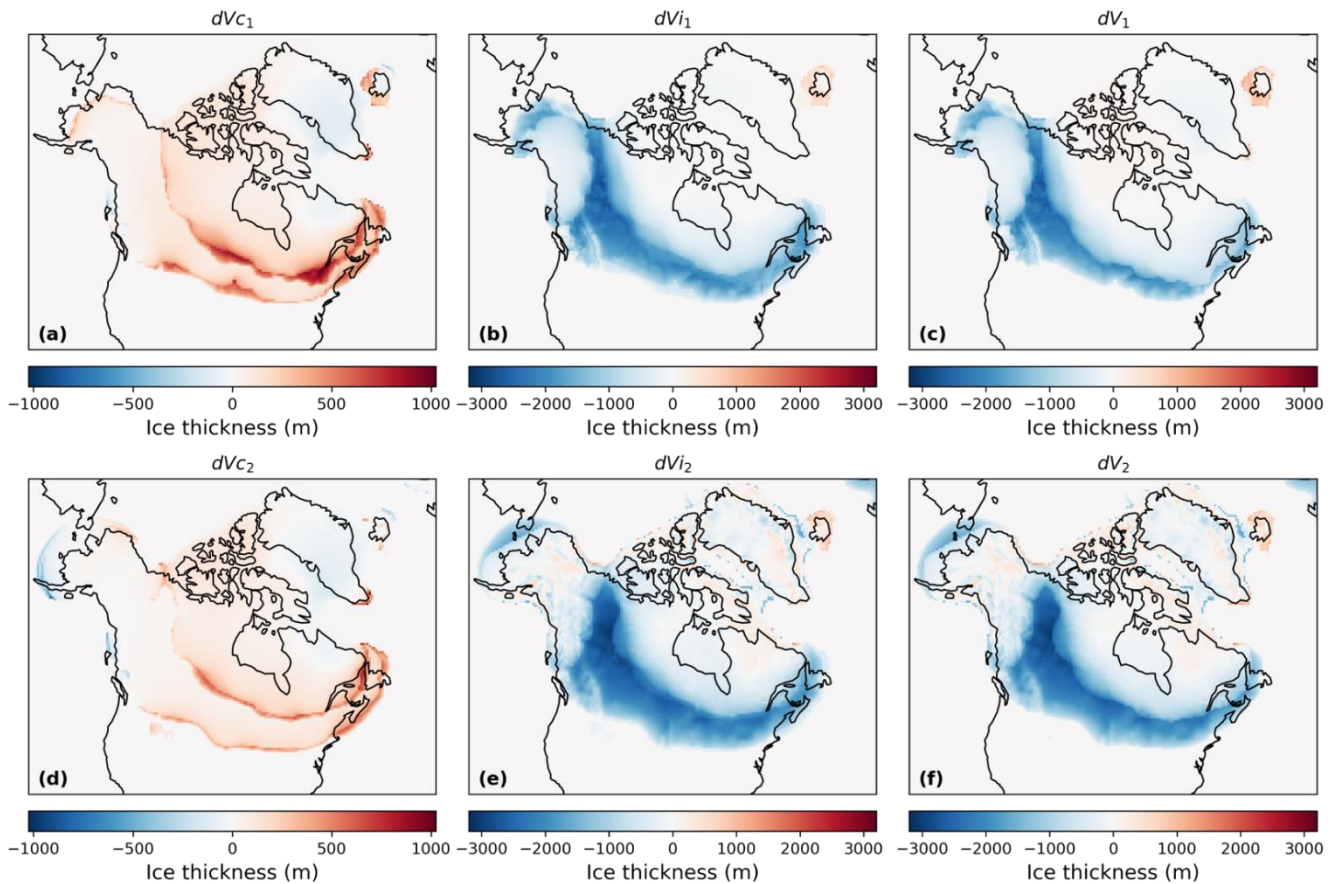
The results of the sensitivity analysis

Experiment (final volume) FAMOUS initial ice sheet Climate (PMIP4)

$E(V)$	LGM-GLAC1D	LGM
$E_e(V_e)$	LGM-GLAC1D	PGM
$E_i(V_i)$	PGM-PMIP4	LGM
$E_{ei}(V_{ei})$	PGM-PMIP4	PGM

325

326 The results show that between the LGM and the PGM there was a total volume decrease ( $dV_t$ ) of  $8.89 \times 10^6 \text{ km}^3$ . The initial  
 327 ice sheet configuration ( $dV_{i1}$ ) alone caused a decrease of  $1.12 \times 10^7 \text{ km}^3$  (125% contribution) but this was offset by the climatic  
 328 conditions ( $dV_{c1}$ ) which resulted in an increase in volume of  $2.27 \times 10^6 \text{ km}^3$  (25% contribution) (Figs. 10a-c). To further  
 329 understand the effect of initial conditions, we performed further simulations in which the initial conditions in the ice sheet  
 330 component Glimmer was set to closely match the initial ice sheet extent and topography set in the climate component FAMOUS.  
 331 ~~Specifically, for the LGM, the Glimmer initial bedrock topography and ice surface elevation was prescribed from the GLAC~~  
 332 ~~4D reconstruction used in the FAMOUS LGM boundary condition. For the PGM, the data needed for PMP4 reconstruction to~~  
 333 ~~be converted to the Glimmer initial condition were not available. Instead, both Glimmer and FAMOUS were initialised with~~  
 334 ~~the final timestep of the PGM experiment (xpkyn) since it closely resembles the PMP4 reconstruction. This produced a similar~~  
 335 ~~result to the original factorial decomposition, with the initial ice conditions ( $dV_{i2}$ ) resulting in a 35% decrease in volume which~~  
 336 ~~was offset by the climate ( $dV_{c2}$ ) by a 4% increase (Figs. 10d-f).~~



337



338 ~~Figure 10. Difference in final ice thickness between the PGM and LGM due to (a) climate parameters; (b) initial ice sheet conditions,~~  
339 ~~and (c) the total difference. (d-f) show the same but for the corrected Glimmer ice sheets.~~

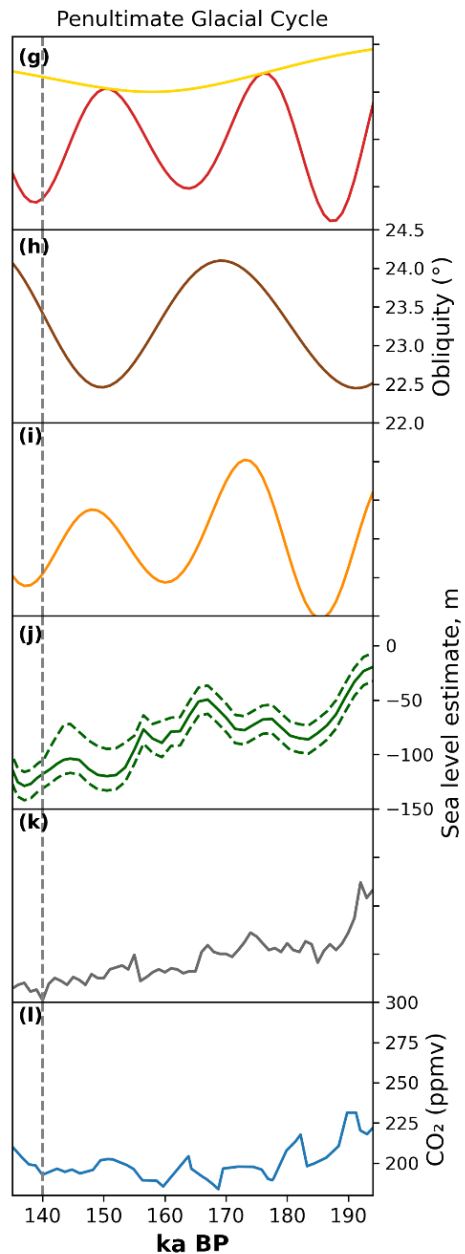
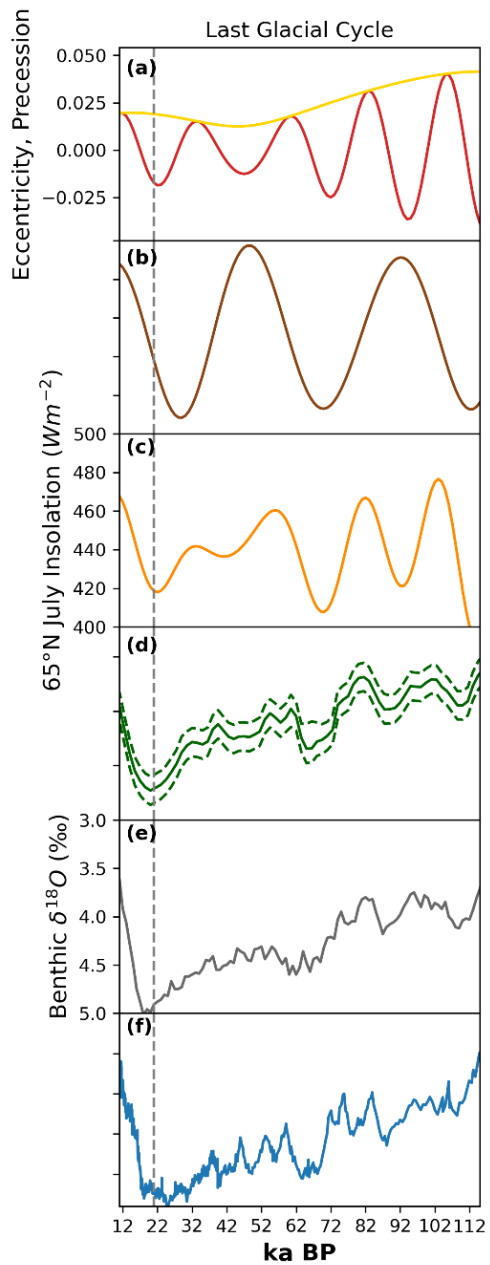
340 ~~Based on these results, it is clear that the difference in initial ice cover, and resulting ice-albedo feedback, the difference in~~  
341 ~~initial ice sheet boundary conditions~~ overwhelmingly determined the difference in final ice volume between the LGM and PGM  
342 in these simulations. Additionally, the vegetation fraction in the non-ice-covered areas in the PGM initial conditions will have  
343 a compounding effect on this difference by introducing a vegetation albedo feedback ~~the ensemble of simulations. We tested~~  
344 ~~the impact of starting from LGM and PGM ice sheet configurations in Glimmer instead of the 18.2 ka BP ice sheet and found~~  
345 ~~that this caused an even larger difference in ice volume between the two glacials. Comparing the simulations that use the same~~  
346 ~~initial ice topography in FAMOUS and Glimmer (first set of experiments), to those that limits the ice growth at the PGM, use~~  
347 ~~different topographies (second set of experiments), whilst keeping the ice cover consistent, reveals that the relative contribution~~  
348 ~~from the initial ice sheet boundary conditions, compared to the climate conditions, to the simulated differences between the~~  
349 ~~LGM and PGM ice sheets, remains similar. This suggests that the dominant feedback responsible for this result is the ice-albedo~~  
350 ~~feedback rather than the temperature-elevation feedback.~~ A similar conclusion was obtained by ~~AbeOuchi~~ Abe-Ouchi et al.,  
351 (2007) who studied the relative contribution to climate over ice sheets from the ice sheet itself and the orbital parameters and  
352 CO<sub>2</sub> concentration. They found the cooling caused by the ice sheet themselves was the dominant effect, mostly due to albedo  
353 feedbacks, which increase with ice sheet area. Kageyama et al., (2004) also highlighted in their study the importance of the  
354 albedo feedback on the maximum modelled North American ice volume. They show that changes in vegetation are needed to  
355 initiate glaciation over North America which is then accelerated by the ice-albedo feedback. ~~Interestingly, The North American~~  
356 ~~ice sheet was larger at the LGM than at the PGM. However, this sensitivity analysis reveals that~~ the difference in orbital  
357 parameters, GHGs and SSTs (climate) between the LGM and PGM ~~caused~~ encourages the growth of a larger North American  
358 ice sheet at the PGM ~~in contrast to what evidence suggests (Fig. 9a). This is mostly a result of the orbital configuration which~~  
359 ~~resulted in the effect would likely be even stronger if we had used the orbit at 137 ka BP (the timing of the minimum in Northern~~  
360 ~~Hemisphere receiving less incoming solar radiation summer insolation; Fig. 11a-c) since the PGM would have received even~~  
361 ~~lower insolation~~ in spring and early summer (Table 1; Fig 2). This reduces the melting of snow that has accumulated in winter.  
362 The winter snow accumulation is also higher at the PGM than the LGM due to warmer air temperatures in autumn and winter,  
363 as a result of the orbital configuration, leading to a wetter climate. Summer SSTs are also cooler at the PGM due to lower spring  
364 insolation, further contributing to reduced runoff. In contrast, the Greenland ice sheet decreases in size due to PGM climate  
365 conditions likely due to higher sea ice concentration south of Greenland reducing the moisture source available for precipitation  
366 (Fig. 2b). This result highlights the importance of the evolution of these climate factors and the ice sheets during the preceding  
367 glacial cycles in determining the glacial maxima configurations.

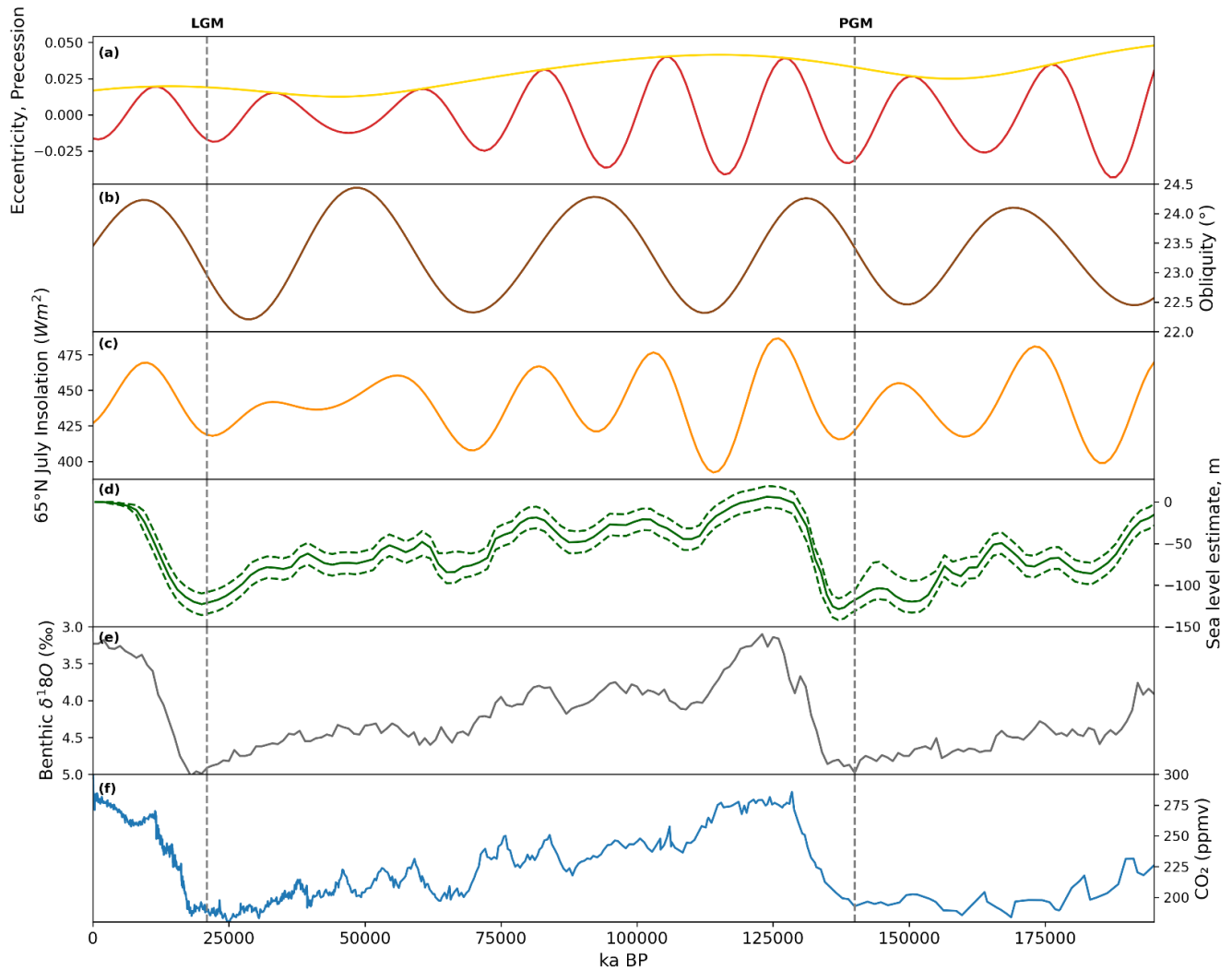
368 For example, during the start of the Last Glacial Cycle (MIS 5; ~115-80 ka BP), the variation in 65° N summer insolation was  
369 relatively large as a result of changes in orbital parameters (Fig 11a-c), which resulted in multiple cycles of growth and recession

370 of the North American Ice Sheets during this period, but total ice volume remained low (Bonelli et al., 2009; Ganopolski et al.,  
371 2010; Dalton et al., 2022). Insolation then reaches a minimum at ~70 ka BP (Fig 11c) which, combined with decreasing  
372 concentrations of CO<sub>2</sub> (~190 ppm at ~65 ka BP; Fig. 11f), ~~lead~~led to a significant increase in ice sheet volume to almost LGM  
373 extent (Fig. 11d) and a switch to more widespread glacial conditions at the MIS 5/MIS 4 transition (Bonelli et al., 2009; Dalton  
374 et al., 2022). The size of the NAIS at this time was large enough to induce positive feedbacks, such as the ice-albedo feedback,  
375 allowing its maintenance throughout MIS 4 and MIS 3 (~70-30 ka BP) despite an increase in insolation from ~50-30 ka BP  
376 (Fig. 11c). This was also supported by a continued decrease in CO<sub>2</sub> (~~Fig. 11f. Bonelli et al., 2009~~). Growth of the ice sheet  
377 could then continue to its glacial maximum extent following a further insolation and CO<sub>2</sub> decrease during MIS 2 (~30-21 ka  
378 BP) (Fig. 11c-f). In contrast, prior to the PGM there were peaks in insolation at ~172 and ~148 ka BP that reached higher levels  
379 than were reached prior to the LGM during MIS 4 and MIS ~~2, respectively, which were significant periods of growth at the~~  
380 ~~LGM 3~~ (Fig. ~~11c~~11c; Berger; 1978). This may have inhibited an initial significant build-up of ice over North America, as during  
381 MIS 4, preventing the initiation of an ice-albedo feedback strong enough to enable the continued growth towards a larger LGM

~~373~~-configuration and/or maintain its volume through the second insolation peak. In addition, there was more time between the ~~374~~ LGM and the insolation maximum at ~50-30 ka BP compared to the PGM and the maximum at ~147 ka BP. Therefore, the ~~375~~-PGM NAIS may have not had enough time to regrow before insolation started to increase again. Thus, investigation of the processes and interactions that took place prior to the glacial maxima will be needed to fully understand why the LGM and PGM NAIS configuration differed.

~~376~~ —





378

379

380

381

382

383

**Figure 11. Evolution of climate proxies over the last two glacial-interglacial cycles: (a-g) precession index (red) with eccentricity as an envelope (yellow); (b,h) obliquity (Berger, 1978); (c,i) July insolation at 65° N (Berger and Loutre, 1999); (d,j) reconstruction of global mean sea level and uncertainty estimate (dotted lines) (Waelbroeck et al., 2002); (e,k) benthic  $\delta^{18}O$  global stack record (Lisiecki and Raymo, 2005), and (f,l) EPICA Dome C carbon dioxide ice core records (Luthi et al., 2008; Bereiter et al., 2015). The PGM and LGM are indicated by the dotted line.**

## 4 Conclusions

~~We have performed and compared ensemble simulations of the LGM and the PGM using a coupled climate ice sheet model (FAMOUS ice) with an interactive North American Ice Sheet. The model was able to successfully simulate the ice sheet at both periods, compared to empirical evidence and other modelling studies, under different LGM and PGM climate boundary conditions and initial ice sheets. Overall, this study has shown that the underlying surface conditions, ice and snow cover and vegetation, used as boundary conditions in coupled climate ice sheet simulations are extremely important in the resulting ice sheet volumes and extents because of the strong influence of the ice albedo and vegetation albedo feedbacks on the expansion of ice. In this study, the climate of each glacial maxima period has only a negligible effect on the simulated ice volume. Thus, investigation of the processes and interactions that took place prior to the glacial maxima will be needed to fully understand why the LGM and PGM NAIS configuration differed.~~

Additional feedbacks that played a role in the development of glacials into either an LGM-like or PGM-like mode are also missing in these simulations due to computational constraints. For example, the low resolution of the atmospheric component of FAMOUS means that it is capable of performing ensembles and long paleopalaeo runs while directly coupled to an ice sheet model, ~~however~~. However, it also means that many small-scale atmospheric processes (e.g. stationary wave response) caused by and affecting the ice sheet topography are not ~~captured~~ represented well (Kageyama and Valdes, 2000; Liakka and Nilsson, 2010; Beghin et al., 2014; 2015; Liakka et al., 2012; 2016). Additionally, the shallow ice approximation used in Glimmer means that the ice sheet will not be able to simulate marine instabilities of advance and retreat (Pattyn et al., 2012). This effect will be minimal for the NAIS, but a more advanced ice sheet model would be required to simulate a marine ice sheet like the EIS.

As ~~previously mentioned~~ a reminder, the vegetation was kept fixed at present day pre-industrial distributions, but the vegetation prior to and next to the ice cover has been shown to be very important for determining ice sheet expansion in models through the vegetation-albedo feedback (Kageyama et al., 2004; Colleoni et al., 2009b; Horton et al., 2010; Stone and Lunt, 2013). Therefore, implementing glacial maxima distributions or dynamical vegetation may affect the results since the reduction in forest and expansion of tundra/shrubs compared to present day would increase the albedo of the surface next to the ice and affect the climate (Meissner et al., 2003). ~~Similarly, the fixed SSTs and sea ice concentrations used introduce uncertainty due to lack of constraint data and neglect any effects changes in ocean conditions and ice sheets have on each other (e.g. Similarly, the prescribed SSTs and sea ice concentrations used introduce an additional source of uncertainty. As well as impacting the global mean temperature and precipitation patterns in the simulations, the SSTs and sea ice used can have local climate impacts that affect the simulated ice sheets. This includes causing a warming or cooling over the more coastal areas affecting the melt rate, and impacting evaporation rates, which affects the amount of snowfall the ice sheets receive. The SSTs used in this study are cooler (as a global average) than the multi-proxy and data assimilation LGM SST reconstructions of Tierney et al., (2020)~~

415 and Paul et al., (2020) and the constrained statistical reconstruction of Gandy et al., (2023) and Astfalck et al., (2024). HadCM3  
416 also tends to simulate cooler SSTs compared to other PMIP4 models, although they are similar to CESM1.2 (Kageyama et al.,  
417 2021). Therefore, the use of colder SSTs in this study causes lower global mean temperature overall, but also would have  
418 caused a cooling next to the ice sheets and reduced snowfall, which would have impacted the ice sheet growth in different  
419 ways (Marsiat and Valdes, 2001; Hofer et al., 2012; Astfalk et al., 2024). The latter impact was shown to be most dominant in  
420 the study by Astfalck et al., 2024, suggesting that our simulated ice sheet volumes may have been larger had we used their  
421 warmer LGM SST reconstruction, due to increased evaporation. Prescribing the ocean forcing also neglects any effects changes  
422 in ocean conditions and ice sheets have on each other (e.g. Timmerman et al., 2010; Colleoni et al., 2011; Ullman et al., 2014;  
423 Sherriff-Tadano et al., 2018; 2021). ~~We recommend the use of a fully coupled atmosphere-ocean~~Using a dynamical ocean  
424 would include the effects of meltwater and changes in atmospheric circulation, arising from the ice sheets, on ocean circulation  
425 and temperature, which would in turn affect the climate, feeding back onto the ice sheets themselves. Further work will be  
426 required to investigate the feedbacks between ice sheets and sea surface at the PGM, but this is beyond the scope of this study.  
427 We recommend the use of a fully coupled atmosphere-ocean-vegetation-ice sheet model to further investigate these feedbacks.  
428 The effect of dust deposition and ice dammed lakes have also been shown to have a large influence on the build-up of ice (e.g.  
429 Krinner et al., 2004; 2006; Naafs et al., 2012; Colleoni et al., 2009a) however further model developments would be needed  
430 to investigate these effects.  
431 Finally, the Eurasian ice sheet also displayed important differences between the LGM and PGM and had a large influence on  
432 the climate. It is likely that some of the differences in the configurations of the NAIS and EIS between the two glacial maxima  
433 resulted from their interactions with each other (Beghin et al., 2014; 2015; Liakka et al., 2016). To investigate the EIS at the  
434 PGM, we recommend the use of an efficient marine ice sheet model such as BISICLES that uses Adaptive Mesh Refinement  
435 to refine the processes occurring at marine margins that are more important for the marine based Eurasian ice sheet (Cornford  
436 et al., 2013; Gandy et al., 2019).

## 437 **5 Conclusions**

438 We have performed and compared ensemble simulations of the LGM and PGM using a coupled atmosphere-ice sheet model  
439 (FAMOUS-ice) with prescribed surface ocean conditions and interactive North American and Greenland Ice Sheets. We tested  
440 the relative importance of the initial ice sheet configuration versus the climate boundary conditions on the resulting ice sheet  
441 volumes through sensitivity tests and factor decomposition analysis. The main conclusions of this study are as follows:

- 442 1. Successful simulations of the LGM and PGM North American and Greenland ice sheets are produced using a coupled  
443 climate-ice sheet model. We find that uncertain model parameters tuned to produce a plausible LGM North American  
444 Ice Sheet also perform well for the PGM.

445 2. The initial ice extents used as boundary conditions in coupled climate-ice sheet simulations have a much larger impact  
446 on the modelled NAIS than the climate boundary conditions, causing a ~30% decrease in ice volume at the PGM  
447 compared to the LGM. This is due to the ice-albedo feedback.

448 3. The climate of the PGM causes an increase in NAIS ice volume of ~6% compared to the LGM due to the orbital  
449 configuration causing the Northern Hemisphere to receive less insolation in spring and early summer. Since the LGM  
450 ice sheet was larger than the PGM, this suggests that the climate and ice sheet evolution prior to the glacial maxima  
451 contributes to the differences seen between the LGM and PGM ice sheets.

## 452 **Appendix A: Eccentricity equation correction**

453 The equation for the role of eccentricity on solar insolation used in the simulations in this paper was:

$$454 S(t) = S_0 (1 + e^2) \left( 1 - \frac{e^2}{2} \right) \frac{1 + e \cos v}{(1 - e)^2} \quad (4)$$

455

$$456 S(t) = S_0 \left( \left( 1 + \frac{e^2}{2} \right) \frac{1 + e \cos v}{(1 - e^2)^2} \right) \quad (4)$$

457

458 However, this is incorrect and has now been corrected in the model to:

$$459 S(t) = S_0 \frac{(1 + e \cos v)}{(1 - e^2)^2} \quad (5)$$

460

$$461 S(t) = S_0 \frac{(1 + e \cos v)}{(1 - e^2)^2} \quad (5)$$

462

463 where; S(t) is the incoming solar insolation, S<sub>0</sub> is the solar constant, e is the eccentricity of the earth's orbit and v is  
464 the true anomaly (the angle of earth's current position on its orbit).

465 The PGM experiment 'xpky0' was re-run with the correct equation and shows that on average the SMB was slightly ~~more~~  
466 ~~negative~~ lower in our simulations than it should have been; (decreased by 16% at the end of the simulations), leading to slightly  
467 smaller ice sheets (Fig. A1). However, the impact is small (and would be even smaller for the LGM given the lower  
468 eccentricity) and does not affect our overall conclusions.



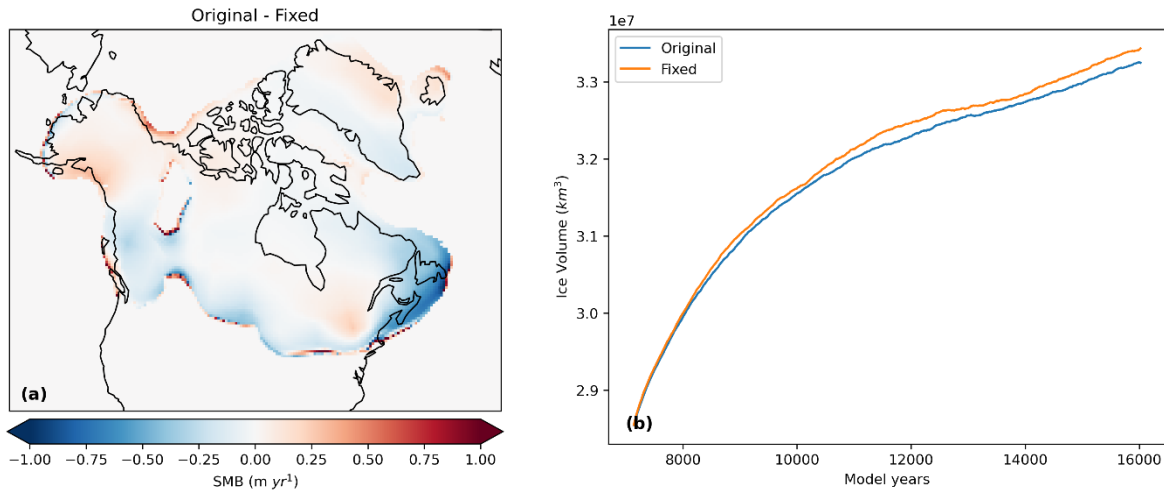
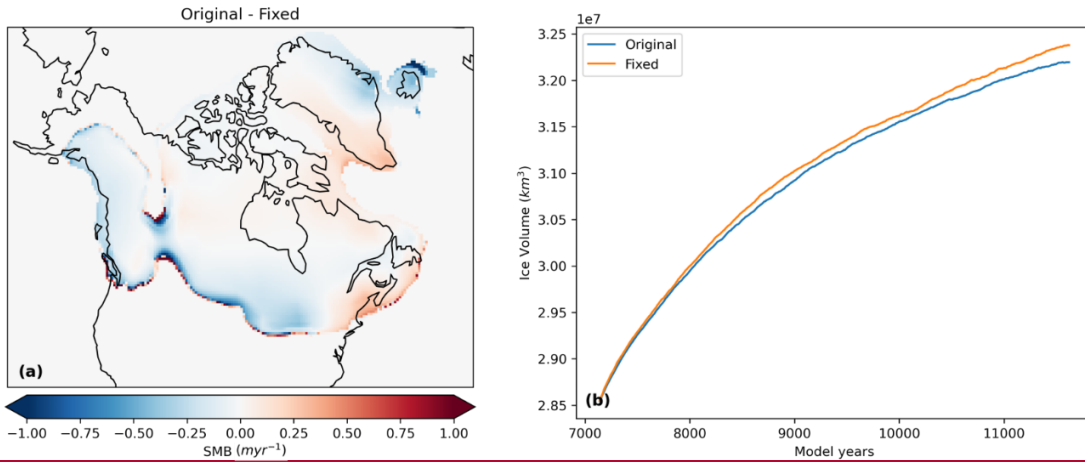
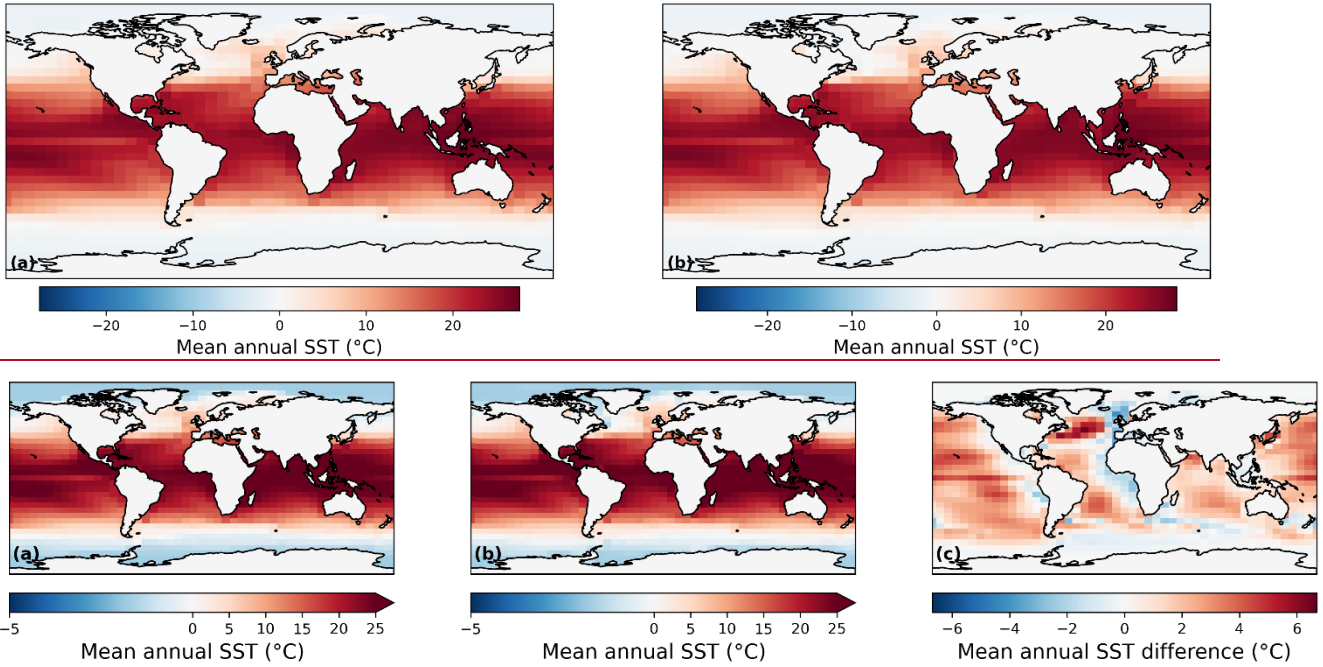


Figure A1. (a) Difference between the SMB after 450 model years at the end of the experiments between the original simulation and the simulation using the corrected eccentricity equation and (b) the evolution of ice sheet volume for both experiments.

476

## Appendix B: Sea surface temperatures



477

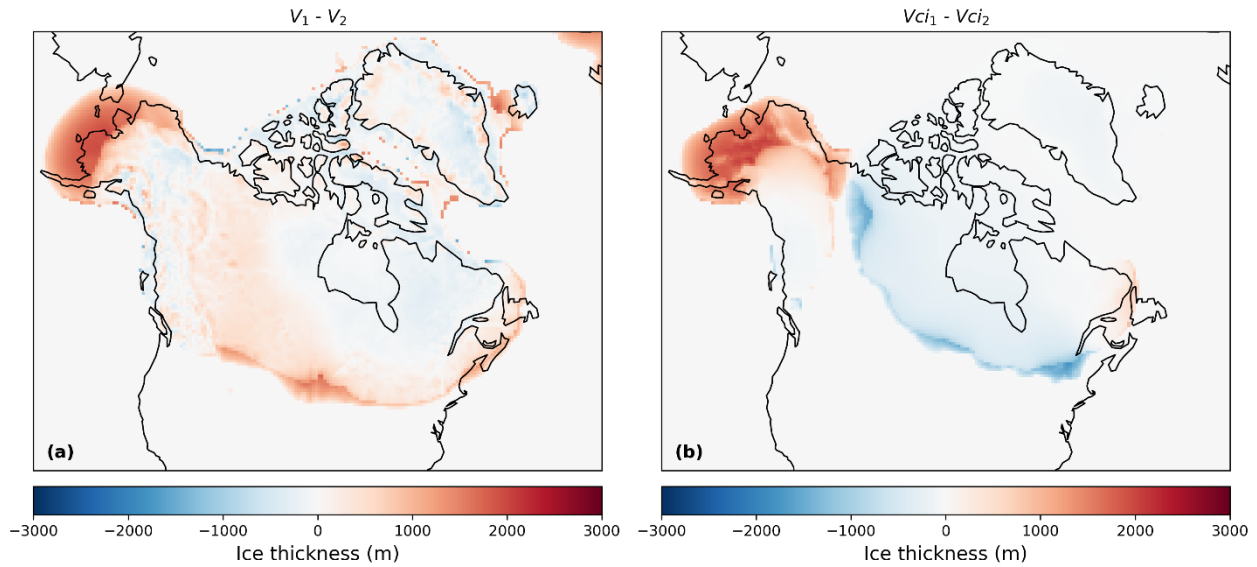
478

479

480

**Figure B1. Mean annual SSTs used in this study from HadCM3 for (a) LGM and (b) PGM- and (c) the difference between the LGM SST reconstruction used in Gandy et al., (2023) and the HadCM3 LGM SSTs.**

481 **Appendix C: Impact of different initial ice sheets**



482

483 **Figure C1. Difference in the final ice thickness between the simulations with matching initial conditions in FAMOUS and Glimmer**  
484 **and the NROYa ensemble member for (a) the LGM and (b) the PGM.**

485 **Appendix D: Wave 2 methodology**

486 The ensemble design in this study was based on the ‘Not Ruled Out Yet’ (NROY) parameter combinations from a second wave  
487 of ensemble members that followed on from the 280 member ensemble performed in Gandy et al., (2023). From the first wave  
488 of simulations, only 18 out of these 280 members produced a large enough LGM North American Ice sheet to meet the volume  
489 and extent criteria they imposed (see details in reference). Further work was thus performed to augment the ensemble of  
490 simulations that met the NROY criteria. We used statistical emulation to identify plausible regions in the parameter space. As  
491 there was limited information to constrain the domain of plausibility in the parameter space, we instead implemented an early-  
492 stopping criteria that allowed us to prevent the full execution of model runs that were not expected to produce good ice sheets.  
493 To do this we first modelled, from Wave 1, the predicted equilibrium area of the ice sheet from the value of the initial surface  
494 mass balance. Mathematically, we specified;

495

496  $A = f(b) + \epsilon,$  (6)

497

498

$$A = f(b) + \epsilon, \tag{6}$$

where A is the ‘equilibrium’ ice sheet area after 10,000 ice sheet years, b is the 20 year averaged SMB value over the ice sheet and  $f(\cdot)$

may be any function. We considered f to be either linear or sampled from a Gaussian Process (GP) and found the linear model gave more conservative uncertainty estimates which was desired since the Wave 2 runs needed to bound the NROY space. The predictive interval for the model is  $P(b) = [f(b) + 3 \sqrt{\text{var}(\epsilon)}, f(b) - 3 \sqrt{\text{var}(\epsilon)}]$  and we targeted equilibrium ice sheet areas in the interval  $T = [1.5 \times 10^7 \text{ km}^2, 2 \times 10^7 \text{ km}^2]$ . The interval T is analogous to the target interval defined using Pukelsheim’s 3-sigma rule in standard history matching (Pukelsheim, 1994). Plausible values of b satisfy the condition that  $P(b) \cap T$  is non-zero, that is, for b to be plausible, the predictive bound P(b) and the plausible equilibrium ice sheet area T must intersect. It was found that the 20-year averaged SMB had to be at least positive to produce a plausible ice sheet.

To further improve efficiency, we used statistical emulation to produce plausible values of b (and hence equilibrium ice sheet areas); iterating the training data of the emulator with each wave of simulator runs. Define by  $\mathbf{x}$  the multivariate vector of parameters that they build the emulator over: here  $\mathbf{x}$  comprised of the 4 most influential parameters Fsnow, AV\_GR, Daice, and Flow Factor. We model b with a random error process,  $b \sim GP(\mathbf{x}) + \eta$ , where the effects of the parameters not explicitly represented in  $\mathbf{x}$  are handled by the stochasticity of the process represented by  $\eta$ . Values of b were sampled using a stratified k-extended Latin Hypercube design (Williamson, 2015) and three sub-waves were executed, from which, a candidate set for the Wave 2 ensemble was extracted.

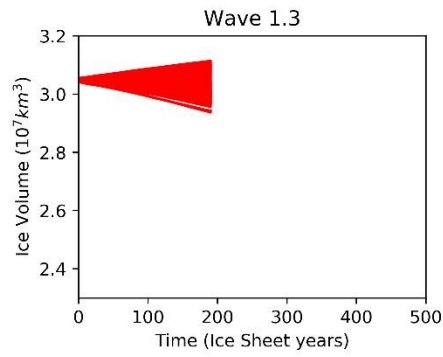
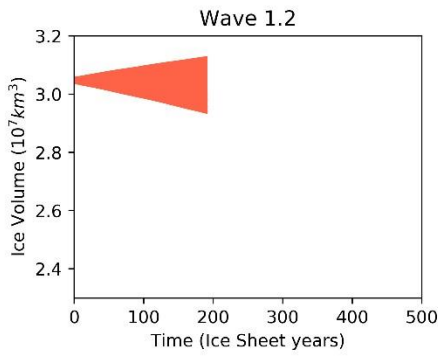
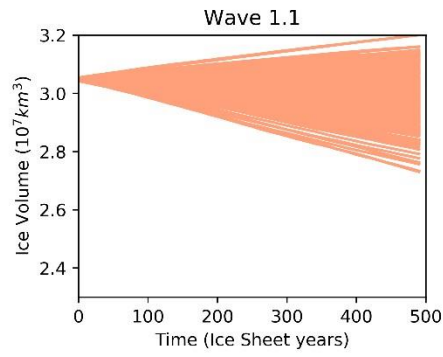
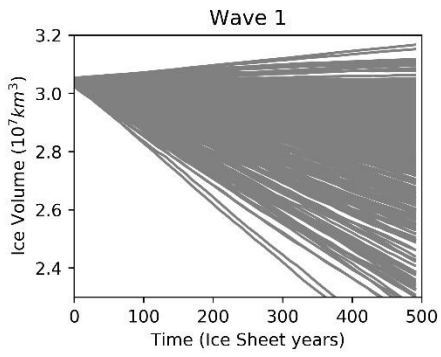
The first sub-wave (Wave 1.1) samples 200 ensemble members, which are predicted from the emulator to have non-negligible probability of positive SMB. This results in around 50% of simulations in this sub-wave having a positive SMB, an increase from 15% in the original wave (Fig. C4D1, Wave 1.1). We attempt to refine the predictive bounds on the GP model twice more (Fig. C4D1, Wave 1.2 and 1.3), with no improvement. This is likely due to the inherent stochasticity of the climate model and cumulative effects of the parameters that they absorb into the predictive error term. At the end of this process of iterative short waves, the candidate set contains over 1000 20-year long simulations that have a positive SMB over the North American ice sheet. From this candidate set, and again using stratified k-extended Latin Hypercubes, we select an optimal (with respect to space-filling and accounting for the previous Wave 1 runs) design of 200 ensemble members to continue for a full 10,000 years to an equilibrium North American Ice Sheet. These 200 simulations make up the Wave 2. For context, this workflow of GP model sub-waves saved around 230,000 core hours (or about two months of real time) compared to running a full second ensemble wave.

Out of these 200 Wave 2 simulations, 176 members were identified to be NROY based on the original volume and extent thresholds. It is based on these results that we sub-sampled 62 parameter combinations for our simulations. This number of

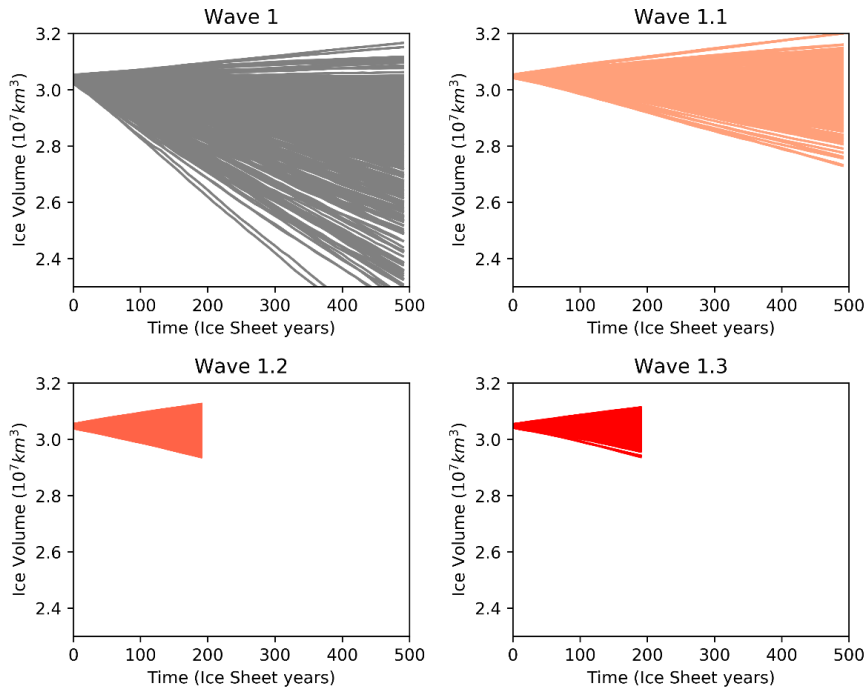
531 simulations was selected to enable us to run long equilibrium LGM and PGM simulations over a full ensemble within  
532 reasonable computational requirements. From the 176 NROY parameter combinations we randomly generated  $10^7$  candidate  
533 designs of size 62 from which we selected an approximate maximin design. This is obtained by: first linearly transforming  
534 each parameter onto the same range of [0, 1] to aid comparability; before computing the minimum distance between a  
535 parameter vector and its nearest neighbour; and then selecting the candidate design that maximised this distance. The resulting  
536 design possesses parameter vectors which are well-spaced and thus adequately cover the NROY space.

537 Our simulations use slightly different orbital parameter values and sea surface conditions to that of Gandy et al., (2023) (see  
538 Sect. 2.3). Thus, we do not expect the sample of 62 parameter combinations to provide full coverage of the NROY space but,  
539 as seen in [section Sect. S2](#) of the supplementary information in Gandy et al., (2023), the output trends are sufficiently similar  
540 that we expect this to be close enough to an optimal sample. Whilst we may have also sampled some parameter combinations  
541 outside of the NROY space, we feel these will still provide valuable information about uncertainty in outputs at the LGM and  
542 PGM. Our detailed comparison to [observations empirical evidence and other model data](#) (see Sect. 2.4 and 3.1) identified six  
543 parameter combinations that match our criteria for LGM and PGM ice extent and volume, thus demonstrating the success of  
544 this approach. Further exploration of the parameter space may produce NROY simulations in a different part of the parameter  
545 space but would not change the conclusion of this paper.

546 Upon analysing the results, we found a technical error in the original Wave 2 ensemble which resulted in the values of the  
547 parameter *Daice* being shifted from its intended range of  $-0.4-0\text{ K}^{-1}$  to  $0-0.4\text{ K}^{-1}$ , this means that the albedo of the bare ice was  
548 increasing with melting, which is likely not the case. This produced larger values of surface albedo and thus larger ice sheets  
549 in these Wave 2 simulations (not shown here). In the ensemble of simulations presented here, we corrected the *Daice* values  
550 to match the intended parameter range. In some simulations, the switch of *Daice* value from a large positive number to a large  
551 negative number would have resulted in a decrease in surface albedo and resulting ice sheet volume. This effect is negligible  
552 for values of *Daice* closer to zero.



554  
555



556

557

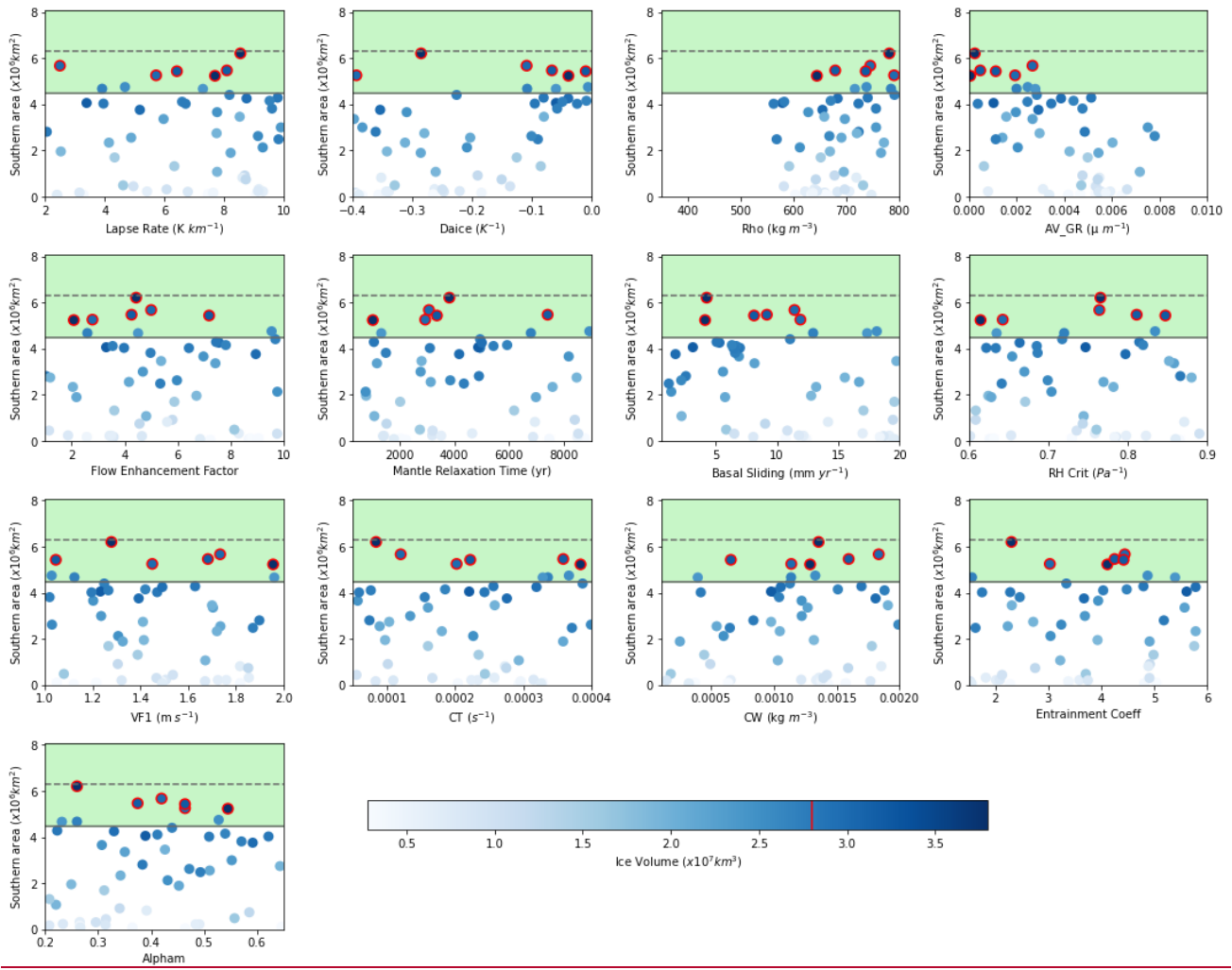
**Figure C1D1.** Ice volumes simulated in the successive ensemble sub-waves of simulations sampled to have a positive initial surface mass balance using the Gaussian Process emulator

558

559

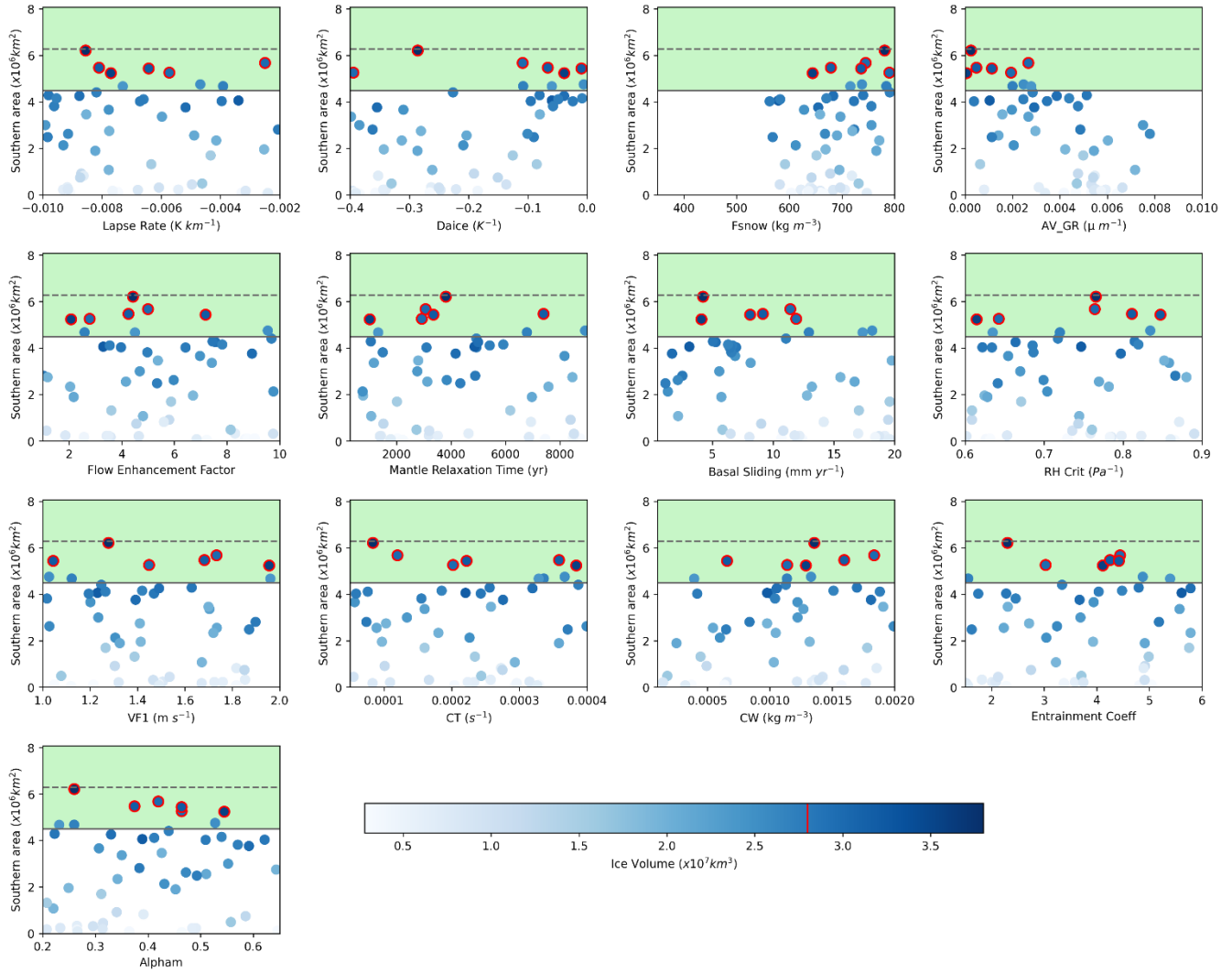
**Appendix DE:** Metrics vs parameters plots

560



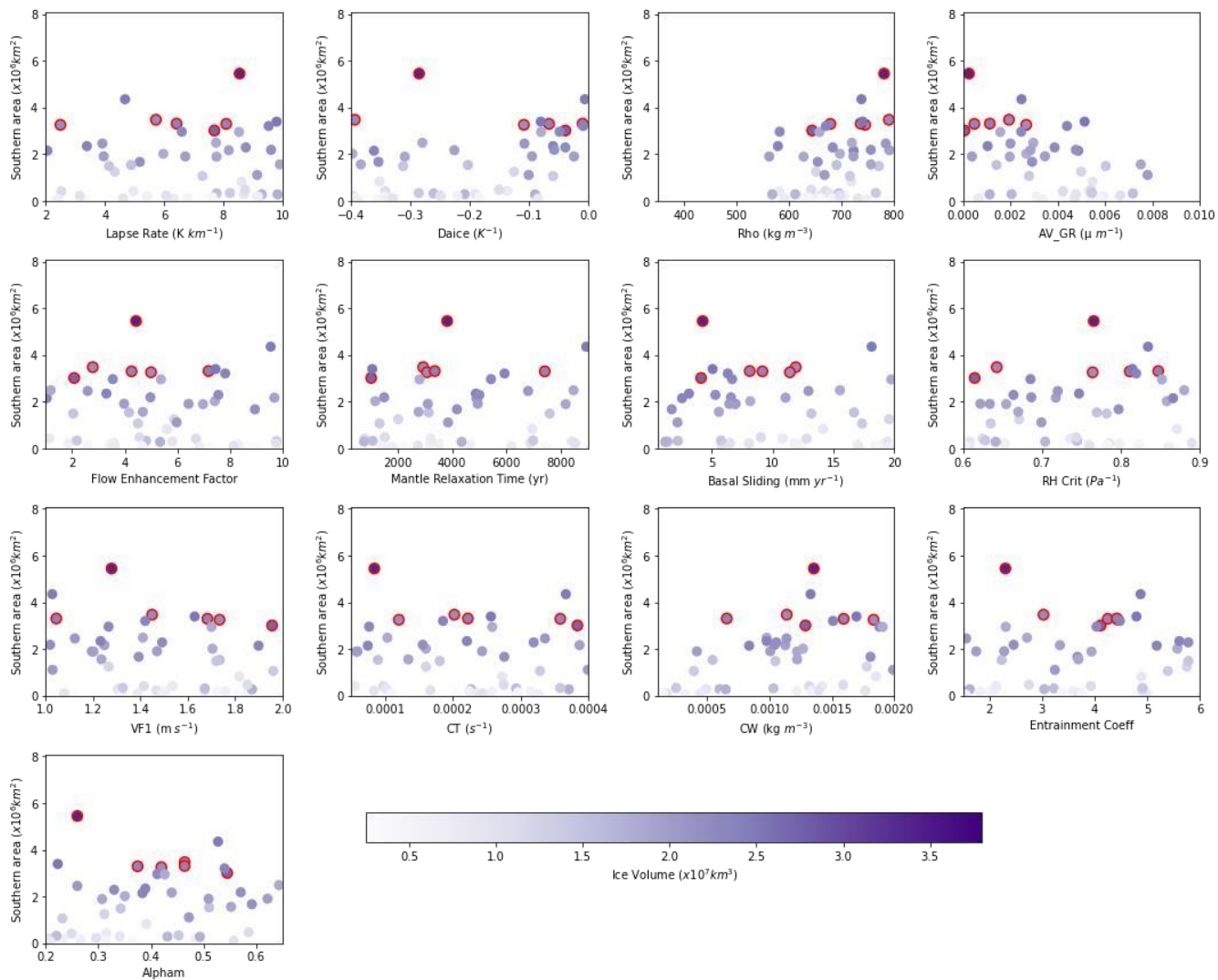
561  
562



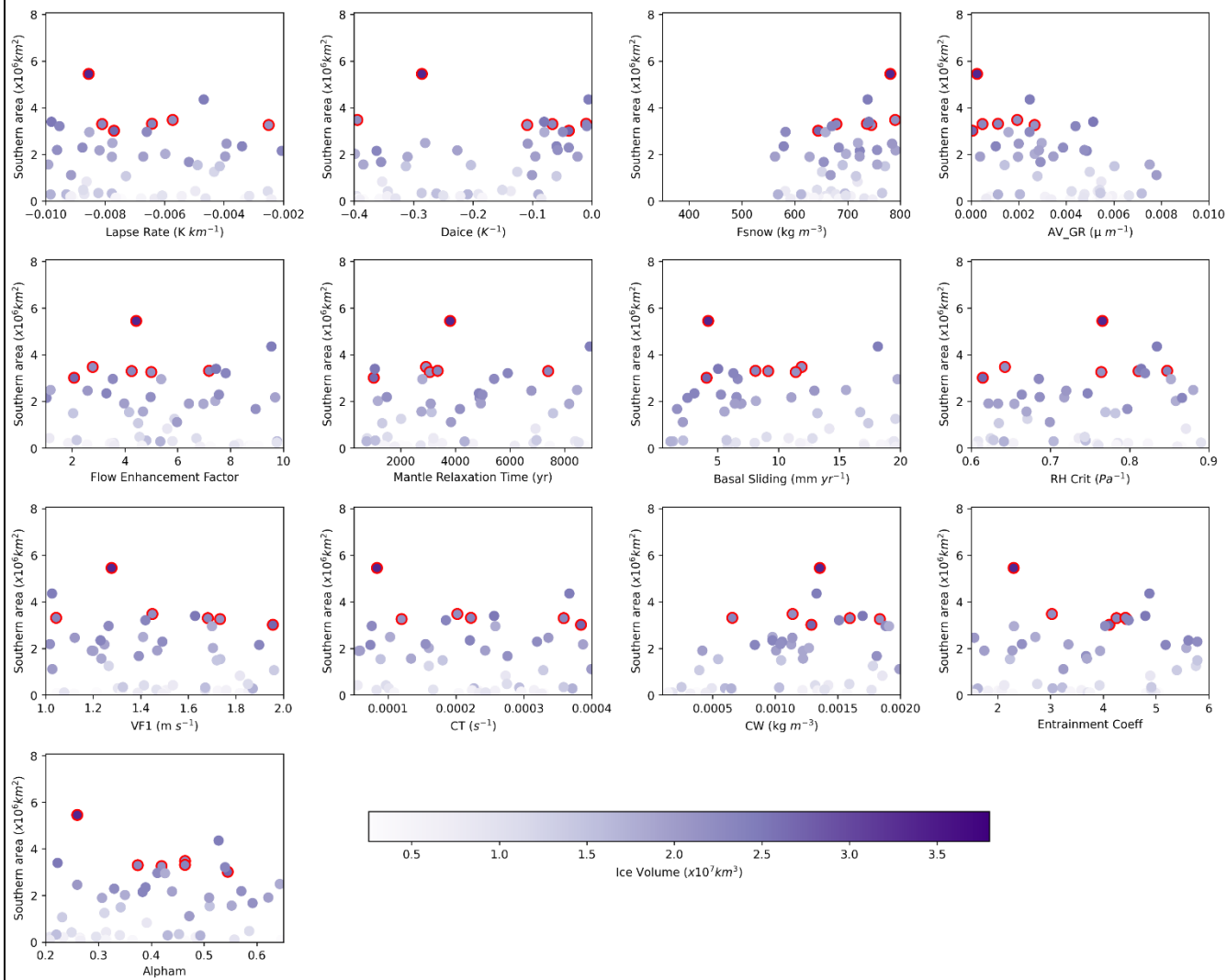


563

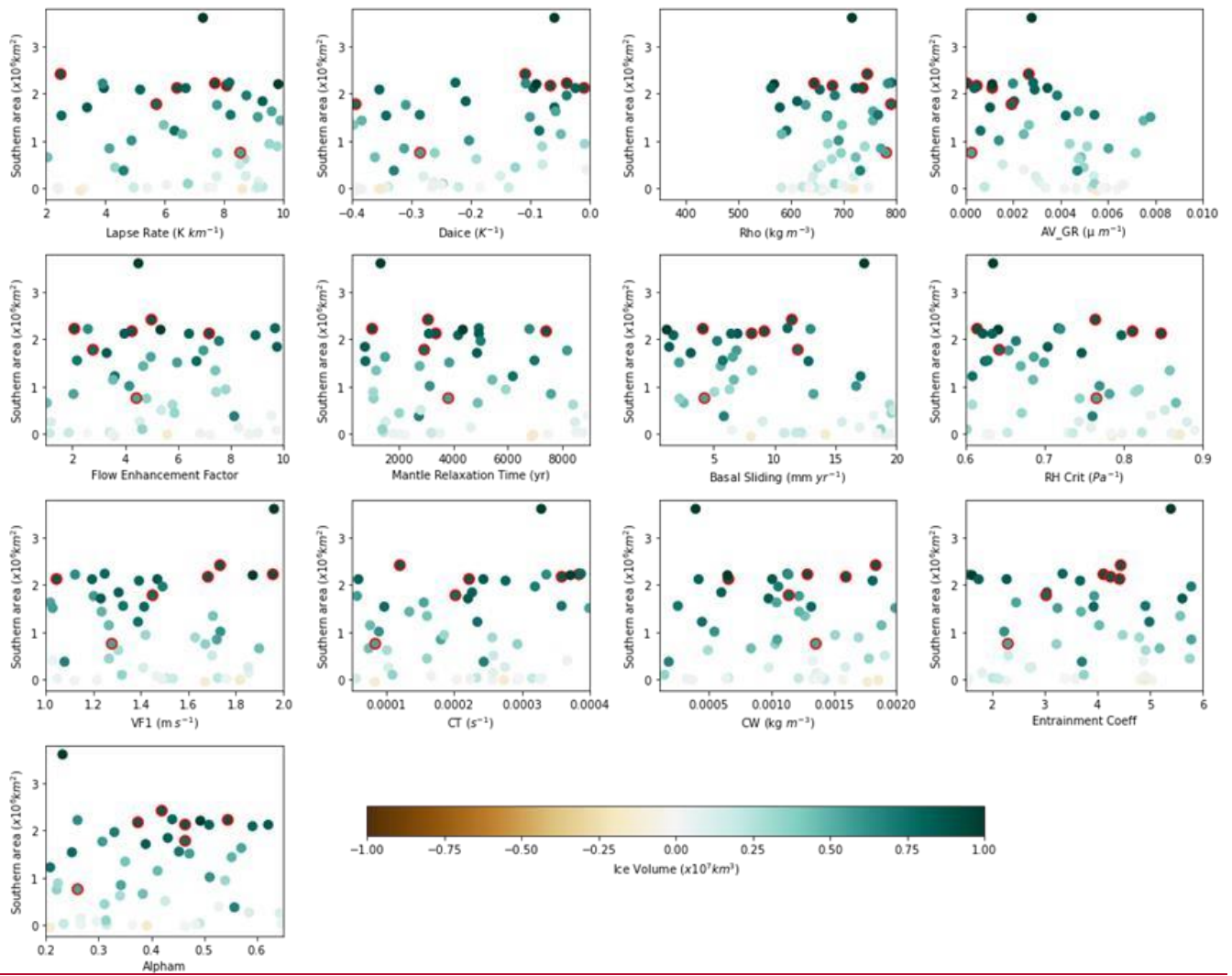
564 **Figure D4E1.** Southern area versus each of the 13 parameters varied for the LGM ensemble. The green shaded region shows the  
 565 southern area constraint applied with the dotted line showing the exact area of the reconstruction and the solid line the solid line the  
 566 minimum bound applied. The colour scale represents ice volume and the dots outlined in red are the six NROY LGM simulations  
 567 with the red line on the colour bar showing the volume constraint.

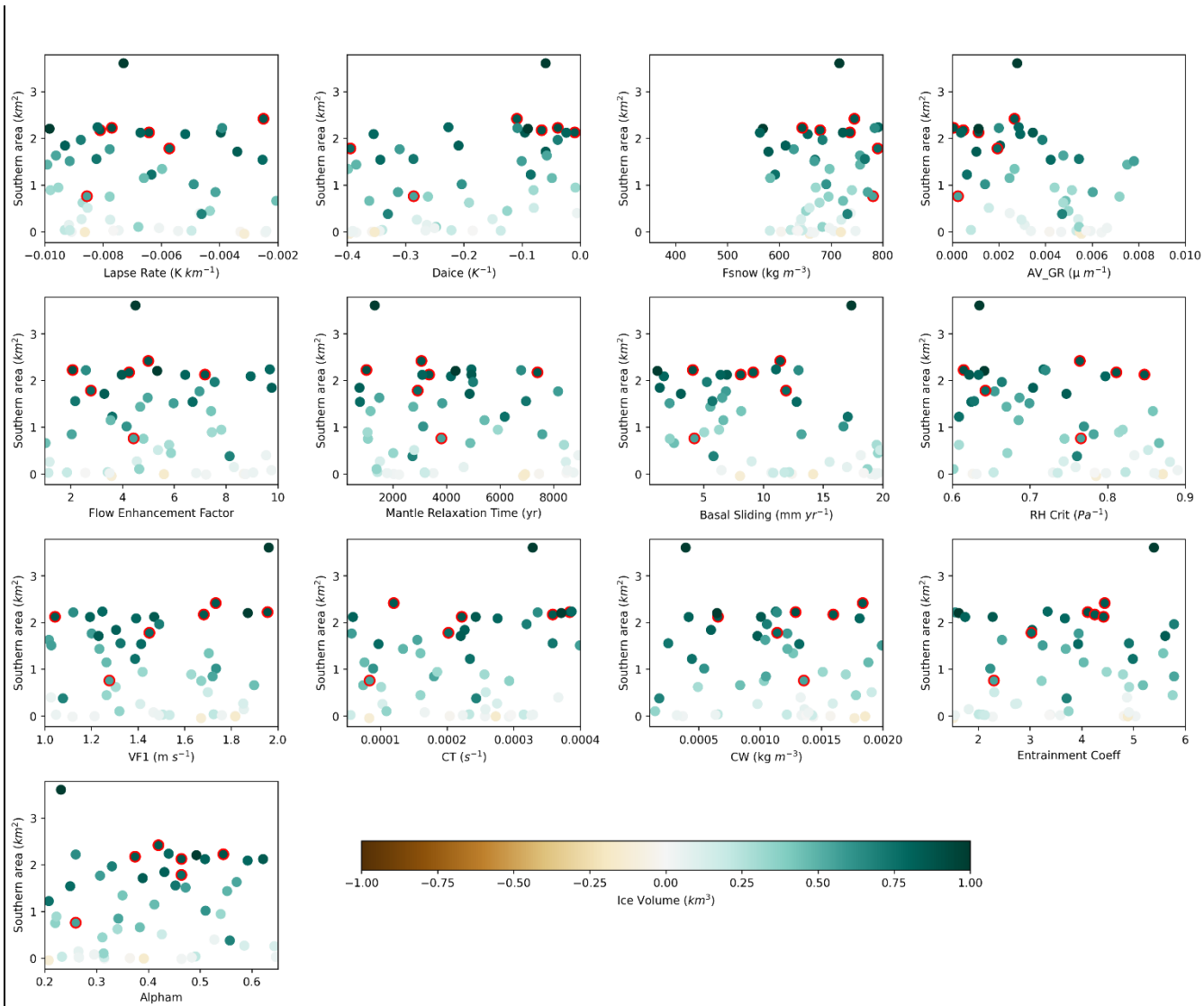


507



508 **Figure D2E2.** Southern area versus each of the 13 parameters varied for the PGM ensemble. The colour scale represents ice volume  
509 and the dots outlined in red are the corresponding six NROY PGM simulations.





§11 — Figure D3E3. Difference in southern area versus each of the 13 parameters varied between the LGM and PGM ensemble members.

§12 The colour scale represents difference in ice volume and the dots outlined in red are the six NROY simulations.

## 1 **Data availability**

2 ~~For this pre print, the~~The boundary conditions used in this study as well as the full ensemble ice sheet model output and volume  
3 and extent metrics, climate timeseries for the NROY simulations and final ice volume data from the sensitivity tests ~~have been~~  
4 ~~made available to reviewers.~~are available at <https://catalogue.ceda.ac.uk/uuid/5e48b31e413b480792e4156191b654f4>. All  
5 other model output data are available on request.

## 6 **Author contributions**

7 VLP lead the project and performed the majority of the work. VLP, LJG, RFI and NG designed the simulations and VLP and  
8 NG prepared the initial and boundary conditions with support from OGP. VLP ran the simulations and analysed the results.  
9 LCA and NG designed and performed the Wave 2 simulations the ensembles were sampled from, and JO did the sampling.  
10 RSS provided technical and scientific support and updates for FAMOUS-Glimmer. PJV provided the PGM HadCM3 sea  
11 surface temperature and sea ice dataset. VLP wrote the manuscript with comments and contributions from all co-authors. LJG,  
12 RFI and NG supervised the project and LJG acquired the funding.

## 13 **Competing interests**

14 The authors declare they have no conflict of interest.

## 15 **Acknowledgements**

16 This research is primarily funded by the ‘SMB-Gen’ UKRI Future Leaders Fellowship MR/S016961/1, with LJG, JO, NG and  
17 ~~JO directly~~LCA supported by the award and VLP’s PhD studentship funded by the University of Leeds. RFI and RSS’s  
18 contributions were supported by the RISICMAP19 NERC standard grant NE/T007443/1. LCA is supported by the ARC ITRH  
19 for Transforming energy Infrastructure through Digital Engineering (TIDE), Grant No. IH200100009. OGP is funded by the  
20 European Union’s Horizon 2020 research and innovation programme RiSeR project (grant agreement no. 802281). The  
21 simulations were run on the high-performance research computing facilities of the University of Leeds and technical support  
22 was provided by Richard Rigby from the Centre for Environmental Modelling and Computation (CEMAC). The authors would  
23 like to thank ~~Paul Valdes for providing the HadCM3 LGM and PGM sea surface temperature and sea ice datasets. Also,~~ Michel  
24 Crucifix, Peter Hopcroft, Pam Vervoort and Paul Valdes for discovering the eccentricity equation error and providing the  
25 corrected equation.

## 26 References

- 27 Abe-Ouchi, A., Segawa, T., and Saito, F: Climatic Conditions for modelling the Northern Hemisphere ice sheets throughout  
28 the ice age cycle, *Clim. Past*, 3, 423–438, <https://doi.org/10.5194/ep-3-423-2007>, 2007., [https://doi.org/10.5194/cp-3-423-](https://doi.org/10.5194/cp-3-423-2007)  
29 [2007, 2007.](https://doi.org/10.5194/cp-3-423-2007)
- 30 Abe-Ouchi, A., Saito, F., Kawamura, K., Raymo, M. E., Okuno, J., Takahashi, K., and Blatter, H.: Insolation-driven  
31 100,000-year-000-year glacial cycles and hysteresis of ice-sheet volume, *Nature*, 500, 190-193,  
32 <https://doi.org/10.1038/nature12374>, <https://doi.org/10.1038/nature12374>, 2013.
- 33 [Allen, J. R. M., Forrest, M., Hickler, T., Singarayer, J. S., Valdes, P. J., and Huntley, B.: Global vegetation patterns of the past  
34 140,000 years, \*J. Biogeogr.\*, 47, 2073-2090. <https://doi.org/10.1111/jbi.13930>, 2020.](https://doi.org/10.1111/jbi.13930)
- 35 [Astfalck, L., Williamson, D., Gandy, N., Gregoire, L., and Ivanovic, R.: Coexchangeable Process Modeling for Uncertainty  
36 Quantification in Joint Climate Reconstruction. \*J. Am. Stat. Assoc.\* 1–14. <https://doi.org/10.1080/01621459.2024.2325705>,  
37 \[2024.\]\(https://doi.org/10.1080/01621459.2024.2325705\)](https://doi.org/10.1080/01621459.2024.2325705)
- 38 Batchelor, C. L., Margold, M., Krapp, M., Murton, D. K., Dalton, A. S., Gibbard, P. L., Stokes, C. R., Murton, J. B., and  
39 Manica, A.: The configuration of Northern Hemisphere ice sheets through the Quaternary, *Nat. Commun.*, 10, 3713,  
40 <https://doi.org/10.1038/s41467-019-11601-2>, 2019. *Commun.*, 10, 3713, <https://doi.org/10.1038/s41467-019-11601-2>, 2019.
- 41 Beghin, P., Charbit, S., Dumas, C., Kageyama, M., Roche, D. M., and Ritz, C.: Interdependence of the growth of the Northern  
42 Hemisphere ice sheets during the last glaciation: the role of atmospheric circulation, *Clim. Past*, 10, 345–358,  
43 <https://doi.org/10.5194/ep-10-345-2014>, 2014. *Past*, 10, 345–358, <https://doi.org/10.5194/ep-10-345-2014>, 2014.
- 44 Beghin, P., Charbit, S., Dumas, C., Kageyama, M., and Ritz, C.: How might the North American ice sheet influence the  
45 northwestern Eurasian climate?, *Clim. Past*, 11, 1467–1490, <https://doi.org/10.5194/CP-11-1467-2015>, 2015.,  
46 <https://doi.org/10.5194/CP-11-1467-2015>, 2015.
- 47 Bereiter, B., Eggleston, S., Schmitt, J., Nehrbass-Ahles, C., Stocker, T. F., Fischer, H., Kipfstuhl, S., and Chappellaz, J.:  
48 Revision of the EPICA Dome C CO<sub>2</sub> record from 800 to 600-kyr before present, *Geophys. Res. Lett.*, 42, 542–549,  
49 <https://doi.org/10.1002/2014GL061957>, <https://doi.org/10.1002/2014GL061957>, 2015.
- 50 Berger, A. L.: Long-Term Variations of Daily Insolation and Quaternary Climatic Changes, *J. Atmos. Sci.*, 35, 2362-2367,  
51 [https://doi.org/10.1175/1520-0469\(1978\)035<2362:LTVODI>2.0.CO;2](https://doi.org/10.1175/1520-0469(1978)035<2362:LTVODI>2.0.CO;2), 1978. [https://doi.org/10.1175/1520-](https://doi.org/10.1175/1520-0469(1978)035<2362:LTVODI>2.0.CO;2)  
52 [0469\(1978\)035<2362:LTVODI>2.0.CO;2](https://doi.org/10.1175/1520-0469(1978)035<2362:LTVODI>2.0.CO;2), 1978.
- 53 Berger, A., and Loutre, M. F.: Insolation values for the climate of the last 10 million years, *Quaternary Sci. Rev.*, 10, 297–317,  
54 [https://doi.org/10.1016/0277-3791\(91\)90033-Q](https://doi.org/10.1016/0277-3791(91)90033-Q), 1991. [https://doi.org/10.1016/0277-3791\(91\)90033-Q](https://doi.org/10.1016/0277-3791(91)90033-Q), 1991.
- 55 Bonelli, S., Charbit, S., Kageyama, M., Woillez, M.-N., Ramstein, G., Dumas, C., and Quiquet, A.: Investigating the evolution  
56 of major Northern Hemisphere ice sheets during the last glacial-interglacial cycle, *Clim. Past*, 5, 329–345,  
57 <https://doi.org/10.5194/ep-5-329-2009>, 2009. *Past*, 5, 329–345, <https://doi.org/10.5194/ep-5-329-2009>, 2009.

58 Briggs, R. D., Pollard, D., and Tarasov, L.: A data-constrained large ensemble analysis of Antarctic evolution since the Eemian,  
59 Quaternary Sci. Rev., 103, 91-115, <https://doi.org/10.1016/j.quascirev.2014.09.003>, 2014.

60 ~~Cheng, H., Edwards, R. L., Broecker, W. S., Denton, G. H., Kong, X.,~~  
61 ~~Wang, Y., Zhang, R., and Wang, X.: Ice age terminations, Science, 326, 248–252. DOI: 10.1126/science.1177840, 2009.~~

62 Colleoni, F., Krinner, G., Jakobsson, M., Peyaud, V., and Ritz, C.: Influence of regional parameters on the surface mass balance  
63 of the Eurasian ice sheet during the peak Saalian (140 kya), Glob. Planet. Change, 68, 132-148,  
64 <https://doi.org/10.1016/j.gloplacha.2009.03.021>, 2009a. <https://doi.org/10.1016/j.gloplacha.2009.03.021>, 2009a.

65 Colleoni, F., Krinner, G., and Jakobsson, M.: Sensitivity of the Late Saalian (140 kyrs BP) and LGM (21 kyrs BP) Eurasian  
66 ice sheet surface mass balance to vegetation feedbacks, Geophys. Res. Lett., 36, L08704, doi:10.1029/2009GL037200, 2009b.

67 Colleoni, F., Liakka, J., Krinner, G., Jakobsson, M., Masina, S., and Peyaud, V.: The sensitivity of the Late Saalian (140 ka)  
68 and LGM (21 ka) Eurasian ice sheets to sea surface conditions, Clim. Dyn., 37, 531–553, [https://doi.org/10.1007/s00382-](https://doi.org/10.1007/s00382-0100870-7)  
69 [0100870-7](https://doi.org/10.1007/s00382-0100870-7), 2011. [Dyn., 37, 531-553, https://doi.org/10.1007/s00382-](https://doi.org/10.1007/s00382-0100870-7)  
[0100870-7](https://doi.org/10.1007/s00382-0100870-7), 2011.

70 Colleoni, F., Wekerle, C., Brandefelt, J., and Masina, S.: Constraint on the penultimate glacial maximum Northern Hemisphere  
71 ice topography (~140 kyrs BP), Quaternary Sci. Rev., 137, 97-112, <https://doi.org/10.1016/j.quascirev.2016.01.024>, 2016.,  
72 <https://doi.org/10.1016/j.quascirev.2016.01.024>, 2016.

73 Cornford, S. L., Martin, D. F., Graves, D. T., Ranken, D. F., le Brocq, A. M., Gladstone, R. M., Payne, A. J., Ng, E. G., and  
74 Lipscomb, W. H.: Adaptive mesh, finite volume modeling of marine ice sheets, J. Comput. Phys., 232, 529–549,  
75 <https://doi.org/10.1016/J.JCP.2012.08.037>, 2013., 2013.

76 Crossley, J. F., and Roberts, D. L.: Thermodynamic/dynamic Sea-ice model, Meteorological office, 1995.

77 Dalton, A. S., Margold, M., Stokes, C. R., Tarasov, L., Dyke, A. S., Adams, R. S., Allard, S., Arends, H. E., Atkinson, N.,  
78 Attig, J. W., Barnett, P. J., Barnett, R. L., Batterson, M., Bernatchez, P., Borns Jr, H. W., Breckenridge, A., Briner, J. P.,  
79 Brouard, E., Campbell, J. E., Carlson, A. E., ... Wright Jr, H. E.: An updated radiocarbon-based ice margin chronology for the  
80 last deglaciation of the North American Ice Sheet Complex, Quaternary Sci. Rev., 234, 106223,  
81 <https://doi.org/10.1016/j.quascirev.2020.106223>, 2020. <https://doi.org/10.1016/j.quascirev.2020.106223>, 2020.

82 Dalton, A. S., Stokes, C. R., and Batchelor, C. L.: Evolution of the Laurentide and Innuitian ice sheets prior to the Last Glacial  
83 Maximum (115 ka to 25 ka), Earth-Sci. Rev., 224, 103875, <https://doi.org/10.1016/j.earscirev.2021.103875>, 2022.,  
84 <https://doi.org/10.1016/j.earscirev.2021.103875>, 2022.

85 [Davies-Barnard, T., Ridgwell, A., Singarayer, J., and Valdes, P.: Quantifying the influence of the terrestrial biosphere on](https://doi.org/10.5194/cp-13-1381-2017)  
86 [glacial–interglacial climate dynamics, Clim. Past, 13, 1381–1401, https://doi.org/10.5194/cp-13-1381-2017](https://doi.org/10.5194/cp-13-1381-2017), 2017.

87 [de Boer, B., van de Wal, R.S.W., Lourens, L.J., Bintanja, R., and Reerink, T. J.: A continuous simulation of global ice volume](https://doi.org/10.1007/s00382-012-1562-2)  
88 [over the past 1 million years with 3-D ice-sheet models, Clim. Dyn., 41, 1365–1384. https://doi.org/10.1007/s00382-012-1562-](https://doi.org/10.1007/s00382-012-1562-2)  
89 [2](https://doi.org/10.1007/s00382-012-1562-2), 2013.



90 Dentith, J. E., Ivanovic, R. F., Gregoire, L. J., Tindall, J. C., and Smith, R. S.: Ocean circulation drifts in multi-millennial  
91 climate simulations: the role of salinity corrections and climate feedbacks, *Clim. Dyn.*, 52, 1761–1781,  
92 <https://doi.org/10.1007/S00382-018-4243-Y/FIGURES/15>, 2019. ~~<https://doi.org/10.1007/S00382-018-4243-Y/FIGURES/15>,~~  
93 ~~2019.~~

94 ~~Denton, G. H., Anderson, R. F., Toggweiler, J.R., Edwards, R. L., Schaefer, J. M., and Putnam, A. E.: The Last Glacial  
95 Termination, *Science*, 328, 1652–1656, DOI:10.1126/science.1184119, 2010.~~

96 ~~Dutton, A., and Lambeck, K.: Ice Volume and Sea Level During the Last Interglacial, *Science*, 337, 216–219,  
97 <https://doi.org/doi:10.1126/science.1205749>, 2012.~~

98 ~~Dutton, A., Carlson, A. E., Long, A. J., Milne, G. A., Clark, P. U., DeConto, R., Horton, B. P., Rahmstorf, S., and Raymo, M.  
99 E.: Sea level rise due to polar ice sheet mass loss during past warm periods, *Science*, 349, 6244,  
100 <https://doi.org/10.1126/science.aaa4019>, 2015.~~

101 Dyer, B., Austermann, J., D’Andrea, W. J., Creel, R. C., Sandstrom, M. R., Cashman, M., Rovere, A., and Raymo, M. E.:  
102 ~~Sealevel~~Sea-level trends across the Bahamas constrain peak last interglacial ice melt, *Proc. Natl. Acad. Sci. U.S.A.*, 118, 33,  
103 <https://doi.org/10.1073/pnas.2026839118>, 2021. ~~<https://doi.org/10.1073/pnas.2026839118>, 2021.~~

104 Dyke, A.S., Andrews, J. T. Clark, P. U., England, J. H., Miller, G. H., Shaw, J., and Veillette, J. J.: The Laurentide and Innuitian  
105 ice sheets during the Last Glacial Maximum, *Quaternary Sci. Rev.*, 21, 9–31, [https://doi.org/10.1016/S0277-3791\(01\)000956-](https://doi.org/10.1016/S0277-3791(01)000956-2)  
106 ~~2002-Rev., 21, 9-31, [https://doi.org/10.1016/S0277-3791\(01\)000956-](https://doi.org/10.1016/S0277-3791(01)000956-2)~~

107 Ehlers, J., Gibbard, P.L. and Hughes, P.D.: Chapter 4 – Quaternary Glaciations and Chronology, in: *Past Glacial Environments*,  
108 Second Edition, edited by: Menzies, J., and van der Meer, J.J.M., Elsevier, 77–101, [https://doi.org/10.1016/B978-0-08-100524-](https://doi.org/10.1016/B978-0-08-100524-8.00003-8)  
109 ~~8.00003-8, 2018.~~, <https://doi.org/10.1016/B978-0-08-100524-8.00003-8>, 2018.

110 Essery, R., Best, M., Betts, R., Cox, P. and Taylor, C.: Explicit Representation of Subgrid Heterogeneity in a GCM Land  
111 Surface Scheme, *J. Hydrometeorol.*, 4, 530–543, [https://doi.org/10.1175/1525-7541\(2003\)004<0530:EROSHI>2.0.CO;2](https://doi.org/10.1175/1525-7541(2003)004<0530:EROSHI>2.0.CO;2),  
112 ~~2003-[Hydrometeorol.](https://doi.org/10.1175/1525-7541(2003)004<0530:EROSHI>2.0.CO;2), 4, 530-543, [https://doi.org/10.1175/1525-7541\(2003\)004<0530:EROSHI>2.0.CO;2](https://doi.org/10.1175/1525-7541(2003)004<0530:EROSHI>2.0.CO;2),~~ 2003.

113 Fyke, J. G., Weaver, A. J., Pollard, D., Eby, M., Carter, L., and Mackintosh, A.: A new coupled ice sheet/climate model:  
114 description and sensitivity to model physics under Eemian, Last Glacial Maximum, late Holocene and modern climate  
115 conditions, *Geosci. Model Dev.*, 4, 117–136, <https://doi.org/10.5194/gmd-4-117-2011>, 2011. ~~[Model Dev.](https://doi.org/10.5194/gmd-4-117-2011), 4, 117–136,~~  
116 ~~<https://doi.org/10.5194/gmd-4-117-2011>, 2011.~~

117 Gandy, N., Gregoire, L. J., Ely, J. C., Cornford, S. L., Clark, C. D., and Hodgson, D. M.: Exploring the ingredients required  
118 to successfully model the placement, generation, and evolution of ice streams in the British-Irish Ice Sheet, *Quaternary Sci.*  
119 ~~*Rev.*, 223, 105915, <https://doi.org/10.1016/j.quascirev.2019.105915>,~~ 2019. ~~*Rev.*, 223, 105915,~~  
120 ~~<https://doi.org/10.1016/j.quascirev.2019.105915>, 2019.~~

121 Gandy, N., Astfalck, L. C., Gregoire, L. J., Ivanovic, R. F., Patterson, V. L., Sherriff-Tadano, S., Smith, R. S., Williamson, D.,  
122 and Rigby, R.: De-tuning a coupled Climate Ice Sheet Model to simulate the North American Ice Sheet at the Last Glacial  
123 Maximum, *J. Geophys. Res. Earth Surf.*, DOI: 10.1002/essoar.10512201.1, 2023.

124 ~~Ganopolski, A. and Brovkin, V.: Simulation of climate, ice sheets and CO2 evolution during the last four glacial cycles with~~  
125 ~~an Earth system model of intermediate complexity, *Clim. Past*, 13, 1695–1716, <https://doi.org/10.5194/cp-13-1695-2017>,~~  
126 ~~2017.~~

127 Ganopolski, A., Calov, R., and Claussen, M.: Simulation of the last glacial cycle with a coupled climate ice-sheet model of  
128 intermediate complexity, *Clim. Past*, 6, 229–244, <https://doi.org/10.5194/cp-6-229-2010>, 2010.

129 ~~Govin, A., Capron, <https://doi.org/10.5194/cp-6-229-2010>, 2010.~~ ~~E., Tzedakis, P. C., Verheyden, S., Ghaleb, B., Hillaire-~~  
130 ~~Marcel, C., St-Onge, G., Stoner, J. S., Bassinot, F., Bazin, L., Blunier, T., Combourieu Nebout, N., el-Ouahabi, A., Genty, D.,~~  
131 ~~Gersonde, R., Jimenez Amat, P., Landais, A.,~~  
132 ~~Martrat, B., Masson Delmotte, V., ... Zahn, R.: Sequence of events from the onset to the demise of the Last Interglacial:~~  
133 ~~Evaluating strengths and limitations of chronologies used in climatic archives, *Quaternary Sci. Rev.*, 129, 1–36,~~  
134 ~~<https://doi.org/10.1016/J.QUASCIREV.2015.09.018>, 2015.~~

135 Gowan, E.J., Zhang, X., Khosravi, S., Rovere, A., Stocchi, P., Hughes, A. L. C., Gyllencreutz, R., Mangerud, J., Svendsen, J-  
136 I., and Lohmann, G.: A new global ice sheet reconstruction for the past 80\_000 years, *Nat. Commun.*, 12, 1199,  
137 <https://doi.org/10.1038/s41467-021-21469-w>, <https://doi.org/10.1038/s41467-021-21469-w>, 2021.

138 ~~Grant, K. M., Rohling, E. J., Bar Matthews, M., Ayalon, A., Medina Elizalde, M., Ramsey, C. B., Satow, C., and Roberts, A.~~  
139 ~~P.: Rapid coupling between ice volume and polar temperature over the past 150,000 years, *Nature*, 491, 744–747,~~  
140 ~~<https://doi.org/10.1038/nature11593>, 2012.~~

141 Gregoire, L., J. Modelling the Northern Hemisphere Climate and Ice Sheets during the Last Deglaciation, Ph.D. thesis, School  
142 of Geographical Sciences, University of Bristol, UK, 2010.

143 Gregoire, L., Payne, A. and Valdes, P.: Deglacial rapid sea level rises caused by ice-sheet saddle collapses, *Nature*, 487, 219–  
144 222, <https://doi.org/10.1038/nature11257>, ~~2012.~~, 2012.

145 Gregoire, L. J., Valdes, P. J., and Payne, A. J.: The relative contribution of orbital forcing and greenhouse gases to the North  
146 American deglaciation, *Geophys. Res. Lett.*, 42, 9970–9979, ~~<https://doi.org/10.1002/2015GL066005>,~~ 2015.,  
147 <https://doi.org/10.1002/2015GL066005>, 2015.

148 Gregoire, L. J., Otto-Bliesner, B., Valdes, P. J., and Ivanovic, R.: Abrupt Bølling warming and ice saddle collapse contributions  
149 to the Meltwater Pulse 1a rapid sea level rise, *Geophys. Res. Lett.*, 43, 9130–9137,  
150 <https://doi.org/10.1002/2016gl070356> ~~<https://doi.org/10.1002/2016gl070356>, 2016.~~, 2016.

151 Gregoire, L. J., Ivanovic, R. F., Maycock, A. C., Valdes, P. J., and Stevenson, S.: Holocene lowering of the Laurentide ice  
152 sheet affects North Atlantic gyre circulation and climate, *Clim. Dyn.*, 51, 3797–3813, [https://doi.org/10.1007/s00382-0184111-](https://doi.org/10.1007/s00382-0184111-9)  
153 ~~9,~~ 2018. <https://doi.org/10.1007/s00382-018-4111-9>, 2018.

154 Gregory, J. M., Browne, O. J. H., Payne, A. J., Ridley, J. K., and Rutt, I. C.: Modelling large-scale ice-sheet–climate  
155 interactions following glacial inception, *Clim. Past*, 8, 1565–1580, <https://doi.org/10.5194/cp-8-1565-2012>, 2012. *Past*, 8,  
156 1565–1580, <https://doi.org/10.5194/cp-8-1565-2012>, 2012.

157 Gregory, J. M., George, S. E., and Smith, R. S.: Large and irreversible future decline of the Greenland ice sheet, *Cryosphere*,  
158 14, 4299–4322, <https://doi.org/10.5194/TC-14-4299-2020>, 2020. <https://doi.org/10.5194/TC-14-4299-2020>, 2020.

159 ~~Heinemann, M., Timmermann, A., Elison Timm, O., Saito, F., and Abe-Ouchi, A.: Deglacial ice sheet meltdown: orbital~~  
160 ~~pacemaking and CO2 effects, *Clim. Past*, 10, 1567–1579, <https://doi.org/10.5194/cp-10-1567-2014>, 2014.~~

161 Hemming, S. R.: Heinrich events: Massive late Pleistocene detritus layers of the North Atlantic and their global climate  
162 imprint, *Rev. Geophys.*, 42, RG1005, <https://doi.org/10.1029/2003RG000128>, 2004. <https://doi.org/10.1029/2003RG000128>,  
163 2004.

164 Hofer, D., Raible, C. C., Dehnert, A., and Kuhlemann, J.: The impact of different glacial boundary conditions on atmospheric  
165 dynamics and precipitation in the North Atlantic region, *Clim. Past*, 8, 935–949, <https://doi.org/10.5194/cp-8-935-2012>, 2012.

166 Horton, D., Poulsen, C. and Pollard, D.: Influence of high-latitude vegetation feedbacks on late Palaeozoic glacial cycles, *Nat.*  
167 *Geosci.*, 3, 572–577, <https://doi.org/10.1038/ngeo922>, 2010. <https://doi.org/10.1038/ngeo922>, 2010.

168 Huybers, P.: Early Pleistocene Glacial Cycles and the Integrated Summer Insolation Forcing, *Science*, 313, 508-511,  
169 DOI:10.1126/science.1125249, 2006.

170 ~~Ivanovic, R. F., Gregoire, L. J., Kageyama, M., Roche, D. M., Valdes, P. J., Burke, A., Drummond, R., Peltier, W. R., and~~  
171 ~~Tarasov, L.: Transient climate simulations of the deglaciation 21–9 thousand years before present (version 1) — PMIP4 Core~~  
172 ~~experiment design and boundary conditions, *Geosci. Model Dev.*, 9, 2563–2587, <https://doi.org/10.5194/gmd-9-2563-2016>,~~  
173 ~~2016.~~

174 ~~Ivanovic, R. F., Gregoire, L. J., Burke, A., Wickert, A. D., Valdes, P. J., Ng, H. C., Robinson, L. F., McManus, J. F., Mitrovica,~~  
175 ~~J. X., Lee, L., and Dentith, J. E.: Acceleration of Northern Ice Sheet Melt Induces AMOC Slowdown and Northern Cooling in~~  
176 ~~Simulations of the Early Last Deglaciation, *Paleoceanogr. Paleoclimatol.*, 33, 807–824,~~  
177 ~~<https://doi.org/10.1029/2017PA003308>, 2018.~~

178 Izumi, K., Valdes, P., Ivanovic, R., and Gregoire, L.: Impacts of the PMIP4 ice sheets on Northern Hemisphere climate during  
179 the last glacial period, *Clim. Dyn.*, 60, 2481-2499, <https://doi.org/10.1007/s00382-022-06456-1>, 2023.

180 ~~Jiménez Amat, P., and Zahn, R.: Offset timing of climate oscillations during the last two glacial interglacial transitions~~  
181 ~~connected with large scale freshwater perturbation, *Paleoceanography*, 30, 768–788, <https://doi.org/10.1002/2014PA002710>,~~  
182 ~~2015. <https://doi.org/10.1007/s00382-022-06456-1>, 2023.~~

183 Kageyama, M., and Valdes, P. J.: Impact of the North American ice-sheet orography on the Last Glacial Maximum eddies and  
184 snowfall, *Geophys. Res. Lett.*, 27, 1515-1518, <https://doi.org/10.1029/1999GL011274>, 2000.  
185 <https://doi.org/10.1029/1999GL011274>, 2000.

186 Kageyama, M., Charbit, S., Ritz, C., Khodri, M., and Ramstein, G.: Quantifying ice-sheet feedbacks during the last glacial  
187 inception, *Geophys. Res. Lett.*, 31, 24, doi:10.1029/2004GL021339, 2004.

188 Kageyama, M., Albani, S., Braconnot, P., Harrison, S. P., Hopcroft, P. O., Ivanovic, R. F., Lambert, F., Marti, O., Peltier, W.  
189 R., Peterschmitt, J.-Y., Roche, D. M., Tarasov, L., Zhang, X., Brady, E. C., Haywood, A. M., Legrande, A. N., Lunt, D. J.,  
190 Mahowald, N. M., Mikolajewicz, U., ... Zheng, W.: The PMIP4 contribution to CMIP6-Part 4: Scientific objectives and  
191 experimental design of the PMIP4-CMIP6 Last Glacial Maximum experiments and PMIP4 sensitivity experiments, *Geosci.*  
192 *Model Dev.*, 10, 4035–4055, <https://doi.org/10.5194/gmd-10-4035-2017>, 2017. <https://doi.org/10.5194/gmd-10-4035-2017>,  
193 [2017](https://doi.org/10.5194/gmd-10-4035-2017).

194 [Kageyama, M., Harrison, S. P., Kapsch, M.-L., Lofverstrom, M., Lora, J. M., Mikolajewicz, U., Sherriff-Tadano, S., Vadsaria,](https://doi.org/10.5194/gmd-10-4035-2017)  
195 [T., Abe-Ouchi, A., Bouttes, N., Chandan, D., Gregoire, L. J., Ivanovic, R. F., Izumi, K., LeGrande, A. N., Lhardy, F., Lohmann,](https://doi.org/10.5194/gmd-10-4035-2017)  
196 [G., Morozova, P. A., Ohgaito, R., Paul, A., Peltier, W. R., Poulsen, C. J., Köpp, R. E., Simons, F., Quiquet, A., Roche, D. M.,](https://doi.org/10.5194/gmd-10-4035-2017)  
197 [Shi, X., Tierney, J. E., Valdes, P. J., Volodin, E., and Zhu, J.: The PMIP4 Last Glacial Maximum experiments: preliminary](https://doi.org/10.5194/gmd-10-4035-2017)  
198 [results and comparison with the PMIP3 simulations, \*Clim. Past\*, 17, 1065–1089, <https://doi.org/10.5194/cp-17-1065-2021>,](https://doi.org/10.5194/gmd-10-4035-2017)  
199 [2021](https://doi.org/10.5194/gmd-10-4035-2017).

200 ~~[J., Mitrovica, J. X., Maloof, A. C., and Oppenheimer, M.: Probabilistic assessment of sea level during the last interglacial](https://doi.org/10.5194/gmd-10-4035-2017)  
201 [stage, \*Nature\*, 462, 863–868, <https://doi.org/10.1038/nature08686>, 2009.](https://doi.org/10.5194/gmd-10-4035-2017)~~

202 Krinner, G., Mangerud, J., Jakobsson, M., Crucifix, M., Ritz, C., and Svendsen, J.-I.: Enhanced ice sheet growth in Eurasia  
203 owing to adjacent ice-dammed lakes, *Nature*, 427, 429–432, <https://doi.org/10.1038/nature02233>, ~~2004.~~  
204 <https://doi.org/10.1038/nature02233>, 2004.

205 Krinner, G., Boucher, O., and Balkanski, Y.: Ice-free glacial northern Asia due to dust deposition on snow, *Clim. Dyn.*, 27,  
206 613–625, DOI:10.1007/s00382-006-0159-z, 2006.

207 Krinner, G., Diekmann, B., Colleoni, F., and Stauch, G.: Global, regional and local scale factors determining glaciation extent  
208 in Eastern Siberia over the last 140,000 years, *Quaternary Sci. Rev.*, 30, 821–831,  
209 <https://doi.org/10.1016/j.quascirev.2011.01.001>, 2011. <https://doi.org/10.1016/j.quascirev.2011.01.001>, 2011.

210 Lambeck, K., Rouby, H., Purcell, A., Sun, Y., and Sambridge, M.: Sea level and global ice volumes from the Last Glacial  
211 Maximum to the Holocene, *Proc. Natl. Acad. Sci. U.S.A.*, 111, 15296–15303, <https://doi.org/10.1073/pnas.1411762111>, 2014.  
212 [U.S.A., 111, 15296–15303, <https://doi.org/10.1073/pnas.1411762111>, 2014.](https://doi.org/10.1073/pnas.1411762111)

213 ~~[Landais, A., Dreyfus, G., Capron, E., Jouzel, J., Masson-Delmotte, V., Roche, D. M., Prié, F., Caillon, N., Chappellaz, J.,](https://doi.org/10.1073/pnas.1411762111)  
214 [Leuenberger, M., Lourantou, A., Parrenin, F., Raynaud, D., and Teste, G.: Two phase change in CO<sub>2</sub>, Antarctic temperature](https://doi.org/10.1073/pnas.1411762111)  
215 [and global climate during Termination II. \*Nature Geoscience\*, 6, 1062–1065, <https://doi.org/10.1038/ngeo1985>, 2013.](https://doi.org/10.1073/pnas.1411762111) Liakka,  
216 J., and Nilsson, J.: The impact of topographically forced stationary waves on local ice-sheet climate, *J. Glaciol.*, 56, 534–544,  
217 <https://doi.org/10.3189/002214310792447824>, 2010. <https://doi.org/10.3189/002214310792447824>, 2010.~~

218 Liakka, J., Nilsson, J. and Löffverström, M.: Interactions between stationary waves and ice sheets: linear versus nonlinear  
219 atmospheric response, *Clim. Dyn.*, 38, 1249–1262, <https://doi.org/10.1007/s00382-011-1004-6>, ~~2012.~~  
220 <https://doi.org/10.1007/s00382-011-1004-6>, 2012.

221 Liakka, J., Löffverström, M., and Colleoni, F.: The impact of the North American glacial topography on the evolution of the  
222 Eurasian ice sheet over the last glacial cycle, *Clim. Past*, 12, 1225–1241, <https://doi.org/10.5194/CP-12-1225-2016>, 2016. ~~Past~~,  
223 <https://doi.org/10.5194/CP-12-1225-2016>, 2016.

224 Lisiecki, L. E., and Raymo, M. E.: A Pliocene-Pleistocene stack of 57 globally distributed benthic  $\delta^{18}\text{O}$  records,  
225 *Paleoceanography*, 20, 1–17, <https://doi.org/10.1029/2004PA001071>, 2005., <https://doi.org/10.1029/2004PA001071>, 2005.

226 Loulergue, L., Schilt, A., Spahni, R., Masson-Delmotte, V., Blunier, T., Lemieux, B., Barnola, J. M., Raynaud, D., Stocker,  
227 T. F., and Chappellaz, J.: Orbital and millennial-scale features of atmospheric  $\text{CH}_4$  over the past 800,000 years, *Nature*, 453,  
228 383–386, <https://doi.org/10.1038/nature06950>, 2008., <https://doi.org/10.1038/nature06950>, 2008.

229 Lunt, D. J., Haywood, A. M., Schmidt, G. A., Salzmann, U., Valdes, P. J., Dowsett, H. J., and Loptson, C. A.: On the causes  
230 of mid-Pliocene warmth and polar amplification. *Earth Planet. Sci. Lett.*, 321-322, 128-138,  
231 <https://doi.org/10.1016/j.epsl.2011.12.042>; <https://doi.org/10.1016/j.epsl.2011.12.042>, 2012.

232 Lüthi, D., le Floch, M., Bereiter, B., Blunier, T., Barnola, J. M., Siegenthaler, U., Raynaud, D., Jouzel, J., Fischer, H.,  
233 Kawamura, K., and Stocker, T. F.: High-resolution carbon dioxide concentration record 650,000–800,000 years before present,  
234 *Nature*, 453, 379–382. <https://doi.org/10.1038/nature06949>, 2008. <https://doi.org/10.1038/nature06949>, 2008.

235 Margari, V., Skinner, L. C., Hodell, D. A., Martrat, B., Toucanne, S., Grimalt, J. O., Gibbard, P. L., Lunkka, J. P., and Tzedakis,  
236 P. C.: Land-ocean changes on orbital and millennial time scales and the penultimate glaciation, *Geology*, 4, 183–186,  
237 <https://doi.org/10.1130/G35070.1>, 2014.

238 ~~Marino, <https://doi.org/10.1130/G35070.1>, 2014. G., Rohling, E. J., Rodríguez-Sanz, L., Grant, K. M., Heslop, D., Roberts, A.~~  
239 ~~P., Stanford, J. D., and Yu, J.: Bipolar seesaw control on last interglacial sea level, *Nature*, 522, 197–201,~~  
240 ~~<https://doi.org/10.1038/nature14499>, 2015.~~

241 Marshall, S. J., James, T. S., and Clarke, G. K. C.: North American Ice Sheet reconstructions at the Last Glacial Maximum,  
242 *Quaternary Sci. Rev.*, 21, 175-192, [https://doi.org/10.1016/S0277-3791\(01\)00089-0](https://doi.org/10.1016/S0277-3791(01)00089-0), 2002., [https://doi.org/10.1016/S0277-](https://doi.org/10.1016/S0277-3791(01)00089-0)  
243 [3791\(01\)00089-0](https://doi.org/10.1016/S0277-3791(01)00089-0), 2002.

244 ~~Marsiat, I., and Valdes, P.: Sensitivity of the Northern Hemisphere climate of the Last Glacial Maximum to sea surface~~  
245 ~~temperatures. *Clim. Dyn.* 17, 233–248, <https://doi.org/10.1007/s003820000108>, 2001.~~

246 Masson-Delmotte, V., Stenni, B., Pol, K., Braconnot, P., Cattani, O., Falourd, S., Kageyama, M., Jouzel, J., Landais, A.,  
247 Minster, B., Barnola, J. M., Chappellaz, J., Krinner, G., Johnsen, S., Röthlisberger, R., Hansen, J., Mikolajewicz, U., and  
248 ~~Otto-Bliesner~~ ~~Otto-Bliesner~~, B.: EPICA Dome C record of glacial and interglacial intensities, *Quaternary Sci. Rev.*, 29, 113-  
249 128, <https://doi.org/10.1016/j.quascirev.2009.09.030>, 2010. <https://doi.org/10.1016/j.quascirev.2009.09.030>, 2010.

250 Meissner, K. J., Weaver, A. J., Matthews, H. D., and Cox, P. M.: The role of land surface dynamics in glacial inception: a  
251 study with the UVic Earth System Model, *Clim. Dyn.*, 21, 515-537, ~~<https://doi.org/10.1007/s00382-003-0352-2>, 2003.~~,  
252 <https://doi.org/10.1007/s00382-003-0352-2>, 2003.

253 Menviel, L., Capron, E., Govin, A., Dutton, A., Tarasov, L., Abe-Ouchi, A., Drysdale, R. N., Gibbard, P. L., Gregoire, L., He,  
254 F., Ivanovic, R. F., Kageyama, M., Kawamura, K., Landais, A., Otto-Bliesner, B. L., Oyabu, I., Tzedakis, P. C., Wolff, E., and  
255 Zhang, X.: The penultimate deglaciation: protocol for Paleoclimate Modelling Intercomparison Project (PMIP) phase 4  
256 transient numerical simulations between 140 and 127 ka, version 1.0, *Geosci. Model Dev.*, 12, 3649–3685,  
257 ~~<https://doi.org/10.5194/gmd-12-3649-2019>, 2019.~~ <https://doi.org/10.5194/gmd-12-3649-2019>,  
258 2019.

259 Naafs, B. D. A., Hefter, J., Acton, G., Haug, G. H., Martinez-Garcia, A., Pancost, R., and Stein, R.: Strengthening of North  
260 American dust sources during the late Pliocene (2.7 Ma), *Earth Planet. Sci. Lett.*, ~~317–318, 8–19,~~  
261 ~~<https://doi.org/10.1016/j.epsl.2011.11.026>, 2012.~~ <https://doi.org/10.1016/j.epsl.2011.11.026>, 2012.

262 Naafs, B. D. A., Hefter, J., and Stein, R.: Millennial-scale ice rafting events and Hudson Strait Heinrich(-like) Events during  
263 the late Pliocene and Pleistocene: a review, *Quaternary Sci. Rev.*, 80, 1–28,  
264 ~~<https://doi.org/10.1016/j.quascirev.2013.08.014>~~ <https://doi.org/10.1016/j.quascirev.2013.08.014>, 2013.

265 Niu, L., Lohmann, G., Hinck, S., Gowan, E., and Krebs-Kanzow, U.: The sensitivity of Northern Hemisphere ice sheets to  
266 atmospheric forcing during the last glacial cycle using PMIP3 models, *J. Glaciol.*, 65, 645–661, doi:10.1017/jog.2019.42,  
267 2019.

268 ~~Niu, L., Lohmann, G., Gierz, P., Gowan, E. J., and Knorr, G.: Coupled climate-ice sheet modelling of MIS-13 reveals a~~  
269 ~~sensitive Cordilleran Ice Sheet. *Glob. Planet. Change*, 200, 103474, <https://doi.org/10.1016/j.gloplacha.2021.103474>, 2021.~~

270 ~~Niu, L., Knorr, G., Krebs-Kanzow, U., Gierz, P., and Lohmann, G.: Rapid Laurentide Ice Sheet growth preceding the Last~~  
271 ~~Glacial Maximum due to summer snowfall. *Nat. Geosci.* 17, 440–449, <https://doi.org/10.1038/s41561-024-01419-z>, 2024.~~

272 Obrochta, S. P., Crowley, T. J., Channell, J. E. T., Hodell, D. A., Baker, P. A., Seki, A., and Yokoyama, Y.: Climate variability  
273 and ice-sheet dynamics during the last three glaciations, *Earth Planet. Sci. Lett.*, 406, 198–212,  
274 ~~<https://doi.org/10.1016/J.EPSL.2014.09.004>, 2014.~~ <https://doi.org/10.1016/J.EPSL.2014.09.004>, 2014.

275 ~~Otto-Bliesner, B. L., Rosenbloom, N., Stone, E. J., McKay, N. P., Lunt, D. J., Brady, E. C., and Overpeck, J. T.: How warm~~  
276 ~~was the last interglacial? New model-data comparisons, *Philos. Trans. Royal Soc. A*, 371, 20130097,~~  
277 ~~<https://doi.org/10.1098/RSTA.2013.0097>, 2013.~~

278 Parker, R. L., Foster, G. L., Gutjahr, M., Wilson, P. A., Littler, K. L., Cooper, M. J., Michalik, A., Milton, J. A., Crocket, K.  
279 C., and Bailey, I.: Laurentide Ice Sheet extent over the last 130 thousand years traced by the Pb isotope signature of weathering  
280 inputs to the Labrador Sea, *Quaternary Sci. Rev.*, 287, 107564, <https://doi.org/10.1016/j.quascirev.2022.107564>, 2022.  
281 <https://doi.org/10.1016/j.quascirev.2022.107564>, 2022.



282 Pattyn, F., Schoof, C., Perichon, L., Hindmarsh, R. C. A., Bueler, E., de Fleurian, B., Durand, G., Gagliardini, O., Gladstone,  
283 R., Goldberg, D., Gudmundsson, G. H., Huybrechts, P., Lee, V., Nick, F. M., Payne, A. J., Pollard, D., Rybak, O., Saito, F.,  
284 and Vieli, A.: Results of the Marine Ice Sheet Model Intercomparison Project, MISMP, *Cryosphere*, 6, 573–588,  
285 <https://doi.org/10.5194/te-6-573-2012>, 2012. <https://doi.org/10.5194/tc-6-573-2012>, 2012.

286 [Paul, A., Mulitza, S., Stein, R., and Werner, M.: Glacial Ocean Map \(GLOMAP\), PANGAEA \[dataset\],  
287 <https://doi.org/10.1594/PANGAEA.923262>, 2020.](https://doi.org/10.1594/PANGAEA.923262)

288 Peltier, W. R., Argus, D. F., and Drummond, R.: Space geodesy constrains ice age terminal deglaciation: The global  
289 [ICE6GICE-6G\\_C \(VM5a\) model, \*J. Geophys. Res. Solid Earth\*, 120, 450–487, doi:10.1002/2014JB011176, 2015.](https://doi.org/10.1002/2014JB011176)

290 Pollard, O. G., Barlow, N. L. M., Gregoire, L. J., Gomez, N., Cartelle, V., Ely, J. C., and Astfalck, L. C.: Quantifying the  
291 uncertainty in the Eurasian ice-sheet geometry at the Penultimate Glacial Maximum (Marine Isotope Stage 6), *Cryosphere*, 17,  
292 4751–4777, <https://doi.org/10.5194/te-17-4751-2023>, 2023. <https://doi.org/10.5194/tc-17-4751-2023>, 2023.

293 Pöppelmeier, F., Joos, F., and Stocker, T.F.: The Coupled Ice Sheet–Earth System Model Bern3D v3.0. *J. Climate*, 36, 7563–  
294 7582, <https://doi.org/10.1175/JCLI-D-23-0104.1>, 2023.

295 Pukelsheim, F.: The Three Sigma Rule, *Am. Stat.*, 48, 88–91, <https://doi.org/10.2307/2684253>, 1994.  
296 <https://doi.org/10.2307/2684253>, 1994.

297 [Quiquet, A., Roche, D. M., Dumas, C., Bouttes, N., and Lhardy, F.: Climate and ice sheet evolutions from the last glacial  
298 maximum to the pre-industrial period with an ice-sheet–climate coupled model, \*Clim. Past\*, 17, 2179–2199,  
299 <https://doi.org/10.5194/cp-17-2179-2021>, 2021.](https://doi.org/10.5194/cp-17-2179-2021)

300 Rabineau, M., Berné, S., Olivet, J.-L., Aslanian, D., Guillocheau, F., and Joseph, P.: Paleo sea levels reconsidered from direct  
301 observation of paleoshoreline position during Glacial Maxima (for the last 500,000 yr), *Earth Planet. Sci. Lett.*, 252, 119–137,  
302 <https://doi.org/10.1016/j.epsl.2006.09.033>, 2006. <https://doi.org/10.1016/j.epsl.2006.09.033>, 2006.

303 Roberts, W. H. G., Valdes, P. J., and Payne, A. J.: Topography's crucial role in Heinrich Events, *Proc. Natl. Acad. Sci. U.S.A.*,  
304 111, 16688–16693, <https://doi.org/10.1073/pnas.1414882111>, 2014. <https://doi.org/10.1073/pnas.1414882111>, 2014.

305 <https://doi.org/10.1073/pnas.1414882111>, 2014.

306 [Robinson, A., Calov, R., and Ganopolski, A.: Greenland ice sheet model parameters constrained using simulations of the  
307 Eemian Interglacial, \*Clim. Past\*, 7, 381–396, <https://doi.org/10.5194/cp-7-381-2011>, 2011.](https://doi.org/10.5194/cp-7-381-2011)

308 Rohling, E. J., Hibbert, F. D., Williams, F. H., Grant, K. M., Marino, G., Foster, G. L., Hennekam, R., de Lange, G. J., Roberts,  
309 A. P., Yu, J., Webster, J. M., and Yokoyama, Y.: Differences between the last two glacial maxima and implications for  
310 ~~icesheet~~ice-sheet,  $\delta^{18}\text{O}$ , and sea-level reconstructions, *Quaternary Sci. Rev.*, 176, 1–28,  
311 <https://doi.org/10.1016/j.quascirev.2017.09.009>, 2017. <https://doi.org/10.1016/j.quascirev.2017.09.009>, 2017.

312 Rutt, I. C., Hagdorn, M., Hulton, N. R. J., and Payne, A. J.: The Glimmer community ice sheet model, *J. Geophys. Res. Earth  
313 Surf.*, 114, 2004, <https://doi.org/10.1029/2008JF001015>, 2009. <https://doi.org/10.1029/2008JF001015>, 2009.

314 Sellevoid, R., van Kampenhout, L., Lenaerts, J. T. M., Noël, B., Lipscomb, W. H., and Vizcaino, M.: Surface mass balance  
315 downscaling through elevation classes in an Earth system model: application to the Greenland ice sheet, *Cryosphere*, 13, 3193–  
316 [3208](https://doi.org/10.5194/te-13-3193-2019), <https://doi.org/10.5194/te-13-3193-2019>, 2019. <https://doi.org/10.5194/tc-13-3193-2019>, 2019.

317 Sherriff-Tadano, S., Abe-Ouchi, A., Yoshimori, M., Oka, A., and Chan W-L.: Influence of glacial ice sheets on the Atlantic  
318 meridional overturning circulation through surface wind change, *Clim. Dyn.*, 50, 2881–2903,  
319 <https://doi.org/10.1007/s00382017-3780-0>, 2018. <https://doi.org/10.1007/s00382-017-3780-0>, 2018.

320 Sherriff-Tadano, S., Abe-Ouchi, A., and Oka, A.: Impact of mid-glacial ice sheets on deep ocean circulation and global climate,  
321 *Clim. Past*, 17, 95–110, <https://doi.org/10.5194/cp-17-95-2021>, <https://doi.org/10.5194/cp-17-95-2021>, 2021. <https://doi.org/10.5194/cp-17-95-2021>, 2021.

322 Sherriff-Tadano, S., Ivanovic, R., Gregoire, L., Lang, C., Gandy, N., Gregory, J., Edwards, T. L., Pollard, O., and Smith, R.  
323 S.: Large ensemble simulations of the North American and Greenland ice sheets at the Last Glacial Maximum with a coupled  
324 atmospheric general circulation-ice sheet model, *EGUsphere* [preprint], <https://doi.org/10.5194/egusphere-2023-2082>, 2023.  
325 <https://doi.org/10.5194/egusphere-2023-2082>, 2023.

326 Smith, R. N. B.: A scheme for predicting layer clouds and their water content in a general circulation model, *Q. J. R. Meteorol.*  
327 *Soc.*, 116, 435–460, <https://doi.org/10.1002/qj.49711649210>, 1990. *Soc.*, 116, 435–460,  
328 <https://doi.org/10.1002/qj.49711649210>, 1990.

329 Smith, R.S., and Gregory, J.: The last glacial cycle: transient simulations with an AOGCM, *Clim. Dyn.*, 38, 1545–1559,  
330 <https://doi.org/10.1007/s00382-011-1283-y>, <https://doi.org/10.1007/s00382-011-1283-y>, 2012.

331 [Smith, R. S., Gregory, J. M., and Osprey, A.: A description of the FAMOUS \(version XDBUA\) climate model and control](https://doi.org/10.5194/gmd-1-53-2008)  
332 [run, \*Geosci. Model Dev.\*, 1, 53–68, <https://doi.org/10.5194/gmd-1-53-2008>, 2008.](https://doi.org/10.5194/gmd-1-53-2008)

333 Smith, R. S., George, S., and Gregory, J. M.: FAMOUS version xotzt (FAMOUS-ice): A general circulation model (GCM)  
334 capable of energy- And water-conserving coupling to an ice sheet model, *Geosci. Model Dev.*, 14, 5769–5787,  
335 <https://doi.org/10.5194/GMD-14-5769-2021>, <https://doi.org/10.5194/GMD-14-5769-2021>, 2021. <https://doi.org/10.5194/GMD-14-5769-2021>, 2021.

336 Snoll, B., Ivanovic, R. F., Valdes, P. J., Maycock, A. C., and Gregoire, L., J.: Effect of orographic gravity wave drag on  
337 Northern Hemisphere climate in transient simulations of the last deglaciation, *Clim. Dyn.*, 59, 2067–2079,  
338 <https://doi.org/10.1007/s00382-022-06196-2>, 2022. <https://doi.org/10.1007/s00382-022-06196-2>, 2022.

339 Stokes, C. R., Tarasov, L., and Dyke, A. S.: Dynamics of the North American Ice Sheet Complex during its inception and  
340 build-up to the Last Glacial Maximum, *Quaternary Sci. Rev.*, 50, 86–104, <https://doi.org/10.1016/j.quascirev.2012.07.009>,  
341 [2012. \*Rev.\*, 50, 86–104, <https://doi.org/10.1016/j.quascirev.2012.07.009>, 2012.](https://doi.org/10.1016/j.quascirev.2012.07.009)

342 Stone, E.J., and Lunt, D.J.: The role of vegetation feedbacks on Greenland glaciation, *Clim. Dyn.*, 40, 2671–2686,  
343 <https://doi.org/10.1007/s00382-012-1390-4>, <https://doi.org/10.1007/s00382-012-1390-4>, 2013.

344 [Stone, E. J., Lunt, D. J., Annan, J. D., and Hargreaves, J. C.: Quantification of the Greenland ice sheet contribution to Last](https://doi.org/10.5194/cp-9-621-2013)  
345 [Interglacial sea level rise, \*Clim. Past\*, 9, 621–639, <https://doi.org/10.5194/cp-9-621-2013>, 2013.](https://doi.org/10.5194/cp-9-621-2013)

346 Svendsen, J. I., Alexanderson, H., Astakhov, V. I., Demidov, I., Dowdeswell, J. A., Funder, S., Gataullin, V., Henriksen, M.,



347 Hjort, C., Houmark-Nielsen, M., Hubberten, H. W., Ingólfsson, Ó., Jakobsson, M., Kjær, K. H., Larsen, E., Lokrantz, H.,  
348 Lunkka, J. P., Lyså, A., Mangerud, J., ... Stein, R.: Late Quaternary ice sheet history of northern Eurasia, *Quaternary Sci.*  
349 *Rev.*, 23, 1229–1271, <https://doi.org/https://doi.org/10.1016/j.quascirev.2003.12.008>, 2004.  
350 ~~*Rev.*, 23, 1229–1271, <https://doi.org/https://doi.org/10.1016/j.quascirev.2003.12.008>, 2004.~~

351 Tarasov, L., and Peltier, W. R.: Greenland glacial history and local geodynamic consequences, *Geophys. J. Int.*, 150, 198–229,  
352 <https://doi.org/10.1046/j.1365-246X.2002.01702.x>, 2002. ~~<https://doi.org/10.1046/j.1365-246X.2002.01702.x>, 2002.~~

353 Tarasov, L., and Peltier, W. R.: A geophysically constrained large ensemble analysis of the deglacial history of the North  
354 American ice-sheet complex, *Quaternary Sci. Rev.*, 23, 359–388, <https://doi.org/10.1016/j.quascirev.2003.08.004>, 2004.  
355 ~~<https://doi.org/10.1016/j.quascirev.2003.08.004>, 2004.~~

356 Tarasov, L., Dyke, A. S., Neal, R. M., and Peltier, W. R.: A data-calibrated distribution of deglacial chronologies for the North  
357 American ice complex from glaciological modelling, *Earth Planet. Sci. Lett.*, 315–316, 30–40,  
358 <https://doi.org/10.1016/j.epsl.2011.09.010>, 2012. ~~<https://doi.org/10.1016/j.epsl.2011.09.010>, 2012.~~

359 ~~[Tierney, J. E., Zhu, J., King, J., Malevich, S. B., Hakim, G., and Poulsen, C.: Last Glacial Maximum SST proxy collection and  
360 data assimilation, PANGAEA \[dataset\], <https://doi.org/10.1594/PANGAEA.920596>, 2020.](https://doi.org/10.1594/PANGAEA.920596)~~

361 Timmermann, A., Knies, J., Timm, O. E., Abe-Ouchi, A., and Friedrich, T.: Promotion of glacial ice sheet buildup 60–115 kyr  
362 B.P. by precessionally paced Northern Hemispheric meltwater pulses, *Paleoceanography*, 25, PA4208,  
363 doi:10.1029/2010PA001933, 2010.

364 ~~[Turney, C. S. M., and Jones, R. T.: Does the Agulhas Current amplify global temperatures during super-interglacials?, \*J. Quat.\*  
365 \*Sci.\*, 25, 839–843, <https://doi.org/10.1002/JQS.1423>, 2010.](https://doi.org/10.1002/JQS.1423)~~

366 Ullman, D. J., Legrande, A. N., Carlson, A. E., Anslow, F. S., and Licciardi, J. M.: Assessing the impact of Laurentide ice  
367 sheet topography on glacial climate, *Clim. Past*, 10, 487–507, ~~<https://doi.org/10.5194/CP-10-487-2014>, 2014~~,  
368 <https://doi.org/10.5194/CP-10-487-2014>, 2014

369 ~~[Valdes, P. J., Armstrong, E., Badger, M. P. S., Bradshaw, C. D., Bragg, F., Crucifix, M., Davies-Barnard, T., Day, J. J.,  
370 Farnsworth, A., Gordon, C., Hopcroft, P. O., Kennedy, A. T., Lord, N. S., Lunt, D. J., Marzocchi, A., Parry, L. M., Pope, V.,  
371 Roberts, W. H. G., Stone, E. J., Tourte, G. J. L., and Williams, J. H. T.: The BRIDGE HadCM3 family of climate models:  
372 HadCM3@Bristol v1.0, \*Geosci. Model Dev.\*, 10, 3715–3743, <https://doi.org/10.5194/gmd-10-3715-2017>, 2017.](https://doi.org/10.5194/gmd-10-3715-2017)~~

373 Vizcaíno, M., Lipscomb, W. H., Sacks, W. J., van Angelen, J. H., Wouters, B., and van den Broeke, M. R.: Greenland Surface  
374 Mass Balance as Simulated by the Community Earth System Model. Part I: Model Evaluation and 1850–2005 Results, *J.*  
375 *Clim.*, 26, 7793–7812, <https://doi.org/10.1175/JCLI-D-12-00615.1>, 2013.

376 Waelbroeck, C., Labeyrie, L., Michel, E., Duplessy, J. C., McManus, J. F., Lambeck, K., Balbon, E., and Labracherie, M.:  
377 Sea-level and deep water temperature changes derived from benthic foraminifera isotopic records, *Quaternary Sci. Rev.*, 21,  
378 295–305, ~~[https://doi.org/10.1016/S0277-3791\(01\)00101-9](https://doi.org/10.1016/S0277-3791(01)00101-9), 2002.~~, [https://doi.org/10.1016/S0277-3791\(01\)00101-9](https://doi.org/10.1016/S0277-3791(01)00101-9), 2002.

379 [Willeit, M. and Ganopolski, A.: The importance of snow albedo for ice sheet evolution over the last glacial cycle, Clim. Past,](https://doi.org/10.5194/cp-14-697-2018)  
380 [14, 697–707, https://doi.org/10.5194/cp-14-697-2018, 2018.](https://doi.org/10.5194/cp-14-697-2018)

381 [Willeit, M., Calov, R., Talento, S., Greve, R., Bernales, J., Klemann, V., Bagge, M., and Ganopolski, A.: Glacial inception](https://doi.org/10.5194/cp-20-597-2024)  
382 [through rapid ice area increase driven by albedo and vegetation feedbacks, Clim. Past, 20, 597–623, https://doi.org/10.5194/cp-](https://doi.org/10.5194/cp-20-597-2024)  
383 [20-597-2024, 2024.](https://doi.org/10.5194/cp-20-597-2024)

384 Williams, J. H. T., Smith, R. S., Valdes, P. J., Booth, B. B. B., and Osprey, A.: Optimising the FAMOUS climate model:  
385 inclusion of global carbon cycling, Geosci. Model Dev., 6, 141–160, ~~https://doi.org/10.5194/gmd-6-141-~~  
386 ~~2013https://doi.org/10.5194/gmd-6-141-2013, 2013.~~, [https://doi.org/10.5194/gmd-6-141-](https://doi.org/10.5194/gmd-6-141-2013)  
387 [2013](https://doi.org/10.5194/gmd-6-141-2013), 2013.

387 Williamson, D.: Exploratory ensemble designs for environmental models using k-extended Latin Hypercubes, Environmetrics,  
388 26, 268–283, [https://doi.org/10.1002/env.2335, 2015.](https://doi.org/10.1002/env.2335) ~~https://doi.org/10.1002/env.2335, 2015.~~

389 Ziemen, F. A., Rodehacke, C. B., and Mikolajewicz, U.: Coupled ice sheet–climate modeling under glacial and pre-industrial  
390 boundary conditions, Clim. Past, 10, 1817–1836, ~~https://doi.org/10.5194/cp-10-1817-2014https://doi.org/10.5194/cp-10-~~  
391 ~~1817-2014, 2014.~~, [https://doi.org/10.5194/cp-10-](https://doi.org/10.5194/cp-10-1817-2014)  
392 [1817-2014](https://doi.org/10.5194/cp-10-1817-2014), 2014.

392 [Zweck, C., and Huybrechts, P.: Modeling of the northern hemisphere ice sheets during the last glacial cycle and glaciological](https://doi.org/10.1029/2004JD005489)  
393 [sensitivity, J. Geophys. Res., 110, D07103, doi:10.1029/2004JD005489, 2005.](https://doi.org/10.1029/2004JD005489)